Thermodynamic Studies of Macromolecular Models

Ola Sommelius

Department of Theoretical Physics
Lund University, Sweden

Thesis for the degree of Doctor of Philosophy

To be presented, with the permission of the Faculty of Mathematics and Natural Sciences of Lund University, for public criticism in the Auditorium of the Department of Theoretical Physics on Thursday May 29, at 10.15 a.m.

This thesis is based on the following publications/papers:

I C. Peterson, O. Sommelius and B. Söderberg,
A Variational Approach for Minimizing Lennard-Jones Energies,
Physical Review **E 53**, 1723 (1996).

II B. Jönsson, M. Ullner, C. Peterson, O. Sommelius and B. Söderberg,
Titrating Polyelectrolytes –Variational Calculations and Monte Carlo Simulations,
Journal of Physical Chemistry **100**, 409 (1996).

III C. Peterson, O. Sommelius and B. Söderberg,
A Blocking Technique for Emulating Very Large Polyelectrolytes,
Physical Review Letters **76**, 1079 (1996).

IV C. Peterson, O. Sommelius and B. Söderberg,
Scaling and Scale Breaking in Polyelectrolytes,
Journal of Chemical Physics **105**, 5233 (1996).

V A. Irbäck, C. Peterson, F. Potthast and O. Sommelius
Local Interactions and Protein Folding: A 3D Off-lattice Approach,
LU TP 96-28 (to appear in *J. Chem. Phys*).

VI B. Jönsson, M. Ullner, C. Peterson, O. Sommelius and B. Söderberg,
The Electrostatic Persistence Length Calculated from Monte Carlo, Variational and Perturbation Methods,
LU TP 96-30 (to appear in *J. Chem. Phys*).

VII O. Sommelius,
On the Kinetic Behavior and Folding Properties of an Off-Lattice Heteropolymer Model,
LU TP 97-04 (submitted to *Europhysics Letters*).

1 Introduction

Macromolecules are large molecules that play a profound role in both biological systems and industrial applications. In fact since the functions of life are carried out by biological macromolecular machines, knowledge of the structure and thermodynamic behavior of biomolecules are of importance in order to understand the function of these machines.

In this thesis we focus on simplified systems. These models are unrealistic in the sense that no model can be said to represent a specific real macromolecule, or phrased in a more positive manner these models focus on properties that can be expected to be shared by many different types of molecules. That is, in the reductionistic spirit of physics, a few aspects of macromolecular interactions are singled out and used in formulating simple models while (for the time being) ignoring the remaining types of interaction. The properties of these models are then to be extracted and compared with experiments in order to judge their merits. To extract the characteristics of the different models is however in itself a nontrivial problem. One obvious reason, indicated by the word macromolecules, is that these systems are large. The many degrees of freedom is an essential feature of macromolecules and although a large amount of coarse graining on both spatial and temporal scales is implicit in the models, they are still complex enough to defy attempts to solve them exactly.

Many macromolecules have a particular simple structure in that the small constituents (monomers) are joined together like beads on a string to form a linear polymer. This is the case for the two types of models considered here, polyelectrolytes and proteins. This partitioning into (flexible) polyelectrolytes and proteins may seem somewhat odd since the two types of system are classified in different ways. Polyelectrolytes are defined in terms of the interaction. The monomeric units are charged and thus the electrostatic interactions will play a dominating role. Proteins are biological macromolecules defined in terms of their constituents. They are linear polymers built up by 20 different types of monomers, the amino acids, and therefore many different interactions including electrostatic ones are present although one or a few effective interactions will be emphasized in the models.

This partitioning is nevertheless useful in that proteins and (flexible) polyelectrolytes on one hand have many properties in common and on the other are quite complementary in nature. They are similar in that both are large polymeric macromolecules. Partly because of this, many of the questions asked are the same for both types of systems. How do various properties, structural like the end-to-end extension of the chain or energetical, change when some parameter of the model, for example the temperature, is changed?

On the other hand the two systems are very different. Polyelectrolytes are homopolymers, that is polymers that are built up by one type of monomer. This is implicit in the definition since we neglect any eventual differences between the monomers and only focus on the electrostatic interactions. Proteins are heteropolymers which are polymers comprised of different types of monomers, in the case of proteins – the twenty amino acids. This difference gives rise to very different structural properties. Polyelectrolytes can be considered as extended objects exhibiting large structural fluctuations. In contrast proteins attain a very stable three dimensional structure under physiological conditions. Furthermore the chains in a polyelectrolyte sample are of different length (polydispersity), while a given protein always has a fixed length.

The outline of this thesis is as follows: Section 2 contains introductions to the systems and models used. Section 3 describes the computational methods applied on these models and section 4 contains short introductions to the papers.

2 Polymers

Polymer means literally something that consists of many parts, which truly is not much of a definition. What we will have in mind here is a large molecule built up by connecting many smaller ones together in a linear chain. The linear topology is not necessary, but is the case for the models considered here. If the small constituents – the monomers – are identical we speak about a homopolymer, otherwise a heteropolymer.

At the core of physics lies the idea of simplification, to strip down a problem until only the essential properties remain. In polymer physics the concept of a monomer is a result of this. We ignore the internal structure of the repeating unit, whether it consists of three or thirty atoms, and treat it as a single entity attributed with some properties that affect the way it interacts with other monomers. This implies a coarse-graining of the length-scale and that, for homopolymers with a short range interaction at least, many different polymers will be described by the same physics at length-scales much larger than the average monomer-monomer separation. The situation is somewhat similar to that of phase transitions where the nature of the phase transition does not depend on the details at small distances and thus it should be possible to describe properties shared by different polymers by using simple models. The simplest possible polymer model is the ideal chain (random walk). The only interaction present in this model is the one maintaining the monomer-monomer connectivity. If we let $\mathbf{r}_i$ denote the vector between monomers i and $i+1$ the end-to-end vector $\mathbf{R}$ can be written as

$$\mathbf{R} = \sum_{i=1}^{N-1} \mathbf{r}_i \tag{1}$$

Since all directions are equally probable $\langle \mathbf{R} \rangle = 0$, where $\langle\,\rangle$ denotes the thermal average, and since the links are independent, $\langle \mathbf{r}_i \cdot \mathbf{r}_j \rangle = 0$, the relevant measure

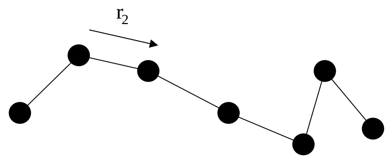

Figure 1.

of the extension of the chain is

$$\langle \mathbf{R}^2 \rangle = \sum_{i=1}^{N-1} \langle \mathbf{r}_i^2 \rangle \tag{2}$$

With a finite monomer-monomer separation $\langle \mathbf{r}_i^2 \rangle = l^2$, indeed a reasonable assumption for a polymer, the average size of an ideal chain is $R = \sqrt{N}l$. This behavior will persist even with non-zero off-diagonal elements $\langle \mathbf{r}_i \cdot \mathbf{r}_{i+m} \rangle$ provided that they decay fast enough with increasing m. More generally, the distribution of the end-to-end vector $\mathbf{R}$ will, according to the central limit theorem, be a Gaussian for all short range interactions in the limit of long chains. But short ranged here is with respect to the "topological distance" along the chain. This means that two distant parts of the chain that happens to be close in space, for example when a large loop is formed in the chain, do not interact. In particular the chain is allowed to intersect itself which is unphysical for real polymers. An ideal chain on which this excluded-volume requirement is imposed, is called a self-avoiding walk. The behavior of this system, at large N, will not be Gaussian. Instead the excluded volume effect will cause the chain to swell, $R \propto N^{\nu}$ with an (dimensional dependent) exponent ν, larger or equal to that of an ideal chain, $\nu_{ideal} = 1/2$. Flory devised a simple method of estimating the value of ν: Assume in d dimensions a density of monomers $c \propto N/R^d$. The repulsive free energy density is taken to be proportional to c^2 and $F_{rep} \propto N^2/R^d$. This is a typical mean field approach where all monomer-monomer correlations are neglected. The stretching caused by the repulsive part will be balanced by an entropic contribution which Flory took to be that of an ideal chain $F_{attr} \sim R^2/N$. After minimizing the total free energy $F = F_{rep} + F_{attr}$ with respect to R one gets $R \sim N^{\nu_F}$ with

$$\nu_F = \frac{3}{2+d} \tag{3}$$

This is a remarkably accurate result. In three dimensions $\nu_F = 0.6$ which is very close to the result obtained with renormalization techniques $\nu = 0.588 \pm 0.001$ [2]. Unfortunately the arguments leading to eq. (3) are not very well founded. There are large errors in both the repulsive and attractive energies that cancel each other. For detailed discussions on these questions see refs. [1, 2]. Nevertheless eq. (3) describes with good precision the large N limit of polymers with short range repulsions. For a system with long range interactions the behavior will be different. For the Coulomb potential $V \sim 1/R^{d-2}$, the repulsive part becomes $F_{rep} \sim N^2/R^{d-2}$ which yields an exponent $\nu = 3/d$. This result is less accurate than was the case for short range interactions. It is in fact wrong for $3 < d < 6$. Renormalization arguments for the Coulomb potential [1] give $\nu = 2/(d-2)$ for $4 < d < 6$ and for $\nu = 1$ for $d < 4$.

To summarize, in the physically relevant case $d = 3$, we can expect any short range polymer to behave like a self-avoiding walk in the large N-limit while a polymer with Coulomb interactions will be of rod-like character and the chain size will be proportional to the number of monomers.

2.1 Polyelectrolytes

Polyelectrolytes are macromolecules with ionizable groups, which dissociate into a charged polymer (poly-ion) and counterions when immersed in a polar solvent. Real world examples are found among biomolecules such as the nucleic acids, DNA and RNA, as well as synthetic polymers used in various technical applications. For a general introduction see for example [3]. The structure of a flexible polyelectrolyte is the result of an interplay between long range electrostatic interactions, covalent bonding forces and other short range forces. Moreover the long range Coulomb forces are screened by the presence of salt in the solution. This introduces an intermediate length scale in the problem. Due to this coupling of length scales the results for polyelectrolytes are expected to be more model-dependent than those of neutral polymers. Nevertheless the approach taken for polyelectrolytes is inspired by the successful application of coarse grained models in theories for neutral polymer systems [1, 2]. Here we only consider single chain properties, which means that the interactions between chains are neglected.

In the limit of no counterions and zero salt concentration the interaction between the segments of the polymer is, apart from nearest neighbor interactions, given by a pure Coulomb potential $V \propto 1/r$. If we for the moment use the notation $\tilde{x}$ to denote a dimensional variable, and x for the corresponding dimensionless variable the total energy can be written

$$\tilde{E} = \frac{k}{2}\sum_{i=1}^{N-1} \tilde{\mathbf{r}}_i^2 + \frac{q^2}{4\pi\epsilon_r\epsilon_0}\sum_{\sigma}\frac{1}{\tilde{r}_\sigma} \tag{4}$$

where $\tilde{\mathbf{r}}_i$ denotes the bond vector between monomers i and $i+1$ and

$$\tilde{\mathbf{r}}_\sigma = \sum_{i\in\sigma} \tilde{\mathbf{r}}_i \tag{5}$$

is the end-to-end vector for a subchain σ. The quadratic term is mainly chosen for convenience but partly stems from the assumption that the neutral backbone which separates the charged monomers can be approximated by a Gaussian chain. The spring constant k can be expressed in terms of the $N = 2$ equilibrium separation $\tilde{r}_0$

$$k = \frac{q^2}{4\pi\epsilon_r\epsilon_0\tilde{r}_0^3} \tag{6}$$

and if we introduce the dimensionless variables $\mathbf{r} = \tilde{\mathbf{r}}/\tilde{r}_0$ and $T = k_B\tilde{T}/(k\tilde{r}_0^2)$ the dimensionless energy becomes

$$E = \frac{1}{2}\sum_{i=1}^{N-1}\mathbf{r}_i^2 + \sum_{\sigma}\frac{1}{r_\sigma} \tag{7}$$

The presence of salt ions in the solution will screen the Coulomb interaction at large distances, and the potential will fall off more rapidly than $1/r$. It is computationally demanding to handle the salt particles explicitly. Instead the screening effect can be taken into account by averaging over the salt ions. From a linearized Poisson-Boltzmann equation one can derive an effective screened Coulomb potential $e^{-\kappa r}/r$. This is a short range potential which means that in the asymptotic $N \to \infty$ limit the behavior of the chain will be that of a self-avoiding walk. The total energy for the screened Coulomb (Debye-Hückel) chain, after a rescaling similar to that for the Coulomb chain with $\kappa = \tilde{r}_0\tilde{\kappa}$, becomes

$$E = \frac{1}{2}\sum_{i=1}^{N-1}\mathbf{r}_i^2 + \sum_{\sigma}\frac{e^{-\kappa r_\sigma}}{r_\sigma} \tag{8}$$

where $\tilde{\kappa}$ is the Debye screening parameter, proportional to the square root of the salt concentration.

2.2 Proteins

Proteins are large biological macromolecules that perform a wide variety of tasks in living organisms [5]. Proteins act as enzymes regulating chemical reactions, they are responsible for transportation of various particles, work as antibodies in the immune system etc. This multitude of functions depends to a large extent on the structural diversity of proteins. That is, a well defined three dimensional structure, the native state, is crucial in order for a protein to be able to carry out its function. This is in sharp contrast to the flexible polyelectrolytes discussed earlier, for which the thermal fluctuations are large.

A protein is a linear chain built up from the 20 amino acids occurring in nature. Each particular protein corresponds to a specific amino acid sequence, often called the primary structure in contrast to the secondary structure which denotes small structural motifs and the tertiary structure which is the overall three dimensional arrangement. The conformational structure of the protein is encoded in the amino acid sequence [4]. This implies that the folding process, i.e. the formation of the native state, is determined by the primary structure. To understand the nature of this process is one of the more challenging problems in structural biology. In particular how can a polypeptide chain find the native state, among the very large number of conformations that exists, without a global search. Proteins fold on time scales from milliseconds to seconds while a global search would require tens of orders of magnitude more time. The resolution to this (Levinthals) paradox is that the chain is guided by the energetical and entropical forces present in the system. That is the shape of the (free) energy landscape is such that the protein is ensured to fold quickly.

There are many types of interactions present in a protein. Electrostatic interactions between charged monomers, hydrogen bonds and van der Waal interactions to mention but a few. They all contribute to the structural stability of the chain. Proteins do however not function in vacuum and apart from the intra-molecular forces, interactions with the solvent, normally water, is of great importance. Since non-polar molecules to a smaller extent partake in the hydrogen-bonding in the water they will prefer a nonaquaeous environment. This can be seen as an effective (hydrophobic) interaction between these molecules. Despite the fact that these interactions are known, fundamental approaches such as quantum chemistry are limited to very small systems, a few tens of atoms, and even molecular dynamics simulations of simplified all-atom models are, due to computational limitations, applicable only to small parts of proteins or short time scales (compared to folding times), and can not be used for simulations of the entire folding process. Because of this, a large number of simplified (computationally manageable) methods have been introduced in which the gross part of the folding process can be studied.

The use of simple protein models may at first seem to be a contradiction in terms since some of the more striking features in proteins are the wide variety of structure and function they can attain. The purpose of many of these models is not primarily to mimic the behavior of a specific protein, although in the long run the hope is to transform the knowledge gained from these models into predictive power. Instead the main idea is to provide a generic scenario for the folding process and to clarify the relative importance of the various types of interactions in this process. As a consequence there is no consensus on a "minimal" protein model. Instead a wide range of approaches has emerged [6].

For the model used in papers V and VII the hydrophobic interactions are in focus. Thus the model, which is defined off-lattice, has only two types of amino acids, hydrophobic A, and hydrophilic B, respectively. The formation of a hydrophobic core is induced by a Lennard-Jones potential,

$$E_{\mathrm{LJ}}(r_{ij}, \sigma_i, \sigma_j) = 4\epsilon(\sigma_i, \sigma_j)\left(\frac{1}{r_{ij}^{12}} - \frac{1}{r_{ij}^{6}}\right) \tag{9}$$

where the depth of the minimum of the potential is chosen somewhat deeper for two hydrophobic residues $\epsilon(A, A) = 1$ than for the other combinations $\epsilon(A, B) = \epsilon(B, B) = 1/2$. Functional proteins have, due to the secondary structure, rather strong local correlations. This is in contrast to what is found for a pure Lennard-Jones chain. Therefore the model also includes species independent local interactions of the form $b_i \cdot b_{i+1}$ and $b_i \cdot b_{i+2}$ where b_i denotes the (rigid) bond vector between monomer i and $i + 1$.

3 Numerical Methods

Given a physical model, characterized by its energy $E(x)$, one of the tasks of statistical physics is to obtain thermal averages of different relevant observables.

$$\langle f \rangle = \frac{1}{Z} \int dx\, f(x) e^{-E(x)/T} \tag{10}$$

Since this, in general, is impossible to do analytically, approximation methods will be of great importance. The integral in eq. (10) can, by replacing it with a sum, be evaluated numerically. This is the basis of the so called Monte Carlo methods. Alternatively one can approximate the integral with one that can be solved analytically. This is the route taken for variational calculations in which the true Boltzmann distribution is replaced with a trial distribution and in perturbative expansions in which the energy is expanded around (for example) a high or low temperature limit.

3.1 Monte Carlo methods

The first thing that comes to mind is to replace the integral over phase space $\int dx$, with a finite sum over a subset of the phase space $\{x_1, ..., x_N\}$.

$$\langle f \rangle \approx \frac{\sum_{i=1}^{N} f(x_i) e^{-E(x_i)/T}}{\sum_{i=1}^{N} e^{-E(x_i)/T}} \tag{11}$$

For many systems this is not very practical since a large number of conformations correspond to high energies and thus will give negligible contributions. Instead one wants to choose the configurations $\{x_1, ..., x_N\}$ from reasonable probable regions (importance sampling). If the configurations were chosen with their proper Boltzmann probabilities $P(x_i) \propto \exp(-E(x_i)/T)$ the thermal average becomes

$$\langle f \rangle \approx \frac{1}{N} \sum_{i=1}^{N} f(x_i) \tag{12}$$

How does one generate configurations with the correct Boltzmann weight? The answer was given by Metropolis et al. [7]. Instead of picking the configurations x_i independently a Markov chain is generated so that configuration x_{i+1} is constructed from x_i in such a way that for large N the distribution converges to the Boltzmann distribution. That is one configuration is generated from the previous one with a transition probability $P(x \to x')$. A sufficient requirement for the method to work is the condition of detailed balance

$$\frac{P(x \to x')}{P(x' \to x)} = \frac{P_{eq}(x')}{P_{eq}(x)} = \exp\left(-\frac{\Delta E}{T}\right) \tag{13}$$

with $\Delta E = E(x') - E(x)$. This is fulfilled if the transition probability is chosen as

$$P(x \to x') = \min(1, e^{-\Delta E/T}) \tag{14}$$

This is the basis of the Metropolis algorithm. Still a few things remain to be specified. How should a new configuration be generated from the old one? If the suggested change is too large the energy difference will in general be large as well and the probability of accepting the change (eq. 14) consequently low. If on the other hand the change is small it is likely to be accepted, but many updates are needed in order to generate independent configurations. For a system like the Coulomb chain (eq. 7) the simplest update would be a trial displacement of one monomer. This is however not very efficient, and a large number of iterations are needed in order to generate statistically independent configurations. A more effective method, at least for global observables like the end-to-end distance, is the pivot algorithm [8, 9]. Here a collective move is carried out as follows: select a monomer i and perform a random rotation of monomers $i+1$ to N around a randomly chosen axis. If the bonds are flexible this is complemented with a random translation.

Heteropolymer chains are very difficult to simulate at low temperatures due to the large free energy barriers separating the different collapsed states. A pure Metropolis algorithm is likely to be very inefficient since in order to pass from one valley to another with a local updating algorithm the separating barriers have to be climbed which will be done with a very low acceptance rate. Thus the system is likely to get stuck is a small region of configuration space for long times. One efficient algorithm to circumvent this problem is the simulated tempering method [10]. The basic idea in this approach is to extend the configurational space and let the temperature become a dynamical variable attaining the values T_k for $k = 1, \ldots, K$. More precisely, the joint probability distribution

$$P(x,k) \propto \exp\left(-g_k - E(x)/T_k\right) \tag{15}$$

is simulated with separate Metropolis updates for x and k. The g_k's are tunable parameters that have to be chosen (carefully) before the simulation starts. In this way the system will apart from a walk in configuration space also move between different temperatures in such a way that the system is always in its proper Boltzmann equilibrium for that given temperature. When the system reaches the high temperatures the free energy barriers get smaller and large configurational changes are easily accepted. As the system moves down in temperature it is therefore likely to end up in a different minimum.

3.2 Variational Calculations

The basic idea with variational calculations in this context is to replace the Boltzmann distribution used in eq. 10 with a distribution for which the integral can be carried out. This trial distribution $P_V = P_V(x; a_i)$ contains a set of free parameters a_i to be chosen so that the averages obtained with the trial distribution resembles the true Boltzmann averages as much as possible. This method is standard in quantum mechanics (the Rayleigh-Ritz variational principle) where it is used to estimate the groundstate energy by minimizing the energy functional $\langle\phi\,|H|\,\phi\rangle/\langle\phi|\phi\rangle$ with respect to the trial wavefunctions ϕ and was proposed in connection to statistical mechanics by Feynman. Given an energy $E(x)$ the free energy with respect to an arbitrary probability distribution $P(x)$ is given by

$$F[P] = E[P] - TS[P] \tag{16}$$

$E[P] = \int dx E(x)P(x)$ is the average energy and $S[P] = -\int dx P(x)\log P(x)$ is the entropy. This free energy is minimized by the Boltzmann distribution $P \propto \exp(-E/T)$.

If we write the trial distribution

$$P_V(x) = \frac{e^{-E_V/T}}{Z_V} \tag{17}$$

with

$$Z_V = \int dx \exp(-E_V/T) \tag{18}$$

the free energy becomes

$$F[P_V] = -T\log Z_V + \langle E - E_V\rangle_V \tag{19}$$

where $\langle\,\rangle_V$ denotes an expectation value in the variational distribution. The values of the free parameters a_i are then given by the equations

$$\frac{\partial F}{\partial a_i} = 0 \tag{20}$$

As a simple example consider an Ising spin system

$$E = -\frac{1}{2}\sum_{ij}\omega_{ij}s_i s_j + \mu\sum_i s_i \tag{21}$$

with binary spins $s_i = 0, 1$. Here a variational approach

$$E_V = -T\sum_i u_i s_i \tag{22}$$

were u_i are the variational parameters, corresponds to a mean field approximation (since the variational probability distribution P_V factorizes). Minimizing the variational free energy one gets

$$v_i = \frac{1}{2}\left(1+\tanh(\frac{u_i}{2})\right) \tag{23}$$

$$u_i = -\frac{1}{T}\frac{\partial\langle E\rangle_V}{\partial v_i} \tag{24}$$

This is precisely the approach taken in paper II when treating titrating polyelectrolytes. $s_i = 1$ (0) indicates the presence (absence) of a charge on monomer i. The "magnetic field" μ then corresponds to a chemical potential controlling the titration

3.3 Perturbative expansions

In general the integral in eq. 10 is of course impossible to calculate analytically. If however the energy is a quadratic form the integral is a Gaussian and can readily be evaluated. Now for the polyelectrolyte models considered the chain becomes large at high temperatures and the electrostatic energy can be considered a perturbation.

$$E = \frac{1}{2}\sum_i \mathbf{r}_i^2 + V \tag{25}$$

where $V = \sum_\sigma v(r_\sigma)$ in this case represents the Coulomb or screened Coulomb potential. The partition function can then be re-written in terms of Gaussian chain averages

$$Z = \int \mathcal{D}\mathbf{r}_i e^{-E/T} = Z_0\langle e^{-V/T}\rangle_0 \tag{26}$$

where subscript 0 refers to the pure Gaussian model. Similarly for an observable f

$$Z\langle f\rangle = Z_0\langle f e^{-V/T}\rangle_0 \tag{27}$$

and if the exponentials are expanded

$$\langle f \rangle = \langle f \rangle_0 - \frac{1}{T}\langle fV \rangle_0^c + \frac{1}{2T^2}\langle fVV \rangle_0^c - \cdots \tag{28}$$

where $\langle\,\rangle_0^c$ refers to the connected expectation values in the Gaussian distribution.

At low temperatures on the other hand the expectation values can be expanded around the minimal energy configuration. If the fluctuations around this ground state are small, the energy can (to lowest order) be considered quadratic with the corrections treated as a perturbation. If we for simplicity consider a one dimensional system with an energy minimum $E(0)$ the expectation value for an observable f becomes

$$\langle f \rangle = f(0) + \frac{T}{2}\left(\frac{f''(0)}{E''(0)} - \frac{E^{(3)}(0)f'(0)}{[E''(0)]^2}\right) + \mathcal{O}(T^2) \tag{29}$$

The coefficients depend on the ground state configuration. For polyelectrolytes, in contrast to the proteins, the ground state is trivial and given by a straight line configuration. Furthermore the pure Coulomb chain is expected to be rod-like in the limit of large systems and consequently the low temperature expansion can be expected to work well.

4 The Papers

This section contains short introductions to the papers. Paper I is about a variational method for minimizing Lennard-Jones energies. Papers II, III, IV and VI are about the thermodynamics of the Coulomb and Debye-Hückel chains while papers V and VII deal with thermodynamics and folding properties of heteropolymer chains.

Paper I

A variational method, made for dealing with angular degrees of freedom "rotors", is used for minimizing Lennard-Jones energies. In this method the dynamic variables (D-dimensional unit vectors) are replaced by their mean-field counterparts which are defined inside the unit sphere. In the limit $T \to 0$ they go on-shell and can be identified with a low-energy configuration.

Two ensembles of Lennard-Jones energies are used, one dense packed and one based on the natural occurrence of amino acids. For the dense-packed problems the mean-field approach outperform the local, gradient descent methods, while the results are less significant for the "protein"-ensemble.

The method is also used to estimate the end-to-end distance for a rigid bond Coulomb chain at finite temperatures. For the unscreened chain surprisingly good results are obtained whereas it breaks down for the screened chains.

Paper II

In this paper variational calculations and Monte Carlo simulations are used to calculate structural and thermodynamical properties of a titrating polyelectrolyte. The variational ansatz consists of harmonic interactions between all pairs of monomers.

Excellent agreement with Monte Carlo data is obtained in the unscreened chain for the end-to-end distance and apparent dissociation constant. For the screened chain the structural properties are less well described while the thermodynamical quantities are described with the same accuracy as for the unscreened chain.

For the highly charged polyelectrolyte the chain is strongly elongated. In this case one can devise a simplified "rigid rod" ansatz with only two parameters, the monomer separation and the degree of dissociation. This approach gives a very good description of the titration behaviour for a highly charged system.

Paper III

A Monte Carlo method for computing thermodynamical properties of large polyelectrolytes is presented. In the spirit of the renormalization group the original polymer of size N is coarse-grained and mapped to a smaller system with N/Q monomers. This is done by using rescaled harmonic and Coulombic interactions and, as a consequence of the N-dependence of the short distance Coulomb cut-off, a corrective nearest-neighbour interaction. For the unscreened chains very large Q-values can be used. Emulating a chain of size $N = 2048$ with one of size $K = 50$ (corresponding to $Q \sim 40$) gives very good results with relative errors for the end-to-end distance less than four percent. For the screened case, the results are less accurate but since the computational gain of the method grows as Q^3 non-negligible savings still result.

Paper IV

The thermodynamics of a polyelectrolyte chain is considered. For the pure Coulomb chain at high temperatures there is an approximate scaling of global properties with chain length divided by temperature. At low temperatures this scaling is broken by the short distance divergence of the Coulomb potential. The scaling is restored by renormalizing the nearest neighbor interaction. This forms the basis of the blocking approach devised in paper III.

The situation is somewhat different for the screened chain due to the presence of a new length scale – the screening length. When this length is smaller than the chain size and simultaneously larger than the monomer-monomer separation scaling, *i.e.* dominating contributions from large length scales, are observed both for conformational and thermodynamical observables.

Paper V

In this paper a three dimensional off-lattice model for protein folding is presented. The model has two types of residues, hydrophobic and hydrophilic respectively, that interact via a sequence dependent Lennard-Jones potential. By including appropriate sequence independent local interactions local correlations qualitatively similar to those found in functional proteins were obtained. Furthermore the local interactions improved the thermodynamic stability. This in contrast to the behaviour with pure Lennard-Jones interactions where the folding properties were poor and fairly sequence independent.

By studying the temperature dependence of various thermodynamic and structural variables the formation of the native state can be understood as a gradual compaction followed by a sequence dependent folding transition. This is in agreement with what has been found in lattice model calculations. In a simplified two-state picture the two coexisting states at the folding temperature correspond to different energy distributions but, in contrast to what is observed for lattice models, the overlap is significant resulting in a unimodal energy distribution.

Paper VI

Monte Carlo methods and variational techniques are used to calculate the stiffness for some different polyelectrolyte chain models. The persistence length which characterizes the stiffness is a correlation length over which a polymer chain remembers its direction. The contributions to the total persistence length are usually partitioned into parts of electrostatic and non-electrostatic origin respectively.

When adding salt to a solution the electrostatic interactions, here represented by a Debye-Hückel potential, are screened out. Consequently the electrostatic persistence length $l_{p,e}$ becomes smaller. For the flexible model three regimes for the persistence length dependence of the screening length κ^{-1} are found. When the screening length is longer than the end-to-end distance $l_{p,e}$ varies only slowly with κ^{-1}. At intermediate salt concentrations $l_{p,e} \sim \kappa^{-1}$ which is in agreement with experimental data. For screening lengths much shorter than the bond length the decrease is faster. Variational calculations suggests a quadratic dependence.

For a sufficiently stiff chain the persistence length varies quadratically with κ^{-1}. This is in agreement with OSF-calculations and has been confirmed experimentally for intrinsically very stiff chains like DNA.

Paper VII

In this paper the folding properties of the model presented in paper V is further studied. The kinetic behaviour is examined in terms of the temporal dependence of the average mean-square displacement between configurations. At short time-scales the sequence dependence, at fixed temperature, is rather weak. This means that when studying the sequences at the same "physical" temperature, high thermodynamic stability implies fast kinetics.

In addition the degree of cooperativity in the folding process is investigated by studying the temperature dependence of the residual number of degrees of freedom contributing to the structural fluctuations. This is done by calculating the eigenvalues to the bond-bond correlation matrix. There is a gradual decrease in the effective number of degrees of freedom as the temperature is lowered. This can be interpreted as an increasing asymmetry of the energy landscape.

Acknowledgments

I would first of all like to thank my supervisor Carsten Peterson for generous guidance and support during these years. Furthermore I also want to thank Bo Söderberg and Anders Irbäck for helpful instructions on arbitrary relevant topics and of course my fellow graduate students and the remaining staff for making the department the nice place it is.

References

[1] P. G. deGennes "Scaling Concepts in Polymer Physics" (Cornell University Press, Ithaca, 1979).

[2] J. des Cloizeaux and G. Jannik "Polymers in Solution, Their Modelling and Structure" (Clarendon Press, Oxford, 1990).

[3] J.-L. Barrat and J. F. Joanny "Theory of Polyelectrolyte Solutions" *Adv. in Chem. Phys.* (1995)

[4] C. B. Anfinsen "Principles that Govern the Folding of Protein Chains" *Science* **181** 223 (1973).

[5] T. E. Creighton "Proteins, Structures and Molecular Properties" (W. H. Freeman and Co., New York, 1984).

[6] For a review, see M. Karplus and A. Šali, "Theoretical Studies of Protein Folding and Unfolding", *Curr. Opin. Struct. Biol.* **5**, 58 (1995).

[7] N.A. Metropolis, A.W. Rosenbluth, M.N. Rosenbluth, A. Teller and E. Teller, "Equation of State Calculations by Fast Computing Machines", *J. Chem. Phys.* **21**, 1087 (1953).

[8] M. Lal, "Monte Carlo Computer Simulations of Chain Molecules", *Molec. Phys.* **17**, 57 (1969).

[9] N. Madras and A. D. Sokal, "The Pivot Algorithm: a Highly Efficient Monte Carlo method for the Self-avoiding Walk", *J. Stat. Phys.* **50**, 109 (1988).

[10] E. Marinari and G. Parisi "Simulated Tempering: A New Monte Carlo Scheme", *Europhys. Lett.* **19**, 451 (1992).

Paper I

LU TP 94-4
August 1995

A Variational Approach for Minimizing Lennard-Jones Energies

Carsten Peterson[1], Ola Sommelius[2] and Bo Söderberg[3]

Department of Theoretical Physics, University of Lund
Sölvegatan 14A, S-223 62 Lund, Sweden

Physical Review **E 53**, 1723 (1996)

Abstract:

A variational method for computing conformational properties of molecules with Lennard-Jones potentials for the monomer-monomer interactions is presented. The approach is tailored to deal with angular degrees of freedom, *rotors*, and consists in the iterative solution of a set of deterministic equations with annealing in temperature. The singular short-distance behaviour of the Lennard-Jones potential is adiabatically switched on in order to obtain stable convergence.

As testbeds for the approach two distinct ensembles of molecules are used, characterized by a roughly dense-packed ore a more elongated ground state. For the latter, problems are generated from natural frequencies of occurrence of amino acids and phenomenologically determined potential parameters; they seem to represent less disorder than was previously assumed in synthetic protein studies.

For the dense-packed problems in particular, the variational algorithm clearly outperforms a gradient descent method in terms of minimal energies. Although it cannot compete with a careful simulating annealing algorithm, the variational approach requires only a tiny fraction of the computer time.

Issues and results when applying the method to polyelectrolytes at a finite temperature are also briefly discussed.

[1]carsten@thep.lu.se
[2]ola@thep.lu.se
[3]bs@thep.lu.se

1 Introduction

The determination of configurations of long molecular chains often is a difficult problem. For polyelectrolytes, consisting of identical charged monomers interacting with Coulomb repulsion forces, the ground state is trivial – the monomers form a straight line. The challenge here lies in predicting statistical quantities for finite temperature configurations; thus, the thermodynamics of the system is crucial. For proteins, modelled as a sequence of point-like amino acids interacting with effective pair potentials having local minima, the situation is somewhat different. Here the groundstate is nontrivial; the energy landscape is typically plagued with many local minima. This is the main difficulty here, while the finite temperature properties often are just considered as minor perturbations around the ground state.

Optimization problems with many local minima as in the the protein case are notoriously difficult, and elaborate methods to search the phase space efficiently have been devised. One such method is Simulated Annealing (**SA**) [1], where noise is introduced to emulate a Boltzmann distribution; this enables the system to escape from local minima. Unfortunately, this procedure is quite CPU demanding. The formal temperature in such an approach is merely an artificial parameter; it need not be identified with the physical temperature of the system.

For some optimization problems it has turned out profitable to abandon stochastic methods like SA in favour of deterministic approaches based on the iterative solution of equations originating from a variational scheme. Successful results with such approaches were reported for combinatorial optimization problems that can be mapped onto spin systems [2, 3].

Variational methods have recently also been used to compute configurational properties of polyelectrolytes. In refs. [4, 5], harmonic trial potentials were used with widths and positions as variational parameters. This approach works well as long as the potentials to be approximated have a milder divergence than $1/r^3$. In the Coulomb case (screened or unscreened), which was treated in refs. [4, 5], this requirement is fulfilled. However, for the strongly diverging ($1/r^{12}$) Lennard-Jones (**LJ**) potential, occuring in protein models, a harmonic Ansatz will lead to divergent integrals, as will indeed any smooth Ansatz.

This problem could be overcome in two different ways: In principle, one could use a modified Ansatz for the trial potential, that leads to finite integrals. However, this is difficult to achieve while maintaining the computational simplicity needed for a competitive algorithm. Alternatively, one could keep the harmonic Ansatz, and instead modify the LJ-potential to make it less singular.

The approach of refs [4, 5] applies only to molecules with flexible bonds, however; in this paper we will consider a slightly simplified model with *rigid bonds*, and the dynamics hence limited to the angular degrees of freedom. This

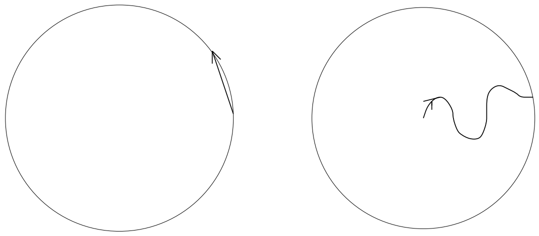

Figure 1: **(a)**. Elementary moves on the unit sphere. **(b)**. Evolution of a MF rotor initialized close to the center, for $T < T_c$.

simplification is motivated by the assumption that the flexibility of bonds is of minor importance for obtaining an accurate spatial structure. Indeed, several calculations using real chains of amino acids focus entirely on the angular degrees of freedom [6].

Thus, we are facing a minimization problem in terms of an energy-function of angular variables. These will be represented by a set of unit vectors, **rotors**, which can be seen as continuous generalizations of discrete Ising spins. In algorithms like gradient descent (**GD**) and SA elementary moves are made with the rotors *on-shell*, ie. restricted to the unit sphere (see fig. 1a).

In ref. [10] the variational mean-field approach, commonly used for discrete spin-systems, was generalized by introducing *mean field rotors*; these can explore the interior of the sphere and can be interpreted as thermal averages of on-shell rotors. The method was successfully explored on the minimal energy problem for charges on a sphere. The corresponding mean field equations are iteratively solved as the temperature T is lowered. Above a critical temperature T_c the system relaxes to a fixed point with all rotors at the center of the sphere. As the temperature is lowered the rotors approach the "shell" (see fig. 1b). Thus, in the variational approach, rather than fully or partly exploring the configuration space, the variables "feel" their ways off-shell in a fuzzy manner towards good on-shell solutions.

The main purpose of this paper is to apply a similar technique to proteins, modelled as a chain of monomers connected by rigid bonds and interacting via LJ-potentials, with the aim of finding the ground state.

Any updating algorithm faces problems with the steepness of the LJ-potential at short distances. We have developed an adiabatic regularization procedure that efficiently handles the short-distance problem, which is useful for any method, not just the variational rotor approach.

Computational simplicity is gained, at the price of sacrificing uniqueness and physical interpretability at non-zero T, by approximating expectation values according to

$$\langle E(\cdot)\rangle \rightarrow E(\langle\cdot\rangle) \tag{1}$$

The resulting algorithm is shown to yield a GD algorithm in the $T \rightarrow 0$ limit.

As LJ-potential testbeds we do not consider real-world proteins. For the purpose of algorithmic development and studies it suffices to study synthetic systems. We have chosen to study two extremes, by considering systems with a dense-packed or elongated ground state, respectively. The latter were generated from empirical independent amino-acid probabilities and phenomenologically determined pairwise forces. As a by-product, it turns out that the resulting LJ-parameters give rise to far less disordered systems than has been assumed in some recent generic investigations of spectra and stability issues [8, 9].

For these testbeds the variational rotor approach is explored for problem sizes N ranging from 10 to 40. For the dense-packed model the variational approach compares favourably with GD with respect to reaching low energy states, while for the elongated model the corresponding gain is smaller. For both models the CPU time consumption is much lower than for SA.

For completeness, we apply the variational rotor approach also to a polyelectrolyte (Coulomb) problem at $T \neq 0$, and discuss the limitations of the approach here.

This paper is organized as follows. In Sect. 2 the variational (mean field) formalism is derived. The generation of synthetic proteins and their LJ-potential couplings are discussed in Sect. 3. The regularization of the LJ-potential is treated in Sect. 4. In Sect. 5 we present the numerical procedures and results for the LJ-potential, and Sect. 6 contains the polyelectrolyte application. A brief summary and outlook can be found in Sect. 7.

2 The Variational Approach

2.1 Proper Variational Approach

Limiting ourselves to angular degrees of freedom, we consider an energy function

$$E = E(\mathbf{s}_1, \ldots, \mathbf{s}_N) \tag{2}$$

to be minimized w.r.t. the directions of a set of N distinct D-dimensional unit vectors $\mathbf{s}_i$ (*rotors*)

$$|\mathbf{s}_i| = 1 \ . \tag{3}$$

In instances where the energy landscape contains many local minima, one would typically employ a stochastic technique like SA. In [10] a *mean field* method was developed and numerically explored for the problem of placing charges on a sphere. We will here generalize this technique, and apply it to the case of a protein model with LJ pair-potentials.

For spin systems the mean field approximation can be derived in (at least) three conceptionally distinct ways; from a *variational principle*, from a *saddlepoint approximation*, or using an *intuitive physical argument.* We will here briefly discuss the variational derivation; for the saddle-point approach we refer the reader to e.g. ref. [10].

The variational approach is based on an effective energy Ansatz, E_V, which is linear in the spins $\mathbf{s}_i$,

$$E_V(\mathbf{s}_1, \ldots, \mathbf{s}_N) = -\sum_i \mathbf{u}_i \cdot \mathbf{s}_i \tag{4}$$

where the (real, unconstrained) coefficient vectors $\mathbf{u}_i$ are to be considered as *variational parameters.*

Based on the corresponding Boltzmann distribution ($\propto \exp(-E_V/T)$), a free energy, F_V, can be defined,

$$F_V(\mathbf{u}_1, \ldots, \mathbf{u}_N) = \langle E \rangle_V - ST, \tag{5}$$

where S is the entropy. F_V is bounded from below by the true equilibrium free energy, F, based on the proper Boltzmann distribution $\propto \exp(-E/T)$.

The variational free energy F_V can be written as

$$F_V = -T \log Z_V + \langle E - E_V \rangle_V \tag{6}$$

where Z_V is the variational partition function, while $\langle\rangle_V$ refers to averages w.r.t. the variational Boltzmann distribution. By minimizing F_V with respect to the parameters $\mathbf{u}_i$, the variational equations result. These are best expressed in terms of the *mean fields*

$$\mathbf{v}_i = \langle \mathbf{s}_i \rangle_V \tag{7}$$

which approximate the exact averages $\langle \mathbf{s}_i \rangle$. The mean fields are simple functions of the coefficients $\mathbf{u}_i$,

$$\mathbf{v}_i = \frac{\mathbf{u}_i}{|\mathbf{u}_i|} g\left(|\mathbf{u}_i|/T\right) = \mathbf{g}\left(\mathbf{u}_i/T\right) \tag{8}$$

where for the case of three dimensions g is given by $g(x) = \coth(x) - 1/x$; its graph is shown in fig. 2. Note that $g(0) = 0$, and that $g(x) \to 1$, when $x \to \infty$; this generic qualitative behaviour holds for any number of dimensions, and implies in particular that as $T \to 0$ the MF rotors $\{\mathbf{v}_i\}$ go on-shell, and can be identified with a low-energy configuration $\{\mathbf{s}_i\}$.

The variation of the entropy term ST yields

$$d(ST) = -\sum_i \mathbf{u}_i d\mathbf{v}_i \tag{9}$$

and we obtain the variational equations in the form

$$\mathbf{v}_i = \mathbf{g}\left(-\nabla_{\mathbf{v}_i} \langle E \rangle_V / T\right) \tag{10}$$

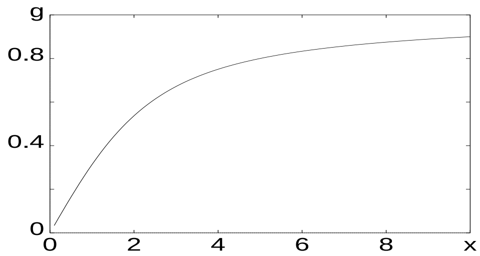

Figure 2: The function $g(x)$ for the case of three dimensions.

2.2 Modified Variational Approach

For a strongly singular potential, like LJ, things are complicated by the fact that $\langle E \rangle_V$ is a diverging integral. In other cases, the corresponding integral may be convergent, but difficult to evaluate. These difficulties can be remedied by making the apparently crude replacement

$$\langle E(\mathbf{s}_1, \ldots, \mathbf{s}_N) \rangle_V \rightarrow E(\langle \mathbf{s}_1 \rangle_V, \ldots, \langle \mathbf{s}_N \rangle_V) = E(\mathbf{v}_1, \ldots, \mathbf{v}_N) \tag{11}$$

in the expression for F_V. This is justified as long as we are only interested in the groundstate, which dominates for $T \rightarrow 0$ where the fluctuations vanish and the above approximation becomes exact. For a finite T, the replacement in eq. (11) is more questionable, and its use must be justified by other means.

Minimization of the thus modified F_V with respect to the trial parameters $\mathbf{u}_i$ (or $\mathbf{v}_i$) yields a modified set of equations:

$$\mathbf{v}_i = \mathbf{g}\left(-\nabla_i E(\mathbf{v}_1, \ldots, \mathbf{v}_N)/T\right) \tag{12}$$

In principle, these could be iterated to find a (local) minimum of F_V.

However, a question of uniqueness arises: since E really is defined only on-shell, i.e. for $|\mathbf{s}_i| = 1$, off-shell values are not uniquely defined. By adding eg. a term $\propto \mathbf{v}_i^2 - 1$ which is zero on-shell, we can alter the off-shell behaviour of E, and hence the solutions to eq. (12). Thus, these make sense only in the $T \rightarrow 0$ limit, where the $\mathbf{v}_i$ are forced on-shell, due to the asymptotic behaviour of $g()$.

Another problem is a possible lack of stability of the iterative dynamics of eq. (12). This can be remedied by formally adding a stabilizing term to the energy of the form $-\beta/2 \sum_i \mathbf{v}_i^2$, which is just a constant on-shell.

We then obtain a modified set of variational equations:

$$\mathbf{u}_i = \beta \mathbf{v}_i - \nabla_i E(\mathbf{v}_1, \ldots, \mathbf{v}_N) \tag{13}$$

$$\mathbf{v}_i = \mathbf{g}\left(\frac{\mathbf{u}_i}{T}\right) \tag{14}$$

to be iterated. For $T \to 0$ this turns into a kind of an (on-shell) gradient descent with β corresponding to a reciprocal step size. This of course could have been obtained in a much simpler way. However, we aim at an annealing approach: start iterating with a high T, for which the modified F_V typically is minimized by a fixpoint with $\mathbf{v}_i \approx 0$. Then keep iterating while slowly letting $T \to 0$. The value of β should be chosen to stabilize the iterative dynamics. The idea is that with the soft high T dynamics, the $\mathbf{v}_i$ are allowed to short-cut through an interpolating (off-shell) space. As T slowly falls to zero, the $\mathbf{v}_i$ are eventually forced on-shell, and finally a local minimum of the on-shell energy function $E(\mathbf{s}_i)$ crystallizes out. This way, one can hope to obtain better minima then by just using gradient descent.

3 The Lennard-Jones Potential

In models of proteins one often uses a potential between the individual atoms consisting in a sum of "bonded" interactions and "non-bonded" ones. The latter consist of Coulomb and LJ interactions between all the atoms.

It has been argued [12] that a reasonable simplification results from considering the amino acids as *effective monomers*, interacting via *effective potentials*. We will focus on effective LJ potentials. Crucial physical properties like hydrophobicity then are efficiently incorporated by a suitable choice of LJ parameters.

The LJ potential between two monomers k and l is given by

$$V_{kl}(r) = \frac{R_{kl}}{r^{12}} - \frac{A_{kl}}{r^6} \tag{15}$$

An example is shown in fig. 3. It is short-range, and has a very strong (and unphysical) short-distance repulsion. If $A_{kl} > 0$ it has a local minimum located at

$$r_{kl}^0 = \left(\frac{2R_{kl}}{A_{kl}}\right)^{1/6} \tag{16}$$

The energy to be minimized is given by the sum of all pair-potentials

$$E = \sum_{kl} V_{kl}(r_{kl}) \tag{17}$$

3.1 Regularizing the $\mathbf{r} \to 0$ Behaviour

The very steep short-distance behaviour of the LJ-potential might cause problems for updating in minimization algorithms – not only for our variational approach but also for e.g. some Monte Carlo (**MC**) algorithms. A convenient

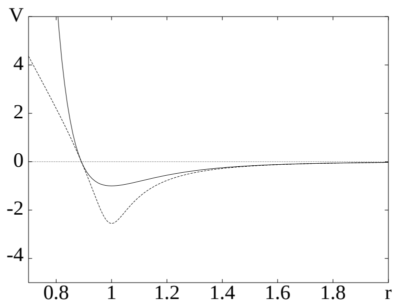

Figure 3: The Lennard-Jones potential (eq. (15)) and a regularized version (eq. (18)) as full and dashed lines, respectively (R=1; A=2).

way of controlling the short-distance singularity is by using a modified potential (see fig. 3)

$$\tilde{V}_{kl}(r) = V_{kl}^0 + \frac{1}{\gamma}\log\left(1 + \gamma(V_{kl}(r) - V_{kl}^0)\right) \tag{18}$$

where V_{kl}^0 is the minimum value of $V_{kl}(r)$. The modified potential only has a logarithmic singularity at the origin, and yields the same result in the limit $\gamma \to 0$ as V. Furthermore, the position of the minimum is preserved for all values of γ. The idea is to start with $\gamma > 0$ and then gradually decrease γ to 0. In minimization schemes of annealing type, where noise is introduced via a temperature T, the decrease in γ should be coupled to the annealing in T (see Sect. 4).

3.2 Coupling Distributions

We choose the LJ parameters R_{kl} and A_{kl} in two different ways; (A) identical values for all monomers, corresponding to dense packing, and (B) using empirical couplings for a random sequence of aminoacids, based on empirical frequencies of occurrence:

A For all pairs, set $R_{kl} = 1$ and $A_{kl} = 2$, leading to $r_{kl}^0 = 1$. This choice implies an approximately dense-packed ground state.

B Choose R_{kl} and A_{kl} in a phenomenological way as follows. Generate a random sequence of amino-acids according to the known frequencies of occurrence in proteins [13]. The various values for R_{kl} and A_{kl} are derived from the empirical effective LJ couplings given in [12]. The resulting A_{kl} distribution is shown in fig. 4. We note that while this distribution exhibits quite some width, it is far from being as dramatic as in the toy models proposed in refs. [8, 9], where $R_{kl} = 1$ and $A_{kl} = 3.8 + 6.0\,\mathtt{rand}[0, 1]$ were used.

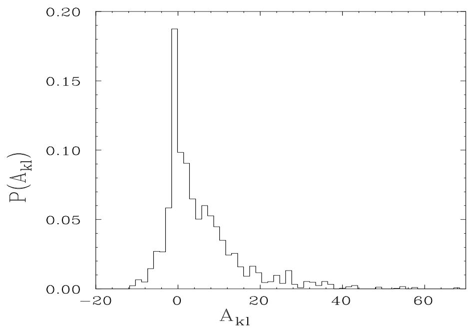

Figure 4: Distribution of A_{kl} according to option **B**.

4 The Variational Rotor Algorithm

We next briefly describe how we implement eqs. (13,14) for the regularized LJ-potential, eqs. (15,18). The non-uniqueness due to eq. (11), and the existence of unique pairwise local minima r^0_{kl} in eq. (16), suggests a modified distance expression:

$$\tilde{r}^2_{kl} = \left(\sum_{i \in \sigma(kl)} \mathbf{v}_i \right)^2 + \frac{\left(r^0_{kl}\right)^2}{|k-l|} \sum_{i \in \sigma(kl)} \left(1 - \mathbf{v}^2_i\right) \tag{19}$$

where $\sigma(kl)$ denotes the set of bonds connecting monomers k and l. To avoid instability in the dynamics, r^0_{kl} is maximized to $\sqrt{|l-k|}$; this value is also used for a negative A_{kl}. On-shell, this yields the correct distance, while at the beginning of the simulation when $\mathbf{v}_i = 0$, most pairs are formally at their distance of minimum energy. The regulator γ is chosen to depend on R_{kl} as

$$\gamma_{kl} = \frac{4\hat{\gamma}}{R_{kl}} \tag{20}$$

where $\hat{\gamma}$ is the same for all pairs; this leads to correct relative normalization of the regularized potentials at short distances.

The resulting variational equations (13,14) read

$$\mathbf{u}_i = \beta \mathbf{v}_i + 6 \sum_{\sigma \ni i} \frac{\left(2R_\sigma - A_\sigma \tilde{r}^6_\sigma\right)\left(\sum_{j \in \sigma} \mathbf{v}_j - \frac{\left(r^0_\sigma\right)^2}{|k-l|}\mathbf{v}_i\right)}{\tilde{r}^2_\sigma \left(\tilde{r}^{12}_\sigma + \hat{\gamma}\left(2 - \frac{A_\sigma}{R_\sigma}\tilde{r}^6_\sigma\right)^2\right)} \tag{21}$$

$$\mathbf{v}_i = \mathbf{g}(\mathbf{u}_i / T) \tag{22}$$

where σ denotes a connected subset of the bonds, that includes bond i.

The variational algorithm then takes the following form:

1. Initialize:

   1.1 Set $T{=}T_0$ and $\hat{\gamma}{=}\hat{\gamma}_0$.

   1.2 Initialize $\mathbf{v}_i$ to small ($\sim .01$) random vectors.

2. Repeat until $\frac{1}{N-1}\sum \mathbf{v}_i^2 > 0.99999$:

   2.1 Update all $\mathbf{v}_i$'s according to eqs. (21) and (22).

   2.2 Anneal: $T = k_T T; \hat{\gamma} = k_\gamma \hat{\gamma}$

The choice of parameter values are shown in table 1; for the stabilizer β the choice is motivated by the empirical observation that the β-values required for high quality solutions scale linearly with N. In the gradient descent limit, where $T = 0$ and the rotors are on-shell, $\mathbf{v}_i = \mathbf{u}_i/|\mathbf{u}_i|$, β plays the role of an inverse step length.

	β	$\hat{\gamma}_0$	k_γ	T_0	k_T
dense	$25N$	0.5	0.99	$\beta/3$	0.995
real	$100N$	0.5	0.99	$\beta/3$	0.995

Table 1: Parameter settings for the variational algorithm (the first three apply also to GD).

5 Numerical Results for the LJ-Potential

We have compared the performance of the variational rotor algorithm to that of (i) a GD algorithm and (ii) a SA method – both for the model A, in which the final structure will be close to a dense-packed configuration, and for the phenomenological model B. The GD method was chosen as the $T = 0$ limit of the variational algorithm, with identical parameter settings for β, $\hat{\gamma}_0$ and k_γ (cf. Table 1); thus, the regularized LJ potentials were used also here. The SA simulations were made using Metropolis updating, with an initial temperature T_0 given by three times the modulus of the lowest energy achieved by the variational method in case A (for simplicity, the same T_0 was used also for the B problems of the same size). With an annealing rate per sweep of $k_T = 0.99999$, approximately $2.5 \cdot 10^6$ sweeps were required, with a sweep defined by N attempted single-rotor updates.

	CPU-time		
	N = 10	20	40
GD	12	70	700
Var.	15	120	1500
MC	4000	25000	200000

Table 2: Approximate CPU consumption for model B in seconds on a DEC Alpha workstation for the different approaches. Similar numbers hold for model A.

These choices of parameters and number of sweeps were based on reasonable trade-offs between solution quality and consumption of CPU time. The reference values for the ground-state energies thus obtained by SA, at the price of very high CPU consumption (see table 2), are not frequently equalled by the energies obtained using the two deterministic approaches.

However, when performing multiple runs with the variational approach using different seeds one do hit solutions comparable with those of SA. Hence the overall advantage taking CPU time consumption into account is very likely be in favour of the variational approach.

In model A (dense-packed) the variational algorithm clearly outperforms the GD one (see table 3). However, for the slightly more realistic model B

	N	$\langle E_{GD} - E_{var} \rangle$	$\pm$	$\langle E_{var} \rangle - E_{SA}$	$\pm$	# probl.	# runs	# sweeps	
								Var.	GD
A	10	0.8	0.1	1.0	0.1	1	100	2200	550
	20	3.0	0.4	4.8	0.2	1	100	2300	1300
	40	7.7	0.8	6.4	0.3	1	100	3000	4400
B	10	0.6	0.5	6.0	0.9	10	10	4100	3800
	20	2.3	1.2	14.9	1.8	10	10	9200	10400
	40	9.1	4.3	59.7	6.1	5	10	16100	15300

Table 3: Average performance differences. The number of runs refers to the variational and GD approaches. For each problem a single run was performed with SA.

the two approaches seem comparable. A possible explanation for this is that the main advantage of the variational approach is the extra degrees of freedom since the rotors can go off-shell; this facilitates the escape from local minima, which probably is more important in the dense packed case.

6 Polyelectrolytes

In this section we briefly discuss how the variational rotor approach can be applied to the case of a polyelectrolyte at a finite temperature. Theoretically, the approach suffers from a certain arbitrariness, but it gives quite good results for the case of unscreened Coulomb forces.

The interaction energy for a polyelectrolyte consisting of N monomers with Coulombic repulsion forces is given by

$$E = \sum_{kl} \frac{1}{r_{kl}} \tag{23}$$

The variational average $\langle E \rangle_V$ is then perfectly convergent. It is however difficult to evaluate, and we will for that reason also here employ the simplifying trick of eq. (11). In this case, the resulting non-uniqueness is used to replace $\mathbf{v}_i^2$ by 1 everywhere; thus, r_{kl} will evaluate to

$$r_{kl} = \sqrt{|k-l| + \sum_{i \neq j} \mathbf{v}_i \cdot \mathbf{v}_j} \tag{24}$$

where i, j are restricted to the set of bonds linking monomers k and l.

Then it is not a priori clear to what degree the results will make sense for a finite T. However, the replacement $\mathbf{v}_i^2 \to 1$ gives the correct result for $\langle r_{kl}^2 \rangle_V$, and we argue that it should be a fair approximation also for $\langle 1/r_{kl} \rangle_V$ — it is certainly correct for $T \to 0$ ($|\mathbf{v}_i| \to 1$), and qualitatively correct for large N when $T \to \infty$ ($\mathbf{v}_i \to 0$).

Thus armed with some confidence, we have used this approach to generate configurations in terms of $\{\mathbf{v}_i\}$ for polyelectrolytes ranging in size from 20 to 1024, by iterating equations analogous to eqs. (21,22). We have chosen to characterize the configurations by their r.m.s. end-to-end distance r_{ee}, which in the variational approach is given by

$$r_{ee}^2 = (N-1) + \sum_{i \neq j} \mathbf{v}_i \cdot \mathbf{v}_j \tag{25}$$

As can be seen from table 4, the results are in surprisingly good agreement with Monte Carlo (**MC**) data.

We have also attempted a similar comparison for polymers with a screened Coulomb interaction. The results in that case are not nearly as good as in the unscreened case, and it is not difficult to see why. With screening, the interaction turns short-range, and for large molecules, essentially all the rotors will be identical in size and direction, $\mathbf{v}_i = \mathbf{v}$, with v independent of N. Thus, we get for the end-to-end distance

$$r_{ee}^2 \approx (N-1) + \frac{(N-1)(N-2)}{2} \mathbf{v}^2 \tag{26}$$

N	Var.	MC	% dev
20	11.53	12.06	-4.6
40	26.80	26.43	1.3
80	59.05	57.07	3.5
160	125.8	122.1	3.0
256	207.6	202.5	2.5
512	429.5	422.0	1.4
1024	880.3	870.2	1.1

Table 4: End-to-end distance r_{ee} for polyelectrolytes. Comparison of variational results with MC data for different N for $T = 0.837808$ (room temperature). The last column lists relative deviations between the variational method and MC results in percentage. The errors in the MC data are approximately 0.1 %.

which goes like N^2 (unless $\mathbf{v} = 0$, which happens for high enough T). Thus, r_{ee} will scale like N, which is clearly unphysical for a short range potential. This failure is probably more due to the linear Ansatz for E_V being unsuitable for this problem, and not so much to the crudeness of the additional approximation of eq. (11).

7 Summary

We have developed a variational approach for finding approximate energy minima for proteins modelled by polymers with Lennard-Jones pair interactions between pointlike monomers. It has been numerically explored for two cases — dense-packed systems and more elongated ones.

In the latter case, phenomenological pair potentials were used with random amino-acid sequences based on natural frequencies of occurrence. This leads to effective coupling distributions far more narrow than those commonly assumed in generic investigations of spectra and stability issues [9, 8].

For dense-packed systems the variational performance compares favourably with a gradient descent method with respect to solution quality, whereas for the more elongated ones the gain is very small. We interpret this difference as being due to the fact that the elongated chain provides less of an optimization challenge as compared to the dense packed ones. Hence there is a less pronounced difference between the methods.

The deterministic variational method fails to find in a consistent way the low energy states produced by a stochastic simulated annealing algorithm when used in a single run mode. However, since simulated annealing requires a factor

$100 - 200$ more in CPU consumption multiple runs with the variational method are relatively efficient.

As a by-product we have devised a regularization of the Lennard-Jones potential, where the short-distance steepness is gradually turned on in the updating process, thereby avoiding ill-behaved dynamics. Most deterministic (and some stochastic) methods will benefit from such a regularization.

The variational method has been applied also to the case of polyelectrolytes at non-zero temperature, where the procedure is somewhat more ambiguous. For the case of unscreened repulsions the method yields good results as judged by MC, whereas it breaks down for the screened case.

Acknowledgements

We thank Anders Irbäck for aiding us with the choice of Lennard-Jones couplings and Bo Jönsson for providing us with polyelectrolyte MC data.

References

[1] S. Kirkpatrick, C.D. Gelatt and M.P. Vecchi, "Optimization by Simulated Annealing", *Science* **220**, 671 (1983).

[2] C. Peterson and B. Söderberg, *International Journal of Neural Systems* **1**, 3 (1989).

[3] C. Peterson, *Neural Computation* **2**, 261 (1990);
M. Ohlsson, C. Peterson and B. Söderberg, *Neural Computation* **5**, 331 (1993);
L. Gislen, B. Söderberg and C. Peterson, *Neural Computation* **4**, 805 (1992).

[4] B. Jönsson, C. Peterson and B. Söderberg, *Physical Review Letters* **71**, 376 (1993).

[5] B. Jönsson, C. Peterson and B. Söderberg, *LU TP 93-15* (to appear in *Journal of Physical Chemistry*).

[6] H. Kawai,T. Kikushi Y. Okamoto, *Protein Engineering* **3**, 85 (1989).

[7] Y. Okamoto, M. Fukugita, T. Nakasawa and H. Kawai, *Protein Engineering* **4**, 639 (1991).

[8] M. Fukugita, D. Lancaster and M.G. Mitchard, *Journal of Physics* **A25**, L121 (1992).

[9] G. Iori, E. Marinari and G. Parisi, *Journal of Physics* **A24**, 5349 (1991).

[10] L. Gislen, C. Peterson and B. Söderberg, *Neural Computation* **4**, 737 (1992).

[11] R.P. Feynman, *Statistical Mechanics, Frontiers in Physics*, Reading, Ma: Benjamin (1972).

[12] A. Wallquist and M. Ullner, *Proteins*, **18**, 267 (1994).

[13] T.E. Chreighton, *Proteins – Structures and Molecular Principles*, W.H. Freeman (New York 1984).

Paper II

LU TP 95-1
May 1995

Titrating Polyelectrolytes – Variational Calculations and Monte Carlo Simulations

Bo Jönsson[1] and Magnus Ullner[2]
Physical Chemistry 2, Chemical Center, University of Lund
Box 124, S-221 00 Lund, Sweden

Carsten Peterson[3], Ola Sommelius[4] and Bo Söderberg[5]
Department of Theoretical Physics, University of Lund
Sölvegatan 14A, S-223 62 Lund, Sweden

Journal of Physical Chemistry **100**, 409 (1996)

Abstract:
Variational methods are used to calculate structural and thermodynamical properties of a titrating polyelectrolyte in a discrete representation. In the variational treatment, the Coulomb potentials are emulated by harmonic repulsive forces between *all* monomers; the force constants are used as variational parameters. The accuracy of the variational approach is tested against Monte Carlo data. Excellent agreement is obtained for the end-to-end separation and the apparent dissociation constant for the unscreened Coulomb chain. The short-range screened Coulomb potential is more difficult to handle variationally and its structural features are less well described, although the thermodynamic properties are predicted with the same accuracy as for the unscreened chain. The number of variational parameters is of the order of N^2, where N is of the number of monomers, and the computational effort scales like N^3. In addition, a simplified variational procedure with only two parameters is pursued, based on a rigid-rod approximation of the polymer. It gives surprisingly good accuracy for certain physical properties.

[1] fk2boj@grosz.fkem2.lth.se
[2] fk2mul@dix.fkem2.lth.se
[3] carsten@thep.lu.se
[4] ola@thep.lu.se
[5] bs@thep.lu.se

1 Introduction

With increasing computer resources and refined algorithms it has now become possible to investigate structural and thermodynamic properties of polymer chains with several thousand monomeric units using simulation techniques. In particular, charged polymers have recently received an increased interest and a number of simulation studies have appeared in the literature [1, 2, 3, 4, 5, 6, 7, 8]. Most polyelectrolytes will under normal solution conditions exhibit an acid-base equilibrium, i.e. titratable groups in a polymer will exchange protons with the solution and the polymer net charge will vary as a function of the solution pH. This extra degree of freedom makes polyelectrolytes particularly versatile in many technical and biological applications [9, 10, 11, 12, 13, 14, 15]. In simulations, this phenomenon can be described by coupling the polyelectrolyte to an external proton bath of fixed chemical potential or pH; such grand canonical Monte Carlo simulations have been performed by several groups [16, 17, 18, 19].

Many polyelectrolytes undergo a dramatic structural change upon a successive ionization, i.e. the Coulombic repulsion between charged monomeric units forces the chain to adopt more extended conformations. This is particularly dramatic at low polymer and salt concentration. Sometimes the Coulombic repulsion is counteracted by attractive interactions leading to a helix-coil transition as a function of pH [20, 21, 22, 23]. In hydrophobically modified polyelectrolytes the attractive interactions tend to dominate and rather modest structural changes are seen upon ionization. Proteins are a special class of polyelectrolytes, which, although they may denature, still show rather small structural changes when going from the isoelectric point to either high or low pH. The competition between electrostatic monomer-monomer repulsion and specific attractive interactions has also been studied with simulation techniques [24, 17].

So far most polyelectrolyte studies have focussed on the behaviour of a single chain at infinite dilution. Additional salt has been introduced in an approximate way via screened Coulomb interactions. Finite polymer concentration and explicit salt particles impose considerable constraints on the chain lengths to be handled. A few studies, however, of non-titrating polyelectrolytes with explicit salt particles have been presented, but then only for fairly short chains [4, 25, 26, 27, 28]. Simulations with finite polymer concentration have also been carried through, but such studies are at present only feasible for a limited chain length [27, 28]. In this paper the accuracy of less computer demanding non-stochastic approaches are investigated using Monte Carlo simulations.

A number of approximate models for titrating polyelectrolytes have been suggested focusing on different phenomena and applying tools of varying mathematical sophistication. Existing theories, however, are seldom based on models that incorporate both a fully flexible chain and a discrete representation of the monomers. Here we suggest a variational approach, which has given excellent results for non-titrating polyelectrolytes [29, 30], based on a discrete representation of the polymer chain. That is, each monomeric unit is connected to its neighbours with a harmonic bond and may carry a unit charge depending on the solution pH. We apply the variational technique to a linear chain although the method is perfectly general and can be applied to any chain topology. The variational solution to the titrating chain is obtained for different chain lengths and salt concentrations and the results are compared to results obtained via Monte Carlo simulations.

The full variational solution is obtained at a much lower computational effort than what is required by simulations. As a further advantage it also provides the chain free energy. Still, the numerical procedure leading to the variational result is non-trivial, and we have also developed a simpler, but of course less accurate, variational scheme based on only two variational parameters.

This paper is organized as follows. In Sect. 2 we describe the details of the model we use for the titrating polymer. The variational technique of refs. [29, 30] is briefly reviewed in Sect. 3 together with some new numerical results for large N for non-titrating chains. In Sect. 4 the variational formalism is generalized to titrating chains, while the details of the Monte Carlo calculations can be found in Sect. 5. Sect. 6 contains the corresponding comparisons between Monte Carlo and variational results for chains in a salt-free environment as well as in salt solutions. Finally a brief summary and our conclusions can be found in Sect. 7.

2 The Model

The polyelectrolyte is regarded as an infinitely diluted polyacid in aqueous solution. The monomers form a linear chain where each monomer represents a titrating site that can be either protonated or deprotonated, i.e. be uncharged or carry one unit of negative charge. The chain is freely jointed, with neighbouring monomers connected by harmonic bonds. The implicit assumption is that the part of the underlying neutral polymer backbone that separates the neighbouring charged groups obeys a Gaussian distribution for its end-to-end separation. This is a reasonable approach for a chain where the separation of neighbouring charges is much larger than the persistence length of the underlying neutral chain.

The solvent is treated as a dielectric continuum with a permittivity equal to that of water at room temperature. It also acts as a proton reservoir via a chemical potential given by

$$\tilde{\mu} = k_B \tilde{T} \ln 10 \, (pK_0 - pH) \tag{1}$$

where pH is that of the bulk, and pK_0 is the intrinsic pK_a of a monomer. In the case of a salt solution, an additional effect of the solvent is a Debye-Hückel screening of the electrostatic interactions between all charged monomers, and the total interaction energy for N monomers becomes

$$\tilde{E} = \tilde{E}_G + \tilde{E}_C + \tilde{E}_\mu = \frac{k}{2}\sum_{i \neq N} |\tilde{\mathbf{x}}_{i,i+1}|^2 + \frac{e^2}{4\pi\epsilon_r\epsilon_0}\sum_i \sum_{j>i} \frac{Z_i Z_j exp(-\tilde{\kappa}|\tilde{\mathbf{x}}_{ij}|)}{|\tilde{\mathbf{x}}_{ij}|} - \tilde{\mu}\sum_i Z_i \tag{2}$$

where $\tilde{\mathbf{x}}_{ij}$ is the distance between monomer i and j, e is the electronic charge, ϵ_r is the dielectric constant of the solution (78.3 in all simulations), ϵ_0 is the permittivity of vacuum and Z_i the amount of charge on monomer i (either 0 or -1). We use the tilde notation $\tilde{E}$, $\tilde{\mathbf{x}}_i$, etc. for physical quantities in conventional units, and reserve E, $\mathbf{x}_i$, etc. for dimensionless ones, which will be used in the variational formalism below. The force constant, k, is implicitly given through the input parameter $\tilde{r}_0 = (e^2/4\pi\epsilon_r\epsilon_0 k)^{1/3}$, which is the equilibrium distance for a fully charged dimer and it is set to 6 Å in all calculations. In the case of a $1:-1$ salt $\tilde{\kappa}$ is given by $\tilde{\kappa} = (2e^2 c_s/\epsilon_r\epsilon_0 N_A k_B \tilde{T})^{1/2}$, where c_s is the salt concentration (in mM), k_B is the Boltzmann constant, N_A is the Avogadro number and $\tilde{T}$ is the temperature.

2.1 Dimensionless Formulation with Relative Coordinates

Using dimensionless coordinates $\mathbf{x}_i$, given by $\tilde{\mathbf{x}}_i = r_0\mathbf{x}_i$, we may define a rescaled temperature T,

$$T = \frac{k_B\tilde{T}}{kr_0^2} \tag{3}$$

and a likewise rescaled chemical potential μ,

$$\mu = \frac{\tilde{\mu}}{kr_0^2} \tag{4}$$

The negative exponent of the Boltzmann factor can then be written as

$$\frac{\tilde{E}}{k_B\tilde{T}} = \frac{E}{T} \tag{5}$$

with the rescaled energy given by

$$E = \frac{1}{2}\sum_i |\mathbf{x}_{i,i+1}|^2 + \sum_{i<j} \frac{s_i s_j e^{-\kappa|\mathbf{x}_{ij}|}}{|\mathbf{x}_{ij}|} + \mu\sum_i s_i \tag{6}$$

where we have replaced Z_i by more convenient $\{0,1\}$ variables $s_i = -Z_i$.

In what follows, relative coordinates will mostly be used; instead of the absolute monomer positions $\mathbf{x}_i$, the *bond vectors* $\mathbf{r}_i$,

$$\mathbf{r}_i \equiv \mathbf{x}_{i+1} - \mathbf{x}_i, \quad i = 1, \ldots, N-1 \tag{7}$$

will be considered the fundamental variables. In this way complications due to the translational zero-modes are avoided; in addition, the convergence of the variational algorithm to be described below becomes considerably faster, especially at high temperatures. The energy of the chain then takes the form

$$E(\mathbf{r}, s) = E_G + E_C + E_\mu = \frac{1}{2}\sum_{i=1}^{N-1} \mathbf{r}_i^2 + \sum_\sigma \frac{s_{l_\sigma} s_{r_\sigma} e^{-\kappa r_\sigma}}{r_\sigma} + \mu \sum_i s_i \tag{8}$$

where σ runs over contiguous non-nil sub-chains, with

$$\mathbf{r}_\sigma \equiv \sum_{i\in\sigma} \mathbf{r}_i \tag{9}$$

corresponding to the distance vector between the endpoints, l_σ and r_σ, of the subchain.

2.2 The Apparent Equilibrium Constant

The average degree of dissociation, $\alpha \equiv \frac{1}{N}\sum_i \langle s_i \rangle$, can be interpreted in terms of an effective chemical equilibrium constant, pK

$$pK = pH - \lg\left(\frac{\alpha}{1-\alpha}\right) \tag{10}$$

Without the interaction, we would have

$$\frac{\alpha}{1-\alpha} = \exp\left(-\frac{\mu}{T}\right) \tag{11}$$

A simple measure of the effect of the interaction on the chemical balance is then given by the change in pK:

$$\Delta pK = pK - pK_0 = -\frac{\mu}{T\ln 10} - \lg\frac{\alpha}{1-\alpha} \tag{12}$$

3 Variational Treatment of Conformational Degrees of Freedom

3.1 Generic Formalism

In this section we will focus on the conformational degrees of freedom, ignoring the titration; thus we consider a non-titrating polymer, with an energy obtained from eq. (8) by setting $s_i = 1$ and disregarding the μ term:

$$E(\mathbf{r}) = E_G + E_C = \frac{1}{2}\sum_{i=1}^{N-1} \mathbf{r}_i^2 + \sum_\sigma \frac{e^{-\kappa r_\sigma}}{r_\sigma} \tag{13}$$

A suitable variational approach to such a system is based on an effective energy Ansatz [31, 32, 29, 30]

$$E_V/T = \frac{1}{2}\sum_{ij} G^{-1}_{ij}\,(\mathbf{r}_i - \mathbf{a}_i)\cdot(\mathbf{r}_j - \mathbf{a}_j) \tag{14}$$

where $\mathbf{a}_i$ define average bond vectors, around which Gaussian fluctuations are allowed, described by the symmetric, positive-definite correlation matrix G_{ij}, the matrix inverse of which appears in the energy.

Using this effective energy, the exact free energy $F = -T\ln Z$ of the polymer is approximated from above [33] by the variational one

$$\hat{F} = -TS_V + \langle E\rangle_V \geq F \tag{15}$$

where S_V is the variational entropy, and $\langle E\rangle_V$ is the average of the true energy in the trial Boltzmann distribution $\propto \exp(-E_V/T)$. The parameters G_{ij} and $\mathbf{a}_i$ are to be determined so as to minimize the variational free energy $\hat{F}$. The resulting effective Boltzmann distribution is then used to approximate expectation values $\langle\cdots\rangle$ by effective (variational) ones $\langle\cdots\rangle_V$. Thus, we have e.g. $\langle\mathbf{r}_i\rangle_V = \mathbf{a}_i$ and $\langle\mathbf{r}_i\cdot\mathbf{r}_j\rangle_V = \mathbf{a}_i\cdot\mathbf{a}_j + 3G_{ij}$. For potentials diverging like $1/r^3$ or worse at short distances, $\langle E\rangle_V$ will be divergent, and the approach breaks down. However, such potentials are not physical.

At high T and/or small N, the resulting $\mathbf{a}_i$ will vanish. By setting $\mathbf{a}_i = 0$ in eq. (14), a restricted Ansatz is obtained, that in the screened case yields better results numerically than the $\mathbf{a}_i \neq 0$ case; this restricted version will be frequently used below.

The minimization of $\hat{F}$ with respect to G_{ij} and $\mathbf{a}_i$ gives rise to a set of matrix equations to be solved iteratively. These are considerably simplified, and the symmetry and positivity constraints on G_{ij} are automatic, if G_{ij} is expressed as the product of a matrix and its transpose:

$$G_{ij} = \sum_{\mu=1}^{N-1} z_{i\mu} z_{j\mu} = \mathbf{z}_i\cdot\mathbf{z}_j \tag{16}$$

The interpretation of the local parameter $\mathbf{z}_i$ is simple – it is a fluctuation amplitude for the ith bond vector $\mathbf{r}_i$. We can write

$$\mathbf{r}_i = \mathbf{a}_i + \sum_{\mu} z_{i\mu}\mathbf{J}_\mu \tag{17}$$

where each component of $\mathbf{J}_\mu \in \mathcal{R}^3$ is an independent Gaussian noise variable of unit variance.

Similarly, we have for a subchain

$$\mathbf{r}_\sigma = \sum_{i\in\sigma}\mathbf{r}_i \equiv \mathbf{a}_\sigma + \sum_{\mu} z_{\sigma\mu}\mathbf{J}_\mu, \tag{18}$$

where $\mathbf{a}_\sigma = \sum_{i\in\sigma} \mathbf{a}_i$ and $\mathbf{z}_\sigma = \sum_{i\in\sigma} \mathbf{z}_i$. Thus, the noise amplitudes are additive.

The matrix inverse of G can be similarly decomposed:

$$G^{-1}_{ij} = \mathbf{w}_i \cdot \mathbf{w}_j \tag{19}$$

where $w_{i\mu}$ is the (transposed) matrix inverse of $z_{i\mu}$:

$$\mathbf{z}_i \cdot \mathbf{w}_j = \delta_{ij} \tag{20}$$

Note that $\mathbf{z}_i$, $\mathbf{w}_i$ and $\mathbf{z}_\sigma$ are vectors in R^{N-1}, not in R^3.

In terms of $\mathbf{a}_i$ and $\mathbf{z}_i$, the variational free energy ignoring trivial additive constants (see ref. [30] for details) is given by

$$\begin{aligned} \hat{F} &= -3T \ln \det z + \frac{1}{2}\sum_i (3\mathbf{z}_i^2 + \mathbf{a}_i^2) \\ &+ \sum_\sigma \frac{1}{2a_\sigma} \exp\left(-\frac{a_\sigma^2}{2z_\sigma^2}\right) \left\{ \Psi\left(\kappa z_\sigma - \frac{a_\sigma}{z_\sigma}\right) - \Psi\left(\kappa z_\sigma + \frac{a_\sigma}{z_\sigma}\right)\right\} \end{aligned} \tag{21}$$

where

$$\Psi(x) \equiv \exp(x^2/2)\ \mathrm{erfc}(x/\sqrt{2}) \tag{22}$$

At high enough temperatures, there is a unique minimum, having all $\mathbf{a}_i = 0$ – a *purely fluctuating solution.* At lower T, an additional solution appears, characterized by aligned $\mathbf{a}_i \neq 0$; this becomes the global minimum at low enough T.

Setting $\mathbf{a}_i = 0$ for the unscreened case ($\kappa = 0$) the variational free energy simplifies to

$$\hat{F} = -3T \ln \det z + \frac{3}{2}\sum_i \mathbf{z}_i^2 + \sqrt{\frac{2}{\pi}} \sum_\sigma \frac{1}{z_\sigma} \tag{23}$$

which very much resembles the energy of an $(N-1)$-dimensional Coulomb chain with bonds $\mathbf{z}_i$, but with an extra *entropy* term (the first) preventing alignment of the ground state.

The equations for a local extremum of $\hat{F}(\mathbf{a}, \mathbf{z})$ are obtained by differentiation with respect to $\mathbf{z}_i$ and $\mathbf{a}_i$,

$$\frac{\partial \hat{F}}{\partial \mathbf{z}_i} = 0\ ,\ \frac{\partial \hat{F}}{\partial \mathbf{a}_i} = 0 \tag{24}$$

Due to the use of relative coordinates and of local noise amplitudes, a simple gradient descent method with a large step-size ϵ can be used, that gives fast convergence to a solution of eqs. (24)

$$\Delta \mathbf{z}_i = -\epsilon_z \frac{\partial \hat{F}}{\partial \mathbf{z}_i},\ \Delta \mathbf{a}_i = -\epsilon_a \frac{\partial \hat{F}}{\partial \mathbf{a}_i}, \tag{25}$$

Further speed is gained by updating the reciprocal variables $\mathbf{w}_i$ (arising from differentiating $\ln \det z$) using incremental matrix inversion (the Sherman-Morrison method [34, 30]) – the increment in $\mathbf{w}_j$ due to a change $\Delta \mathbf{z}_i$ is given by

$$\Delta \mathbf{w}_j = -\frac{\mathbf{w}_i(\mathbf{w}_j \cdot \Delta \mathbf{z}_i)}{1 + \mathbf{w}_i \cdot \Delta \mathbf{z}_i} \tag{26}$$

The resulting computational demand of the method is $\propto N^3$.

The high and low T properties of the variational approach were analyzed in ref. [30]. In contrast to the case in MC simulations, the free energy is directly accessible with the variational method. Furthermore, the approach respects the virial identity, $2\langle E_G \rangle - \langle E_C \rangle = 3(N-1)T$, in the sense that it holds also for the corresponding variational averages.

3.2 Non-Titrating Variational Results Revisited

The method, restricted to $\mathbf{a}_i = 0$, was extensively confronted with MC results in ref. [30]. Very good agreement was found for configurational quantities in the case of an unscreened Coulomb interaction (the error is well within the theoretical 11% limit [30]). In the screened case the method does not reproduce the MC results equally well although it gives a qualitatively correct picture of conformational properties.

Prior to dealing with the titration case we will augment the comparisons in [30] on the end-to-end distance r_{ee} with those arising from the $\mathbf{a}_i \neq 0$ solutions and also with those produced by the simplest possible variational Ansatz [35]. The latter is a highly constrained version of eq. (14), with $\mathbf{z}_i = 0$ and constant $\mathbf{a}_i = \mathbf{a}$, corresponding to a *rigid rod*. This simplification leads to simple scaling behaviour [35],

$$r_{ee} \approx N(\ln N)^{1/3} \tag{27}$$

which seems to be approximately correct in MC calculations [30]; it is certainly correct at $T \to 0$. In fig. 1 we compare the results of the three different variational approaches ($\mathbf{a}_i = 0$, $\mathbf{a}_i \neq 0$, and the rigid rod) to MC data. The large N behaviour of the $\mathbf{a}_i = 0$ and $\mathbf{a}_i \neq 0$ variational curves is consistent with approaching the theoretical limits derived in ref. [29]; 11% and 0% respectively. The average monomer-monomer distances are also very well reproduced by both the $\mathbf{a}_i = 0$ and $\mathbf{a}_i \neq 0$ variational approaches.

The simple rigid rod approach is more or less tailored to reproduce r_{ee}, but it lacks the degrees of freedom to properly describe local properties along the chain. A similar approach was pursued in ref. [8] in which good results were reported, at temperatures significantly higher than those at which the calculations in this paper are performed. We expect the accuracy of the rigid rod approximation to increase with decreasing temperature.

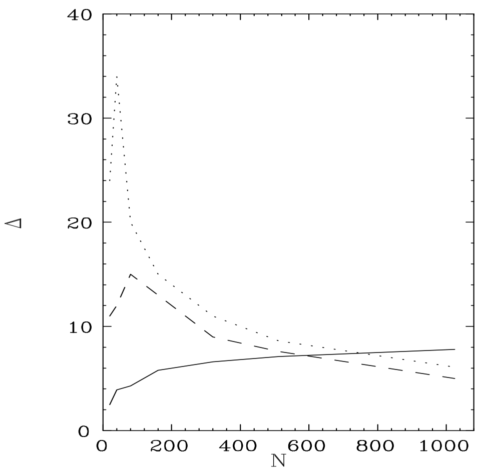

Figure 1: Relative difference (Δ=(Var-MC)/MC) in % for r_{ee} between different variational versions and MC data for unscreened Coulomb chains as functions of N. The $\mathbf{a}_i = 0$, $\mathbf{a}_i \neq 0$, and the rigid rod variants of the variational method are denoted by full, dashed and dotted lines respectively.

For screened Coulomb chains the $\mathbf{a}_i \neq 0$ results do not compare favourably with MC data – the chain tends to elongate more than the screened potentials call for. The same is true for the rigid rod approximation.

4 Variational Approach to Titration

4.1 Variational Treatment of Titratable Charges

So far the variational approach has been confined to the situation with fixed identical charges along the chain. Next we generalize to allowing charge exchange with the solvent, with the total charge governed by a chemical potential. This amounts to considering s_i in eq. (8) as dynamical variables, that each can be either 0 or 1. Thus, suppressing for a moment the coordinate degrees of freedom, the system is isomorphic to an Ising spin system.

$$E = -\frac{1}{2}\sum_{ij} w_{ij} s_i s_j + \mu \sum_i s_i \tag{28}$$

where the chemical potential μ has been introduced and coordinate dependencies etc. are lumped into the "couplings" w_{ij}. Such systems have been subject to much attention in the solid state community, in particular for describing magnetic properties of so called spin glasses. A powerful alternative to computing thermodynamical properties of eq. (28) by means of MC techniques is the mean field (MF) approximation. This can be considered as a variational approach along the lines above, with the variational energy Ansatz

$$E_V = -T \sum_i u_i s_i \tag{29}$$

where the coefficients u_i are the variational parameters. Minimizing the corresponding variational free energy one gets the MF equations

$$v_i = g(u_i) \equiv \frac{1}{2}\left(1 + \tanh\left(\frac{u_i}{2}\right)\right) \tag{30}$$

$$u_i = -\frac{\partial E}{\partial v_i}\frac{1}{T} \tag{31}$$

which can be solved by iteration. The *mean fields* v_i have the interpretation of mean charges $\langle s_i \rangle_V$, while u_i are conventionally referred to as *local fields*.

We will next merge the variational treatments of relative coordinates and charges treating the unscreened and screened cases separately. For simplicity we limit the presentation to the $\mathbf{a}_i = 0$ solutions. The corresponding expressions for the $\mathbf{a}_i \neq 0$ solutions can be found in Sect.2.

4.2 Unscreened Coulomb Chain

For an unscreened Coulomb chain, the energy expression of eq. (8) simplifies to

$$E = \frac{1}{2}\sum_i r_i^2 + \sum_\sigma \frac{s_{l_\sigma} s_{r_\sigma}}{r_\sigma} + \mu \sum_i s_i \tag{32}$$

where s_{l_σ} and s_{r_σ} are the charges at the left and right endpoints of the sub-chain σ, respectively. With a variational effective energy Ansatz

$$E_V/T = \frac{1}{2}\sum_{ij} G_{ij}^{-1}\mathbf{r}_i \cdot \mathbf{r}_j - \sum_i u_i s_i \tag{33}$$

including both coordinate and charge degrees of freedom, the variational free energy becomes, ignoring additive constants

$$\hat{F} = -3T \ln\det z + T\sum_i \{u_i v_i - \ln(1+e^{u_i})\} + \frac{3}{2}\sum_i {\mathbf{z}_i}^2 + \sqrt{\frac{2}{\pi}}\sum_\sigma \frac{v_{l_\sigma} v_{r_\sigma}}{z_\sigma} + \mu \sum_i v_i \tag{34}$$

where v_i and u_i are related according to eq. (30); the first two terms give the entropy part $-TS_V$, while the remaining terms correspond to $\langle E \rangle_V$. The equations for a local extremum of $\hat{F}(\mathbf{z},\mathbf{v})$ are obtained by differentiation with respect to $\mathbf{z}_i$ and v_i. One gets

$$-3T\mathbf{w}_i + 3\mathbf{z}_i - \sqrt{\frac{2}{\pi}} \sum_{\sigma \ni i} \frac{v_{l_\sigma} v_{r_\sigma} \mathbf{z}_\sigma}{z_\sigma^3} = 0 \tag{35}$$

and

$$\mu + T u_i + \sqrt{\frac{2}{\pi}} \sum_{l \neq i} \frac{v_l}{z_{il}} = 0 \tag{36}$$

respectively.

4.3 Screened Coulomb Chain

The variational free energy for the screened case modifies to

$$\begin{aligned} \hat{F} &= -3T \ln \det z + T \sum_i \{u_i v_i - \ln(1 + e^{u_i})\} \\ &+ \frac{3}{2} \sum_i {\mathbf{z}_i}^2 + \sum_\sigma v_{l_\sigma} v_{r_\sigma} \left(\sqrt{\frac{2}{\pi}} \frac{1}{z_\sigma} - \kappa \Psi(\kappa z_\sigma) \right) + \mu \sum_i v_i \end{aligned} \tag{37}$$

The derivatives then become

$$\frac{\partial \hat{F}}{\partial \mathbf{z}_i} \equiv -3T\mathbf{w}_i + 3\mathbf{z}_i - \sum_{\sigma \ni i} \frac{v_{l_\sigma} v_{r_\sigma} \mathbf{z}_\sigma}{z_\sigma^3} \left\{ \sqrt{\frac{2}{\pi}} (1 - \kappa^2 z_\sigma^2) + \kappa^3 z_\sigma^3 \Psi(\kappa z_\sigma) \right\} = 0 \tag{38}$$

$$\frac{\partial \hat{F}}{\partial v_i} \equiv \mu + T u_i + \sum_{l \neq i} v_l \left(\sqrt{\frac{2}{\pi}} \frac{1}{z_{li}} - \kappa \Psi(\kappa z_{li}) \right) = 0 \tag{39}$$

4.4 Properties of the Variational Solution

The Apparent Equilibrium Constant

The variational approximation to α is simply given by

$$\alpha = \frac{1}{N} \sum v_i = \overline{v} = \overline{g(u)} \tag{40}$$

The local fields u_i can be expressed in terms of v_i (inverting eq. (30)) as

$$u_i = g^{-1}(v_i) = \ln \frac{v_i}{1 - v_i} \tag{41}$$

Thus, the variational ΔpK is given by

$$\Delta pK \ln 10 = -\frac{\mu}{T} - g^{-1}\left(\overline{g(u)}\right) \approx -\frac{\mu}{T} - \overline{u} \tag{42}$$

In the unscreened case (for simplicity), the last expression amounts to

$$\frac{1}{NT}\sqrt{\frac{2}{\pi}}\sum_i\sum_{j\neq i}\frac{v_j}{z_{ij}}=\frac{1}{NT}\sum_i\sum_{j\neq i}\left\langle\frac{s_j}{r_{ij}}\right\rangle_V \tag{43}$$

where the interpretation of ΔpK as an average energy cost per dissociated charge is very clear.

The Virial Identity

In the unscreened case, there is, also in the titrating version, a virial identity,

$$2\langle E_G\rangle-\langle E_C\rangle=3(N-1)T \tag{44}$$

obeyed by the exact thermodynamic ensemble. By taking the scalar product of eq. (35) with $\mathbf{z}_i$ and summing over i, we obtain

$$-3T(N-1)+3\sum_i\mathbf{z}_i^2-\sqrt{\frac{2}{\pi}}\sum_\sigma\frac{v_{l_\sigma}v_{r_\sigma}}{z_\sigma}=0 \tag{45}$$

and by a comparison with eq. (34), it is seen that the virial identity is indeed satisfied also for the variational expectation values. The same goes for the $\mathbf{a}_i\neq 0$ solutions.

Structure of the Effective Energy

By taking the scalar product of eq. (35) with $\mathbf{w}_j$, we obtain the effective force-constants

$$TG_{ij}^{-1}=\delta_{ij}-\frac{1}{3}\sqrt{\frac{2}{\pi}}\sum_{\sigma\ni i,j}\frac{v_{l_\sigma}v_{r_\sigma}}{z_\sigma^3} \tag{46}$$

while eq. (36) gives the effective local fields

$$-Tu_i=\mu+\sqrt{\frac{2}{\pi}}\sum_{l\neq i}\frac{v_l}{z_{il}} \tag{47}$$

Thus, we can rewrite the variational energy, eq. (33), as

$$E_V(\{\mathbf{r}_i,s_i\})=\frac{1}{2}\sum_i\mathbf{r}_i^2+\sum_\sigma\sqrt{\frac{2}{\pi}}\left(\frac{v_{l_\sigma}s_{r_\sigma}+v_{r_\sigma}s_{l_\sigma}}{z_\sigma}-\frac{1}{6}\frac{v_{l_\sigma}v_{r_\sigma}\mathbf{r}_\sigma^2}{z_\sigma^3}\right)+\mu\sum_i s_i \tag{48}$$

where the first and the last term reproduce the true bond and chemical potential terms of eq. (32), while the middle term emulates the effect of the Coulomb interaction on the charges (by appropriate local fields), and on the conformation (by suitable repulsive spring forces).

The variational optimization thus forces the effective energy to have an intuitively appealing (and indeed very reasonable) structure.

4.5 Algorithm Implementation

For the numerical minimization of the free energy of eqs. (34) or (37) with respect to the variational parameters $\mathbf{z}_i$ ($\mathbf{w}_i$) and v_i (u_i) a modified gradient descent is used;

$$\Delta z_i = -\epsilon_z \frac{\partial \hat{F}}{\partial \mathbf{z}_i}, \; \Delta u_i = -\epsilon_u \frac{\partial \hat{F}}{\partial v_i}. \tag{49}$$

where the use of the v (rather than u) derivative in the u-update implies a dynamical step size

$$\tilde{\epsilon}_u = \frac{\epsilon_u}{v(1-v)} \tag{50}$$

which is found to speed up the calculations. The $\mathbf{w}_i$:s are obtained using incremental matrix inversion (eq. (26)).

The complete algorithm looks as follows:

1. Initialize all $\mathbf{z}_i$ and v_i at random.
2. Repeat until convergence:

   For all i:

   - Update $\mathbf{z}_i$ (if $i < N$) and $v_i = g(u_i)$ according to eq. (49).
   - Correct all $\mathbf{w}_j$ according to eq. (26)
3. Extract $G_{ij} = \mathbf{z}_i \cdot \mathbf{z}_j$ and compute variational averages of interest.

Typical step-sizes are $\epsilon_z \approx 0.15$ and $\epsilon_u \approx 0.5$. The number of of computations for each iteration step is proportional to N^3. An $N = 80$ system converges within about 100 iterations, which is somewhat slower than in the non-titrating case.

4.6 A Simplified Variational Approach

For a highly charged polyelectrolyte in the absence of salt, the conformation is strongly elongated. This fact motivates a simplified variational Ansatz, based on a rigid rod conformation and a constant degree of dissociation α along the chain. Such a simplified picture allows for analytical estimates of quantities of interest like ΔpK and r_{ee}. To this end, consider the non-fluctuating limit $\mathbf{z}_i \to 0$ with $\mathbf{a}_i = \mathbf{a} = \mathbf{R}/(N-1)$ for all i, in which the variational Boltzmann distribution is given by

$$\exp(-E_V/T) = \exp\left(u \sum s_i\right) \prod_i \delta\left(\mathbf{r}_i - \mathbf{a}\right) \tag{51}$$

This is similar to approximating the interactions by an applied stretching force at the ends of the chain; here, all fluctuations are killed, however. Identifying α with $g(u)$ gives for large N the variational free energy

$$\begin{aligned}\hat{F} &= NT\{\alpha\ln(\alpha)+(1-\alpha)\ln(1-\alpha)\}+\frac{R^2}{2(N-1)}+\\ &\frac{\alpha^2}{R}N(N-1)(\ln N+\gamma-1)+N\mu\alpha \qquad (52)\end{aligned}$$

Here the sum $\sum_1^N 1/k$ has been approximated by $\ln N+\gamma$, where γ is the Euler constant. Minimizing $\hat{F}$ with respect to α and R gives for large N

$$r_{ee}=R\approx\alpha^{2/3}N(\ln N)^{1/3} \qquad (53)$$

$$\langle E_C\rangle\approx\alpha^{4/3}N(\ln N)^{2/3} \qquad (54)$$

$$\Delta pK\approx\frac{2}{T\ln 10}\alpha^{1/3}(\ln N)^{2/3} \qquad (55)$$

where μ has been eliminated in favour of α. This simplified model should give good results in the highly charged limit $\alpha\to 1$, whereas its lack of fluctuations should give rise to poor performance in the $\alpha\to 0$ limit.

A similar approximation can of course be used for a screened Coulomb potential. In this case, however, there is no analytical solution, but the relevant equations are readily solved by a simple numerical iteration scheme.

5 Monte Carlo Methods

The Monte Carlo (MC) simulations were performed with the traditional Metropolis algorithm [36] in a semi-grand canonical ensemble. A single polyelectrolyte chain was simulated with the charges/protons moving between the monomers and an implicit bulk of fixed chemical potential.

When a proton move is attempted, a monomer is picked at random and the charge state of the monomer is switched. The associated (free) energy change, ΔE, which determines if the move is to be accepted or rejected according to the Metropolis scheme, is the sum of the change ΔE_C in the intramolecular Coulomb energy and a term $\pm\mu$ that corresponds to the change in free energy for the acid-base reaction of an isolated monomer; the minus sign is used when the monomer is to be protonated, and the plus sign when it is to be deprotonated.

In a single MC step a proton is only moved from the chain to the bulk or *vice versa*. Adding a step where a proton moves within the polymer does not affect the averages but increases the calculation time.

When a conformational change is attempted, the associated energy change is given by the change in bond energy, ΔE_G, plus the electrostatic energy change, ΔE_C. The sampling of chain conformations is made highly efficient by using a pivot algorithm, which allows chain lengths of more than 2000 monomers. The pivot algorithm was first described by Lal [37], and its efficiency for self-avoiding walks has been thoroughly discussed by Madras and Sokal [38].

A traditional move to update the coordinate variables is to attempt a translation of only one monomer at a time. The number of interactions that have to be calculated is of the order N for a highly charged chain and a large number of attempts per monomer is needed to generate independent chain conformations. In the pivot algorithm, however, each monomer i (except the first one) is translated in turn but together with the remaining semi-chain (monomers $i+1$ to N). Furthermore, the semi-chain is then rotated as a rigid body around one of the coordinate axes with monomer i as origin. The number of interactions calculated in one step is of the order N^2 but independent conformations are obtained after only a few attempted moves, on the order of one per monomer or N in total. The net effect is a greatly reduced simulation time for a given degree of precision and a computational cost that grows approximately as N^3. A completely different and even slightly more efficient procedure has recently been described by Irbäck [39].

A change in conformation is attempted once in every 20 steps; in the remaining steps, a change in the charge state is attempted. The total number of steps is around 10^8. Every run is preceded by an equilibration of 10^5–10^6 steps, where a change in conformation is attempted every other step, starting from a straight line with a charge on every other monomer. The simulations are faster at high $\tilde{\mu}$, since fewer monomers are charged and thus the number of interactions that have to be calculated is smaller.

6 Results and Discussion

6.1 Unscreened Coulomb Chain

We now compare the variational and Monte Carlo results for r_{ee} and ΔpK as a function of chain length and degree of dissociation. Fig. 2 shows an excellent agreement between the $\mathbf{a}_i = 0$ variational results for r_{ee} and MC data, with a maximal relative error of 8% for the $N = 1000$ chain at $\alpha = 1$, well within the theoretical high-N limit of 11%. The difference between the variational and MC results increases with α as expected, but is indeed satisfactory for all cases studied. The $\mathbf{a}_i \neq 0$ variational solution is slightly inferior to the purely fluctuating solution, except for the $N = 1000$ curve at high degree of ionization. Thus, we find a qualitative behaviour of the two variational solutions similar to that seen in fig. 1.

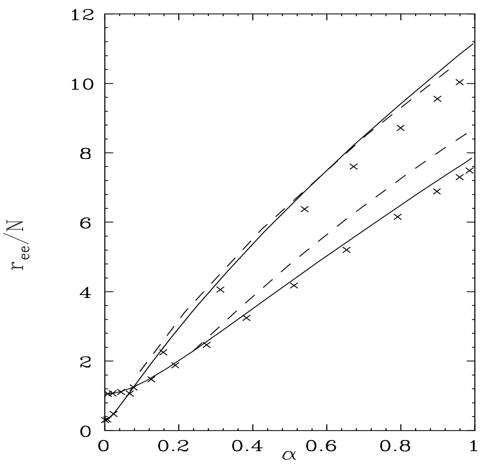

Figure 2: $\tilde{r}_{ee}/N$ as a function of α for for an unscreened polyelectrolyte chain. Monte Carlo results are denoted by crosses and the $\mathbf{a}_i = 0$ and $\mathbf{a}_i \neq 0$ variational solutions are drawn as solid and dashed lines, respectively. The upper curves are for $N = 1000$ and the lower for $N = 80$ and the unit of length is Å.

The rigid rod approximation suggests that r_{ee}/N should increase linearly with $\alpha^{2/3}(\ln N)^{1/3}$, which seems to be verified in fig. 3. Similar scaling behaviour for an analogous non-titrating polyelectrolyte has been derived in the literature [35, 7, 8]. We have, however, made numerical estimates of the exponents from logarithmic plots of r_{ee}/N against α from both variational and MC data. For the α dependence we find exponents in the range 0.80-0.85 from both approaches, which is significantly larger than the value of 2/3 predicted by the rigid rod approximation. The origin of the discrepancy is unclear. A similar discrepancy is seen for the $\ln N$ exponent, which in the rigid rod case is given by 1/3, while numerical estimates from variational and MC data suggest a value of 0.6-0.7. One possible explanation could be that the chain expands via two different mechanisms. One is the expansion of each monomer bond, which should give rise to an $\ln N$ exponent of 1/3 [30]; Another is the increasing alignment of monomer bonds with N, which reaches its limit when the coupling becomes strong and should level off for large N.

Fig. 4 shows the shift in the apparent dissociation constant upon ionization of the chain and one finds that the $\mathbf{a}_i = 0$ variational results differ significantly from the MC results for the longer chains. The $\mathbf{a}_i \neq 0$ results, on the other hand, are always in excellent agreement with the MC data with negligible

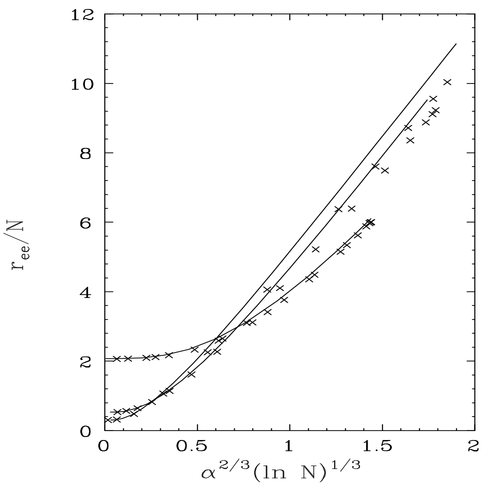

Figure 3: $\tilde{r}_{ee}/N$ as a function of $\alpha^{2/3}(\ln N)^{1/3}$ for different chain lengths ($N = 20, 320, 1000$) in the case of an unscreened Coulomb potential. Variational ($\mathbf{a}_i = 0$) and MC results are denoted by solid lines and crosses, respectively. The unit of length is Å.

differences for all systems studied. The largest error seen is of the order of one tenth of a pK unit.

The global conformational properties of the polymer depends on the electrostatic coupling strength via an *effective coupling*, approximately given by

$$\frac{\alpha^{4/3}N}{T} \tag{56}$$

The two variational solutions coincide for a weakly coupled chain, while at higher coupling two distinct solutions appear. This is seen in fig. 4 where the $\mathbf{a}_i \neq 0$ solution appears at a lower α value for the longer chains. Lowering the temperature (or decreasing r_0) would have a similar effect.

The asymptotic behaviour in the rigid rod approximation can be investigated by plotting ΔpK against $\alpha^{1/3}(\ln N)^{2/3}$. Fig. 5 shows that the α dependence is not well described by a power law over the parameter range studied and that it is only for very large N and α close to unity, that the slope seems to approach the rigid rod result $1/3$. One possible explanation for the lacking agreement could be the fact that α is not uniform, but varies along the chain. A similar plot can be made for the $\ln N$ dependence with a slightly better agreement and with a linear relation between $\ln \Delta pK$ and $\ln(\ln N)$. The

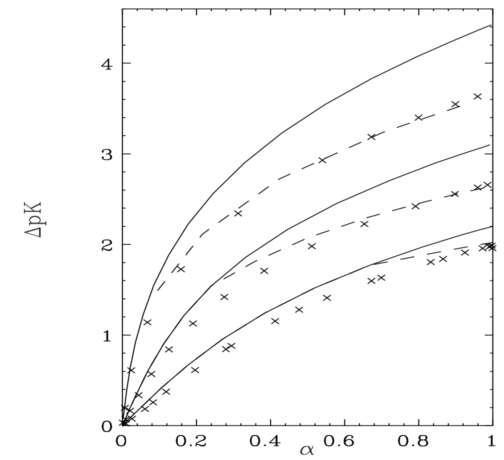

Figure 4: ΔpK as a function of α for different chain lengths with an unscreened Coulomb potential. Monte Carlo results are denoted by crosses and the $\mathbf{a}_i = 0$ and $\mathbf{a}_i \neq 0$ variational solutions are drawn as solid and dashed lines, respectively. The chain lengths are from top to bottom, $N = 1000, 80, 20$.

slope is approximately 0.7 for $\alpha = 1.0$, in good agreement with the rigid rod prediction of $2/3$, but it increases with decreasing α. This is again consistent with two different expansion mechanisms.

The rigid rod approximation gives an excellent description of the titration behaviour for a highly charged chain, while it slightly deviates from the MC results for short chains at low α. Fig. 6 shows that the rigid rod actually gives a better approximation to the MC data for ΔpK at high α values than the full $\mathbf{a}_i = 0$ variational solution. A similarly good agreement is found in fig. 7 where the MC and rigid rod numbers are virtually indistinguishable. The agreement between the rigid rod and the MC results holds for r_{ee} and the apparent dissociation constant, but not for local properties like the monomer-monomer separation. The rigid rod does not distinguish between different positions along the chain and it also strongly underestimates the average monomer-monomer separation. For such properties, the more sophisticated variational approaches are definitely superior and in general in good agreement with the exact MC results.

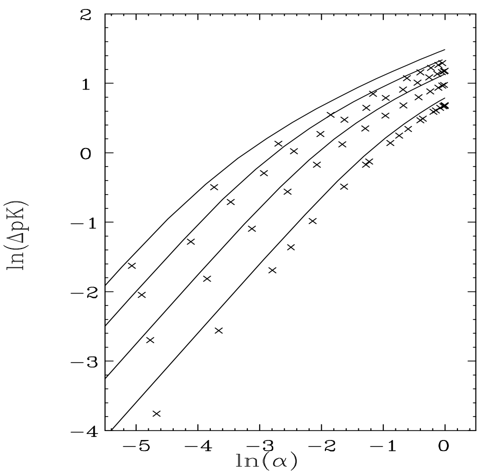

Figure 5: $\ln \Delta pK$ as a function of $\ln \alpha$ for unscreened polyelectrolyte chains. From bottom to top: $N = 20$, 80, 320, and 1000. Variational ($\mathbf{a}_i = 0$) and MC results are denoted by solid lines and crosses, respectively.

6.2 Screened Coulomb Chain

A discussion of the accuracy of the screened Coulomb approximation is beyond the scope of the present communication [4, 25]. Our principal aim is to investigate the variational techniques and we will use the screened Coulomb potential assuming that it contains the main physical features relating to screening. We will be primarily interested in r_{ee} and ΔpK. These quantities will be functions of chain length and degree of ionization as before, but they will also depend on the screening parameter κ. In a real solution κ will contain contributions from added salt as well as any other charged molecule like the polyelectrolyte chain itself. Here we will neglect all these complications and we will refer to different screening conditions by stating the corresponding univalent salt concentration. Effects of solvent quality will be similarly neglected. These can be modelled by introducing additional effective interactions between monomers [6].

A polyelectrolyte chain in a salt solution will be approximately independent of electrolyte concentration as long as the screening length is larger than the end-to-end separation, and the screening will start to play a role when κ^{-1} is smaller than or of the same order as r_{ee}.

The accuracy of the variational result for r_{ee} from the purely fluctuating

[6] Work along these lines is in progress at our laboratory.

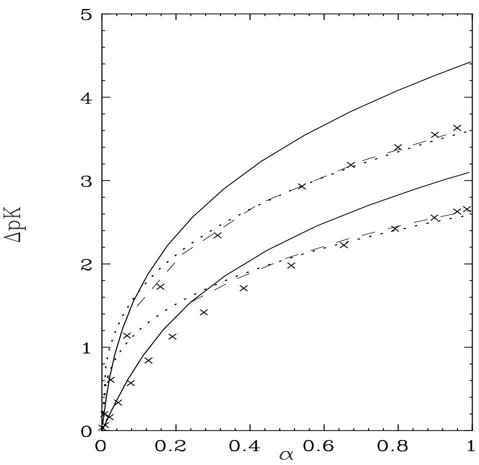

Figure 6: ΔpK as a function of α for an unscreened Coulomb chain. Monte Carlo results are denoted by crosses and the $\mathbf{a}_i = 0$, $\mathbf{a}_i \neq 0$ and the rigid rod solutions are drawn as solid, dashed and dotted lines, respectively. The upper curves are for $N = 1000$ and the lower for $N = 80$.

solution ($\mathbf{a}_i = 0$) deteriorates with increasing chain length for a given salt concentration. The discrepancy to the MC data also becomes worse with increasing degree of ionization - see fig. 8. With increasing salt concentration, the accuracy will deteriorate up to some point, whereafter it improves. In the limit of very high screening the chain becomes perfectly Brownian, leading to an exact agreement. The variational predictions for r_{ee} consistently overshoots; this can be attributed to an overestimate of the interaction with a Gaussian Boltzmann distribution.

The variational solution with $\mathbf{a}_i \neq 0$ is absent at low α and high salt concentration. In the other limit there will always be two solutions and we find that the purely fluctuating one is the most accurate one in predicting the end-to-end separation. The $\mathbf{a}_i \neq 0$ solution on the other hand predicts much too large r_{ee} - see fig. 8. The failure to describe the global structure of a screened chain is mainly due to the alignment of the bond vectors $\mathbf{a}_i$, which leads to the wrong asymptotic behaviour. The chain will expand like N instead of $N^{3/5}$, which approximately seems to describe the MC results. The rigid rod approximation for the screened chain will of course show a behaviour for the end-to-end separation similar to that of the full $\mathbf{a}_i \neq 0$ solution.

The apparent dissociation constant in the presence of salt (see fig. 9) is not

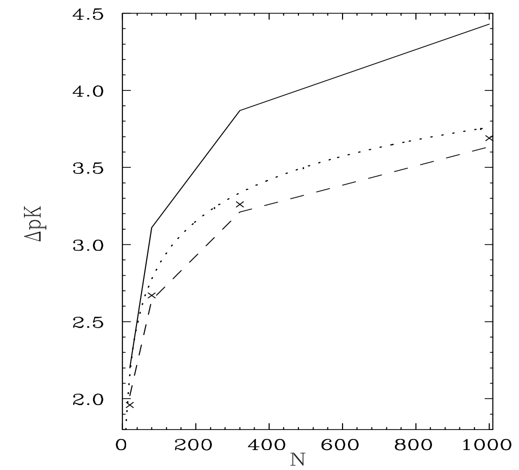

Figure 7: ΔpK as function of N for $\alpha = 1.0$ for an unscreened polyelectrolyte chain. Monte Carlo results are denoted by crosses and the $\mathbf{a}_i = 0$, $\mathbf{a}_i \neq 0$ and the rigid rod solutions are drawn as solid, dashed and dotted lines, respectively.

well described by the fluctuating solution. Instead we find the $\mathbf{a}_i \neq 0$ solution, despite its obvious structural failure, to be superior and in fair agreement with MC data. Obviously the coupling between thermodynamic derivatives, like the apparent dissociation constant, and the global structure is rather weak, and it is the local structure and fluctuations that determine the thermodynamics of a screened chain. The relative error is of the same size as for the unscreened chain - typically of the order of 10% or less. We find that ΔpK is consistently too large in the variational approximations, in accordance with the variational overestimate of the interaction.

For the rigid rod approximation, the overall agreement with MC data is not as good as for the unscreened chain, and ΔpK is predicted to be essentially independent of α. However, as seen in fig. 9, the numerical values obtained for $\alpha = 1$ agree very well with simulated numbers, and the salt dependence of ΔpK for the fully ionized chain is accurately reproduced.

7 Conclusions

The variational calculations accurately reproduce structural and thermodynamic properties of a titrating polyelectrolyte interacting via an unscreened Coulomb potential. For a highly charged polyelectrolyte we find two distinct

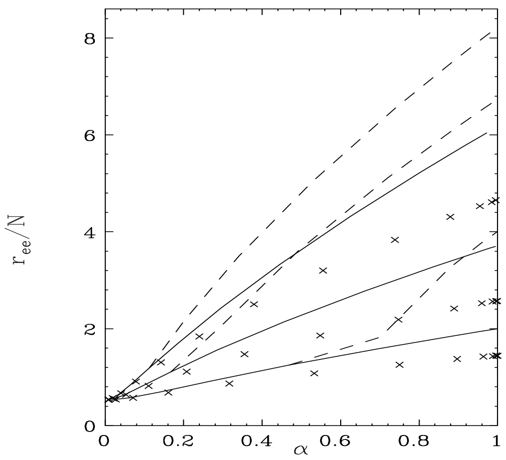

Figure 8: $\tilde{r}_{ee}/N$ as a function of α for a screened Coulomb chain with $N = 320$. Monte Carlo results are denoted by crosses and the $\mathbf{a}_i = 0$ and $\mathbf{a}_i \neq 0$ solutions are drawn as solid and dashed lines, respectively. The salt concentrations are from top to bottom 0.001, 0.01 and 0.1 M and the unit of length is Å.

solutions to the Gaussian variational Ansatz, which at weak coupling collapse into one – a purely fluctuating solution with $\mathbf{a}_i = 0$. At strong effective coupling – i.e. for large N, low T and large α – the $\mathbf{a}_i \neq 0$ solution always gives the lowest free energy, as well as the best approximation to structural and thermodynamic properties. At intermediate coupling strength, the purely fluctuating solution can produce superior structural data, while the apparent dissociation constant seems to be best described by the $\mathbf{a}_i \neq 0$ solution.

With increasing electrostatic coupling, the chain becomes stiffer and more rodlike and a less extensive variational approach, like the rigid rod, becomes applicable. This can be solved analytically, and turns out to be fairly accurate both for thermodynamics and for certain structural properties.

The screened Coulomb potential is more difficult to emulate with a Gaussian Ansatz, although reasonable predictions for the end-to-end separations are obtained from the purely fluctuating solutions. When the bond vectors $\mathbf{a}_i$ are non-zero they tend to align and the end-to-end separation increases linearly with N. For the purely fluctuating solution on the other hand, the end-to-end separation increases approximately as $N^{0.6}$ at high salt concentration, which is expected for a polymer with short range interactions. The apparent dissociation constant is well described also for a screened chain and we find that the

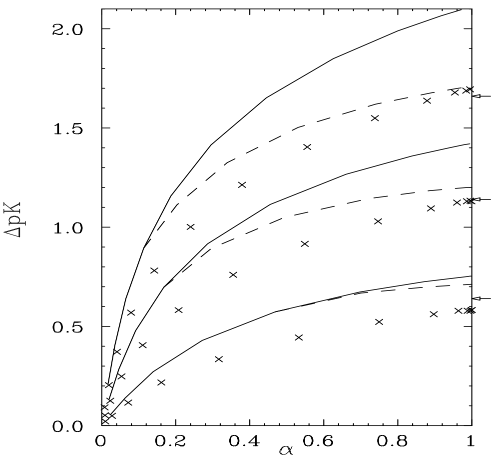

Figure 9: ΔpK as a function of α for a screened Coulomb chain with $N = 320$. Monte Carlo results are denoted by crosses and the $\mathbf{a}_i = 0$ and $\mathbf{a}_i \neq 0$ solutions are drawn as solid and dashed lines, respectively. The rigid rod results for $\alpha = 1$ are indicated with arrows. The salt concentrations are from top to bottom 0.001, 0.01 and 0.1 M.

$\mathbf{a}_i \neq 0$ solution, despite its structural shortcomings, is the best approximation for this property.

References

[1] C. Brender, M. Lax, and S. Windwer, J. Chem. Phys. **74**, 2576 (1981).

[2] A. Baumgärtner, J. Physique Lett. **45**, 515 (1984).

[3] S. L. Carnie, G. A. Christos, and T. P. Creamer, J. Chem. Phys. **89**, 6484 (1988).

[4] J. P. Valleau, Chem. Phys. **129**, 163 (1989).

[5] H. H. Hooper, H. W. Blanch, and J. M. Prausnitz, Macromolecules **23**, 4820 (1990).

[6] C. E. Reed and W. F. Reed, J. Chem. Phys. **92**, 6916 (1990).

[7] P. G. Higgs and H. Orland, J. Chem. Phys. **95**, 4506 (1991).

[8] J.-L. Barrat and D.Boyer, J. Phys. II. **3**, 343 (1993).

[9] T. L. Pugh and W. Heller, J. Polym. Sci. **47**, 219 (1960).

[10] G. D. Jones, *Polyelectrolytes* (Technomic, Westerport, CT, 1976).

[11] F. Mabire, R. Audebert, and C. Quivoron, J. Colloid and Interface Sci. **97**, 120 (1984).

[12] B. Eriksson and A. M. Härdin, in *Flocculation in Biotechnology and Separation Systems* (Elsevier Science Publishers, Amsterdam, 1987).

[13] K. J. Sasaki *et al.*, Langmuir **5**, 363 (1989).

[14] K. Thalberg and B. Lindman, J. Phys. Chem. **93**, 1478 (1989).

[15] I. Iliopoulos, T. K. Wang, and R. Audebert, Langmuir **7**, 617 (1991).

[16] C. E. Reed and W. F. Reed, J. Chem. Phys. **96**, 1609 (1992).

[17] A. P. Sassi *et al.*, J. Chem. Phys. **97**, 8767 (1992).

[18] M. Ullner, B. Jönsson, and P.-O. Widmark, J. Chem. Phys. **100**, 3365 (1994).

[19] M. Ullner, B. Jönsson, C. Peterson, and B. Söderberg, submitted to J. Chem. Phys. .

[20] R. L. Snipp, W. G. Miller, and R. E. Nylund, J. Amer. Chem. Soc. **87**, 3547 (1965).

[21] D. S. Olander and A. Holtzer, J. Am. Chem. Soc. **90**, 4549 (1968).

[22] M. Mandel, Eur. Polymer J. **6**, 807 (1970).

[23] W. Zhang, L. Piculell, and S. Nilsson, Biopolymers **31**, 1727 (1992).

[24] H. H. Hooper *et al.*, J. Chem. Phys. **93**, 2715 (1990).

[25] C. Woodward and B. Jönsson, Chem. Phys. **155**, 207 (1991).

[26] A. Lyubartsev and P. N. Vorontsov-Velyaminov, Macromolecular Compounds **32**, 721 (1990).

[27] M. J. Stevens and K. Kremer, Phys. Rev. Lett. **71**, 2228 (1993).

[28] M. J. Stevens and K. Kremer, to appear in J. Chem. Phys. (1995).

[29] B. Jönsson, C. Peterson, and B. Söderberg, Phys. Rev. Lett. **71**, 376 (1993).

[30] B. Jönsson, C. Peterson, and B. Söderberg, J. Phys. Chem. **99**, 1251 (1995).

[31] J.-P. Bouchaud, M. Mezard, G. Parisi and J. S. Yedida, Journal of Physics. **A24**, L1025 (1991).

[32] J.-P. Bouchaud, M. Mezard and J.S. Yedida, in *Neural Networks: from Biology to High Energy Physics*, edited by O. Benhar, C. Bosio, P. Del Giudice and E. Tabet (ETS Editrice, Pisa, 1991).

[33] R. Feynman, *Statistical Mechanics* (Frontiers in Physics, Benjamin, Reading, 1972).

[34] W.P. Press, B.P Flannery, S.A. Teukolsky and W.T. Vettering, *Numerical Recipes, The Art of Scientific Computing* (Cambridge University Press, Cambridge, 1986).

[35] P. G. de Gennes, P. Pincus, R. M. Velasco, and F. Brochard, J. Phys. **37**, 1461 (1976).

[36] N. A. Metropolis *et al.*, J. Chem. Phys. **21**, 1087 (1953).

[37] M. Lal, Mol. Phys. **17**, 57 (1969).

[38] N. Madras and A. D. Sokal, J. Stat. Phys. **50**, 109 (1988).

[39] A. Irbäck, J. Chem. Phys. **101**, 1661 (1994).

Paper III

LU TP 95-24
December 1995

A Blocking Technique for Emulating Very Large Polyelectrolytes

Carsten Peterson[1], Ola Sommelius[2] and Bo Söderberg[3]
Department of Theoretical Physics, University of Lund
Sölvegatan 14A, S-223 62 Lund, Sweden

Physical Review Letters **76**, 1079 (1996)

Abstract:
A new Monte Carlo method for computing thermodynamical properties of very large polyelectrolytes is presented. It is based on a renormalization group relating the original polymer to a smaller system, where in addition to the naively rescaled forces, a corrective nearest-neighbor interaction originating from the short distance Coulomb cutoff is introduced. The method is derived for low T but is in the unscreened case valid for all T. Large polymers with N monomers are emulated by Monte Carlo calculations on smaller systems, $K = N/Q$. The computational gain of the method is Q^3. It is explored with emphasis on room temperature.

[1]carsten@thep.lu.se
[2]ola@thep.lu.se
[3]bs@thep.lu.se

The thermodynamics of polyelectrolytes consisting of linear chains of monomers, with covalent harmonic bonding forces and Coulomb interactions, have been extensively studied with Monte Carlo Methods. Recently, high statistics results have emerged for relatively long (N=2048) chains [1]. A reliable measurement of e.g. the end-to-end distance r_{ee} is very CPU time consuming, even when employing state-of-the-art updating methods [2, 3].

In order to circumvent the computational bottleneck, and to facilitate estimates of free energies, a variational scheme was proposed [4, 1], relying upon an Ansatz in the form of a generic Gaussian distribution. For the unscreened case the variational method overestimates r_{ee} by 5-6 % at room temperature whereas for the screened case the approximation is less accurate.

In this letter we develop an alternative Monte Carlo (MC) approach, where the chains are "coarse grained" in the spirit of the renormalization group. This is accomplished by using an energy expression for blocked monomers with appropriately renormalized harmonic and Coulomb terms and an additional corrective nearest-neighbor interaction. Superficially, this is reminiscent of the well-known blob-picture of de Gennes [6], but the idea is quite different.

The approach is designed for low T. Indeed, at least in the absence of screening, T_r turns out to be low for large N [5]; thus, the approach should give good results precisely where it is needed. Our blocking scheme is derived in two ways, using (i) a real space renormalization philosophy, and (ii) a cut-off continuum formulation.

In terms of dimensionless quantities, the energy of a Coulomb chain is given by [1]

$$E = E_G + E_C = \frac{1}{2}\sum_{i=1}^{N-1} \mathbf{r}_{i,i+1}^2 + \sum_i \sum_{j>i} V(r_{ij}) \tag{1}$$

$$V(r) = \frac{e^{-\kappa r}}{r} \tag{2}$$

with a Boltzmann distribution $\propto \exp(-E/T)$. Here, $\mathbf{r}_{ij} = |\mathbf{x}_i - \mathbf{x}_j|$ with $\mathbf{x}_i$ as the monomer positions, while κ is the inverse Debye screening length. Assuming a length unit of 6Å, defining the unscreened N=2 equilibrium distance, the temperature in physical units is defined [1] by $(e^2T)/(4\pi\epsilon_0\epsilon_r r_0 k_B)$. Assuming a dielectric constant $\epsilon_r = 78.3$, $T_r = 0.837808$ will correspond to room temperature (298K). Similarly, with κ given by $r_0\sqrt{(2e^2N_Ac_s)/(\epsilon_r\epsilon_0 k_B 298\mathrm{K})}$, salt concentrations of $c_s = 0.01$M, 0.1M and 1.0M correspond to $\kappa = 0.1992$, 0.630 and 1.992, respectively [1].

In this paper we limit our discussion to the Debye potential model of eq. (1) for the Coulomb chain, in order to illustrate our ideas; a similar approach can of course be applied to other potentials.

Naively, one would coarse-grain the chain into blocks of Q monomers, and represent each of them by a single effective position carrying its entire charge.

The remaining position variables can then be integrated out (being Gaussian), leaving a system of $K = N/Q$ effective monomers, each carrying a charge Q. They would be connected by harmonic bonds being a factor Q weaker than the original ones.

This would be fine, were it not for the divergent short-distance behavior of the Coulomb interaction. This mainly affects neighboring blocks, where the naive effective interaction underestimates the repulsion.

This shortcoming can be remedied by a corrective interaction term between neighboring effective monomers, and we are lead to consider the following blocked energy:

$$E_B^{(K)} = \frac{1}{2Q}\sum_{i=1}^{K-1} r_{i,i+1}^2 + \frac{3}{2}(N-K)T \;+\; Q^2\sum_i\sum_{j>i} V(r_{ij}) + \sum_{i=1}^{K} W(r_{i,i+1}) \quad (3)$$

where r_{ij} are distances between blocked monomers. The different terms represent, in order of appearance: (1) the naive effective bond energy, (2) a correction to the bond energy, to account for the bond energy of the N-K eliminated position variables, (3) the naive effective interaction, and (4) a corrective nearest-neighbour interaction.

The correction term is determined as follows. In the low temperature limit the chain is a straight line with a slowly varying nearest-neighbour distance, which we approximate by a constant a. For the blocked system, the corresponding nearest-neighbour distance is then $b = Qa$. In this approximation, the true Coulomb energy is given by

$$U_N = \sum_{l=1}^{N}(N-l)V(la) \quad (4)$$

while the blocked interaction energy (including the correction term) reads

$$U_K = Q^2\sum_{l=1}^{K}(K-l)V(lb) + KW(b) \quad (5)$$

The objective is to choose $W(b)$ such that U_N and U_K become identical. For the Coulomb potential of eq. (1) one obtains for U_N:

$$U_N = \sum_{l}^{N}(N-l)\frac{e^{-\kappa la}}{la} \approx \frac{N}{a}\sum_{l}^{\infty}\frac{e^{-\kappa la}}{l} = -\frac{N}{a}\log(1-e^{-\kappa a}) \quad (6)$$

and similarly for U_K:

$$U_K \approx -\frac{Q^2K}{b}\log(1-e^{-\kappa b}) + KW(b) \quad (7)$$

where only the leading term in the sums have been included. Equating U_N with U_K for $b = Qa$ yields

$$W(r) = -\frac{Q^2}{r}\left[\log\left(1 - e^{-\kappa r/Q}\right) - \log\left(1 - e^{-\kappa r}\right)\right] \tag{8}$$

In the absence of screening (κ=0) this becomes

$$W(r) = \frac{Q^2 \log(Q)}{r} \tag{9}$$

representing an enhancement of the nearest-neighbour Coulomb interaction.

The results above are also transparent in a continuum formulation, where the ultraviolet divergence of the Coulomb interaction is regularized via an N-dependent cutoff, as implied by the discrete nature of the original chain. The W-term then corrects for the shift in the cutoff. We illustrate this in the unscreened case only.

A continuum formulation of the chain is obtained by replacing the discrete index i by a continuous parameter $\sigma = i/N$, such that $\mathbf{x}_i = \mathbf{x}(\sigma)$. Then the energy of eq. (1) (in the unscreened case) transforms into:

$$E \approx \frac{1}{2N}\int_0^1 \dot{\mathbf{x}}^2(\sigma)d\sigma + N^2\int_0^1\int_{\sigma+1/N}^1 \frac{d\sigma d\sigma'}{|\mathbf{x}(\sigma') - \mathbf{x}(\sigma)|} \tag{10}$$

Were it not for the short-distance cutoff ($1/N$) in σ, needed to regularize the Coulomb potential, all the N-dependence could be collected in a global factor N, by making the rescaling $\mathbf{x}(\sigma) \to N\mathbf{x}(\sigma)$. This corresponds to a mere rescaling of the temperature, and we would have the naive scaling

$$\mathbf{x}_{Qi}^{(QN,QT)} \Leftrightarrow Q\mathbf{x}_i^{(N,T)} \tag{11}$$

The N-dependent cutoff introduces a scale-breaking, though, and for $K < N$ the last term of eq. (10) can be rewritten as

$$\begin{aligned} N^2\int_0^1\int_{\sigma+1/N}^1 \frac{d\sigma d\sigma'}{|\mathbf{x}(\sigma') - \mathbf{x}(\sigma)|} &= \\ N^2\int_0^1\int_{\sigma+1/K}^1 \frac{d\sigma d\sigma'}{|\mathbf{x}(\sigma') - \mathbf{x}(\sigma)|} &+ N^2\int_0^1\int_{\sigma+1/N}^{\sigma+1/K} \frac{d\sigma d\sigma'}{|\mathbf{x}(\sigma') - \mathbf{x}(\sigma)|} \end{aligned} \tag{12}$$

In the low-temperature regime, where the chain is more or less linear, we can use the approximation

$$\mathbf{x}(\sigma') - \mathbf{x}(\sigma) \approx (\sigma' - \sigma)\dot{\mathbf{x}}(\sigma) \tag{13}$$

and obtain for the last term of eq. (12)

$$\begin{aligned} N^2 \int_0^1 \int_{\sigma+1/N}^{\sigma+1/K} \frac{d\sigma d\sigma'}{|\mathbf{x}(\sigma') - \mathbf{x}(\sigma)|} &\approx N^2 \int_0^1 \int_{\sigma+1/N}^{\sigma+1/K} \frac{d\sigma d\sigma'}{(\sigma' - \sigma)|\dot{\mathbf{x}}(\sigma)|} \\ = N^2 \int_0^1 \frac{d\sigma}{|\dot{\mathbf{x}}(\sigma)|} \int_{1/N}^{1/K} \frac{d\sigma'}{\sigma'} &= N^2 \log(N/K) \int_0^1 \frac{d\sigma}{|\dot{\mathbf{x}}(\sigma)|} \end{aligned} \quad (14)$$

Switching back to the discrete representation, the integral becomes the sum of nearest neighbour interactions; after rescaling with K^2, it corresponds precisely to the last term of eq. (3).

The correction to the naive blocked energy function was derived for low temperatures, and the method, as will be demonstrated below, indeed gives excellent results at low T, both for r_{ee} and E_C, for unscreened as well as screened Coulomb interactions.

At higher temperatures, the polymer will be less linear, and it is not *a priori* certain, that the method will work there. For the *unscreened* case in the high T limit, the exact results for r_{ee} and E_C for large N can be expanded in a series in $1/T$, yielding [5]

$$\begin{aligned} < r_{ee}^2 > &\approx 3(N-1)T + \frac{4}{15}\sqrt{\frac{2}{\pi}} \frac{N^{5/2}}{T^{1/2}} \\ < E_C > &\approx \frac{4}{3}\sqrt{\frac{2}{\pi}} \frac{N^{3/2}}{T^{1/2}} \end{aligned} \quad (15)$$

while E_G can be determined from the virial identity [1] $2E_G = E_C + 3(N-1)T$. We note, that the expressions are consistent with the naive scaling behavior of eq. (11), in that both r_{ee}/N and E_C/N are functions of T/N only for large N. The relevant small parameter of the high-T expansion is obviously N/T. For the blocked system of K effective monomers, the corresponding results are identical to the order shown. Thus, in the unscreened case the high T performance is under control.

In the presence of screening, the situation is somewhat different. The correct and blocked high-T expansions for E_C differ, and it is actually the contribution from the correction term that dominates [5]. Hence, in the screened case the blocking method is reliable only at low T.

We have made extensive numerical evaluations of the blocking approach. All MC runs, both standard and blocked, were performed using the pivot algorithm [2]. Most results are based on 10^4 thermalization sweeps and 10^5 measured configurations. Some results were taken from ref. [1]. Initially exploratory comparisons were made in order to find Q, T and κ ranges where the blocked approach is trustworthy. It turns out that realistic values for T (T_r) for unscreened chains are within the domain of application even with

N	Q=8	Q=4	Q=2	Q=4/3
40	1.10	1.04	1.01	1.00
80	1.06	1.03	1.01	1.00
160	1.05	1.02	1.00	1.00

Table 1: $r_{ee}(K)/r_{ee}(N)$ as a function of N and $Q = N/K$ at T=T_r for unscreened chains.

very high Q-values. As expected, in the presence of screening the blocking approach breaks down when the screening length becomes smaller than the blocked resolution. The results are nevertheless encouraging since even with strong screening (κ=1.992), $Q \leq 10$ is feasible.

When investigating the power of the method, the relevant parameter is $Q = N/K$. However, in addition one expects finite-N corrections due to end-point effects. This is illustrated in table 1, where the ratios between r_{ee} computed with blocked and standard method, $r_{ee}(K)$ and $r_{ee}(N)$ respectively, are shown for T=T_r and κ=0.0. As can be seen from table 1 finite N effects diminish as N increases and should not pose problems for large system sizes, $1000-10000$ monomers, at which the method is aimed.

We next compare the power of our blocking approach on r_{ee} and E_C for $T = T_r$ and κ=0.0 and 0.630 respectively. The results for r_{ee} can be found in figs. 1 and 2. The corresponding energies, which very well approximate the "true" MC values, are found in table 2.

	N	80	160	320	512	1024	2048
κ=0.0	E_C (K)	2.46	2.76	3.04	3.22	3.48	3.72
	(N)	2.46	2.76	3.04	3.22	3.48	3.73
κ=0.63	E_C (K)	0.47	0.50	0.54	0.56	0.58	
	(N)	0.47	0.48	0.48	0.48	0.48	

Table 2: Average internal Coulombic energies per monomer for unscreened and screened Coulomb potentials. N and K stands for full MC and blocked with $K = 50$ respectively.

As can be seen from fig. 1 and table 2 the r_{ee} and E_C are amazingly well described by the blocked approach for the unscreened case. The value of r_{ee} is within 10% from the true value even for $Q \approx 100$. For even larger N the situation should be even better with diminishing finite N effects. Indeed, using

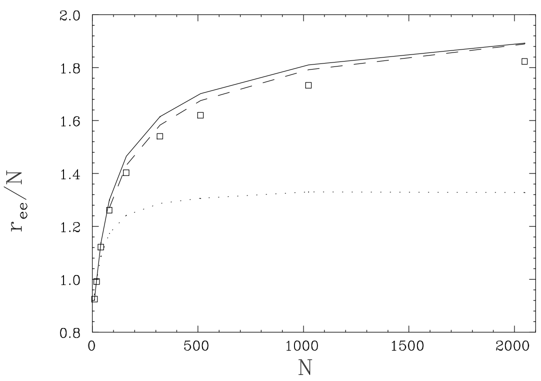

Figure 1: r_{ee}/N as a function of N for an unscreened Coulomb chain. Full and dashed lines denote K=20 and K=50 blocked MC runs including logarithmic correction respectively. Also shown as dotted lines are the naive blocked results for K=20. The squares denote results from original MC runs with N degrees of freedom.

κ	r_{ee}(N)	Q	r_{ee}(K)	% diff	Q	r_{ee}(K)	% diff
0.1992	185	4	186	0.6	8	187	1.1
0.630	104	4	105	1.0	8	110	5.8
1.992	61	4	62	1.6	8	68	11.4

Table 3: Comparison of r_{ee}(K,N) and $r_{ee}(N, N)$ for N=512 screened chains with Q=4 and 8.

the blocked method we have estimated r_{ee} and E_C for a N=10000 unscreened chain with K=250 and find r_{ee}/N = 2.04 and E_C/N = 4.25. The relative errors should be less than those found for K = 50 and N = 2048: 3.6% for r_{ee} and 0.3% for E_C. The computational speedup here is substantial, growing as Q^3.

For the screened case (see fig. 2) the approximation is less accurate but still good enough to be of practical relevance. In table 3 detailed comparisons are made for Q=4 and 8 for different screening strengths. As can be seen there, the blocking gives a reasonable approximation even for Q=8, giving a speedup factor of 512.

The approximation is of course not relevant for quantities more local than the blocking allows for.

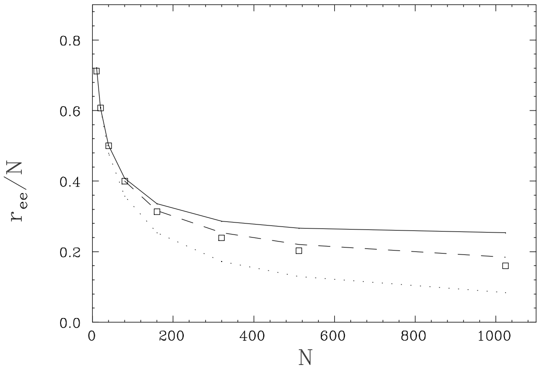

Figure 2: r_{ee}/N as a function of N for a κ=0.630 screened Coulomb chain. Same notation as in fig. 1.

In summary, we have developed an efficient Monte Carlo blocking scheme that allows for estimating certain thermodynamical quantities of polyelectrolytes with very substantial computational speedup factors for temperatures around T_r. The method is excellent for unscreened chains, but even with screening non-neglible savings result.

Our method is of course not confined to Monte Carlo implementations. Other schemes, like Molecular Dynamics, will benefit from it as well.

Acknowledgment:

We thank Bo Jönsson for valuable comments on the manuscript.

References

[1] B. Jönsson, C. Peterson and B. Söderberg, *J. Phys. Chem.* **99**, 1251 (1995).

[2] M. Lal, *Mol. Phys.* **17**, 57 (1969);
N. Madras and A.D. Sokal, *J. Stat. Phys.* **50**, 109 (1988). **50**, 109 (1988).

[3] A. Irbäck, *J. Chem. Phys.* **101**, 1661 (1994).

[4] B. Jönsson, C. Peterson and B. Söderberg, *Phys. Rev. Lett.* **71**, 376 (1994).

[5] C. Peterson, O. Sommelius and B. Söderberg, "Scaling and Scale Breaking in Polyelectrolytes", *LU TP 95-25* (to be submitted to *J. Chem. Phys*).

[6] P.G. deGennes, *Scaling Concepts in Polymer Physics*, Cornell University Press, Ithaca 1979.

Paper IV

LU TP 95-25
February 1996

Scaling and Scale Breaking in Polyelectrolytes

Carsten Peterson[1], Ola Sommelius[2] and Bo Söderberg[3]
Department of Theoretical Physics, University of Lund
Sölvegatan 14A, S-223 62 Lund, Sweden

Journal of Chemical Physics **105**, 5233 (1996)

Abstract:

We consider the thermodynamics of a uniformly charged polyelectrolyte with harmonic bonds. For such a system there is at high temperatures an approximate scaling of global properties like the end-to-end distance and the interaction energy with the chain-length divided by the temperature. This scaling is broken at low temperatures by the ultraviolet divergence of the Coulomb potential. By introducing a renormalization of the strength of the nearest-neighbour interaction the scaling is restored, making possible an efficient blocking method for emulating very large polyelectrolytes using small systems.

The high temperature behaviour is well reproduced by the analytical high-T expansions even for fairly low temperatures and system sizes. In addition, results from low-T expansions, where the coefficients have been computed numerically, are presented. These results approximate well the corresponding Monte Carlo results at realistic temperatures.

A corresponding analysis of screened chains is performed. The situation here is complicated by the appearance of an additional parameter, the screening length. A window is found in parameter space, where scaling holds for conformational as well as thermodynamical properties. This window corresponds to situations where the range of the potential interpolates between the bond length and the size of the chain. This scaling behaviour, which is verified by Monte Carlo results, is, for the end-to-end distance, consistent with Flory scaling. Also for the screened chain a blocking approach can be devised, that performs well for low temperatures, whereas the low-T expansion is inaccurate at realistic temperatures.

[1]carsten@thep.lu.se
[2]ola@thep.lu.se
[3]bs@thep.lu.se

1 Introduction

Thermodynamical properties of uniformly charged polyelectrolytes consisting of linear chains of monomers, with covalent harmonic bonding forces and Coulomb interactions (screened or unscreened), have been extensively studied e.g. with Monte Carlo methods [1, 2, 3, 4, 5, 6] and variational techniques [7, 5]. Less attention has been paid to the low-T and high-T expansions for these systems. To some extent the lack of interest in these two limits has been motivated by the conjecture that "realistic" temperatures fall outside the range of such expansions.

In this work we study the scaling properties of polyelectrolytes starting out from systematic studies of the low-T and high-T expansions both for Coulomb and screened chains. The latter are based upon perturbative treatment of the interaction. Extensive Monte Carlo (MC) calculations are used to evaluate the results.

For the Coulomb chain in dimensionless units there are only two parameters, the number of monomers N and the temperature T. For global quantities such as the end-to-end distance r_{ee} and the interaction energy it turns out that one has approximate scaling for large *rescaled temperatures* $\hat{T} = T/N$. This scaling is broken at low temperatures due to the short-distance divergence of the Coulomb energy. By appropriate renormalization of the harmonic and Coulomb terms and by introducing an additional corrective nearest-neighbor interaction, a blocking scheme results that allows for fairly accurate MC calculations of very large systems with quite modest computational investments [8]. Superficially, this might seem reminiscent of the well-known blob picture of de Gennes [9]. Renormalization group techniques have also been used in the context of polyelectrolytes to extend $(4-\epsilon)$ expansions to d=3 [10]. The idea here is however not to iterate the blocking procedure to a fixed point, but to obtain an effective Hamiltonian with fewer degrees of freedom than the original Hamiltonian. Thus, e.g., when emulating a N=2048 system at room temperature using a system of 50 blocked monomers, approximately a factor 70000 is gained in computing speed at the modest expense of 3.6% error in r_{ee} [8]. At large N the rescaled temperature becomes small and hence one should be able to estimate the thermodynamical quantities using a low-T expansion. Such expansions are systematically developed, and when evaluating the coefficients numerically one is indeed able to compute r_{ee} within 3% for large systems at room temperatures.

For a Debye-Hückel screened chain the situation is quite different. In addition to the parameters N and T one has the Debye screening parameter κ, introducing an additional length scale for the chain. For large κ-values the potential is short range and the chain is essentially Brownian, whereas for low κ the Coulombic chain is recovered. As $N \to \infty$ for fixed (κ, T), scaling relations are obtained, consistent with Flory scaling [11]. When the range of the potential is much larger than the average bond length, but much smaller than the overall chain size, a high temperature expansion indicates a simple dependence on the combination $N/\kappa^4 T^5$ of the deviation from Brownian behaviour, as measured by r_{ee}^2/NT. The blocking approach works reasonably well also for the screened case, at least for relatively low temperatures, despite less firm theoretical foundation. The low-T expansions of global quantities, r_{ee} and the energy, do not provide as accurate results as in the Coulomb case.

Due to the different nature of the unscreened Coulomb and Debye screened chains our presentation is structured such, that each of the two systems is dealt with separately in a self-contained way. We also include in one of the appendices underlying details of the blocking approach[8].

The paper is organized as follows: In Section 2 the Coulomb model is presented together with scaling and scale breaking properties and numerical results. The corresponding discussion and results for the screened chain can be found in Section 3. In Section 4 a brief summary is given. Most of the details concerning high- and low-T expansions are given in the Appendix A and B respectively.

2 The Coulomb Chain

2.1 The Model

In terms of dimensionless quantities, the energy of a Coulomb chain is given by [5]

$$E^{(N)} \;=\; E_G + E_C \;=\; \frac{1}{2}\sum_{i=1}^{N-1} \mathbf{r}_i^2 + \sum_{\sigma} \frac{1}{r_\sigma} \tag{1}$$

where instead of the absolute monomer positions $\mathbf{x}_i$, the *bond vectors*

$$\mathbf{r}_i \equiv \mathbf{x}_{i+1} - \mathbf{x}_i, \quad i = 1, \ldots, N-1 \tag{2}$$

are used, and where σ runs over contiguous non-nil sub-chains, with

$$\mathbf{r}_\sigma \equiv \sum_{i \in \sigma} \mathbf{r}_i \tag{3}$$

corresponding to the distance vector between the endpoints of the subchain.

Due to the simple properties of the Hamiltonian under rescaling of the coordinates, the thermal expectation values for E_G and E_C are related by a simple virial identity [5],

$$2\langle E_G \rangle - \langle E_C \rangle \;=\; 3(N-1)T \tag{4}$$

2.2 Zero Temperature

At zero temperature, the polymer is locked in a minimum energy configuration: an aligned configuration with the nearest-neighbour distances b_i satisfying

$$b_i \;=\; \sum_{\sigma \ni i} \frac{1}{b_\sigma^2} \tag{5}$$

By assuming that the bond length is locally approximately constant, this is solved by [5]

$$b_i \approx \left\{ \log \left(C \frac{i(N-i)}{N} \right) \right\}^{1/3} \tag{6}$$

with $C = \exp(1+\gamma) \approx 4.8$ (γ is Euler's constant ≈ 0.5772). For r_{ee}, E_G and E_C, this implies

$$\begin{aligned} r_{ee} &\approx N \left(\log N\right)^{1/3} \\ E_G &\approx \frac{1}{2} N \left(\log N\right)^{2/3} \\ E_C &\approx N \left(\log N\right)^{2/3} \end{aligned} \tag{7}$$

consistently with the virial identity (eq.(4)) with $T = 0$.

2.3 Low Temperature Expansions

At low temperature, one can make an expansion around the minimum energy configuration. Counting degrees of freedom, removing three for translational invariance and two for rotational symmetry, we have

$$\langle E \rangle \;=\; E_0 + \frac{1}{2}\left(3N-5\right) T + O\left(T^2\right) \tag{8}$$

Using this in combination with the virial identity (eq. (4)), we obtain for the partial energies, E_C and E_G,

$$\begin{aligned} \langle E_C \rangle &= \frac{2}{3} E_0 - \frac{2}{3} T + O\left(T^2\right) \\ \langle E_G \rangle &= \frac{1}{3} E_0 + \left(\frac{3}{2} N - \frac{11}{6} \right) T + O\left(T^2\right) \end{aligned} \tag{9}$$

The corresponding expansions for the correlations $\langle \mathbf{r}_i \cdot \mathbf{r}_j \rangle$, needed e.g. for r_{ee}, can be found in Appendix A, eq. (A5). These expansions contain coefficients that have to be evaluated numerically.

2.4 High Temperature Expansions

In the high-T limit, the results for r_{ee} and E_C can be expanded in power series in $1/T$. For large N, the first few terms yield (see Appendix B)

$$\begin{aligned} \langle r_{ee}^2 \rangle &\approx 3NT + \frac{4}{15}\sqrt{\frac{2}{\pi}}\frac{N^{5/2}}{T^{1/2}} \\ \langle E_C \rangle &\approx \frac{4}{3}\sqrt{\frac{2}{\pi}}\frac{N^{3/2}}{T^{1/2}} \end{aligned} \tag{10}$$

The corresponding expansion for the bond energy E_G can be obtained from E_C using the virial identity (eq.(4)).

We note that the expressions are consistent with a simple scaling behaviour since for large N both r_{ee}/N and E_C/N are functions of the rescaled temperature, T/N, only. The relevant small parameter of the high-T expansion is obviously N/T. In Appendix B the high-T expansion is discussed in some detail.

2.5 Scaling From a Continuum Formulation

The scaling properties indicated by the high-T expansion can be understood as follows. For large N, we can approximate the discrete polymer by a continuous chain, by rescaling i, $\mathbf{x}_i$ and T,

$$\mathbf{x}_i = N\mathbf{y}\left(\frac{i}{N}\right), \quad T = N\hat{T} \tag{11}$$

in effect replacing the discrete index i by a continuous one, $\tau = i/N$, $0 < \tau < 1$. Then in terms of $\mathbf{y}(\tau)$, the Boltzmann exponent E/T is approximated by $\hat{E}/\hat{T}$, with the *effective continuum Hamiltonian* $\hat{E}$ given by

$$\hat{E}^{(N)} = \int_0^1 d\tau \frac{1}{2}\dot{\mathbf{y}}(\tau)^2 + \int_0^1 d\tau \int_{\tau+1/N}^1 \frac{d\tau'}{|\mathbf{y}(\tau') - \mathbf{y}(\tau)|} \tag{12}$$

The remaining N-dependence sits entirely in the short-distance cutoff, necessary to prevent a potential logarithmic divergence. Without the cutoff, the following naive scaling behaviour would be exact:

$$\langle E_C \rangle \approx Nf(\hat{T}), \quad \langle E_G \rangle \approx \frac{3}{2}N^2\hat{T} + \frac{1}{2}Nf(\hat{T}), \quad \langle r_{ee}^2 \rangle \approx N^2 g(\hat{T}) \tag{13}$$

Indeed, at high $\hat{T}$ the scale-breaking is not important; the singularity is washed out by the Brownian fluctuations. From the high-T expansions above, we infer the asymptotic behaviour of the scaling functions f and g:

$$\begin{aligned} f(\hat{T}) &\approx \frac{4}{3}\sqrt{\frac{2}{\pi}}\hat{T}^{-1/2} + O(\hat{T}^{-2}) & (14) \\ g(\hat{T}) &\approx 3\hat{T} + \frac{4}{15}\sqrt{\frac{2}{\pi}}\hat{T}^{-1/2} + O(\hat{T}^{-2}) \end{aligned}$$

At low T, on the other hand, the scaling is more seriously broken:

$$f_N(\hat{T}) \approx (\log N)^{2/3} - \frac{2}{3}\hat{T} \tag{15}$$

2.6 Blocking Degrees of Freedom

Neglecting the residual N-dependence in eq. (12), the scaling properties suggest the possibility of emulating a large system of N monomers by a blocked system of $K = N/Q < N$ effective monomers [8], using the following rescaled Hamiltonian for the latter:

$$E^{(K)}_{\mathrm{B,naive}} = \frac{1}{2Q'}\sum_{i=1}^{K-1} r^2_{i,i+1} + \frac{3}{2}(N-K)T \; + \; Q^2\sum_i\sum_{j>i}\frac{1}{|r_{ij}|} \tag{16}$$

where r_{ij} are distances between blocked monomers, each representing Q real monomers, while $Q' = (N-1)/(K-1)$. This simple renormalization technique should work well at high T, where the detailed short-distance properties of the chain are smoothed out by large fluctuations, and less well at low T.

However, the approach can be improved. The N-dependence in the effective continuum Hamiltonian, eq. (12), implies the discrepancy

$$\hat{E}^{(N)} - \hat{E}^{(K)} = \int_0^1 d\tau \int_{\tau+1/N}^{\tau+1/K} \frac{d\tau'}{|\mathbf{y}(\tau') - \mathbf{y}(\tau)|} \tag{17}$$

In the low-T regime, where the chain is more or less linear, the discrepancy is approximately given by

$$\hat{E}^{(N)} - \hat{E}^{(K)} \approx \log(N/K)\int_0^1 \frac{d\tau}{|\dot{\mathbf{y}}(\tau)|} \tag{18}$$

This indicates a possible low-T improvement to the blocking approach: simply add a corrective interaction term corresponding to eq. (18) to the blocked Hamiltonian:

$$\begin{aligned} E^{(K)}_{\mathrm{B}} &= E^{(K)}_{\mathrm{B,naive}} + \sum_{i=1}^{K} W(r_{i,i+1}) & (19) \\ W(r) &= \frac{Q^2\log(Q)}{r} & (20) \end{aligned}$$

With this improved blocked Hamiltonian, very large chains can be emulated (using MC) with relatively small blocked systems with quite small errors all the way down to $T = 0$ [8].

The correction term can also be derived directly for the discrete system by considering eq. (19), with an unspecified corrective nearest-neighbour interaction $W(r)$. At low temperatures we approximate the nearest-neighbour distance by a constant a. For the blocked system, the corresponding nearest-neighbour distance then is $b = Qa$. In this approximation, the Coulomb energy for large N is given by

$$U_N \approx \frac{N}{a}\sum_{l}^{N}\frac{1}{l} \approx \frac{N}{a}\log N \tag{21}$$

while the blocked interaction energy for large K reads

$$U_K \approx \frac{Q^2 K}{b}\log K + KW(b) \tag{22}$$

Choosing $W(r)$ such that $U_N = U_K$ for $b = Qa$ yields precisely eq. (20).

Appendix B contains a discussion of the high-T properties of the blocked system.

2.7 Numerical Comparisons

In this section we compare the results from the high- and low-T expansions as well as scaling properties with MC data. All MC calculations, both for Coulomb and screened chains (see next section) were performed using the pivot algorithm [12]. Most results are based on 10^4 thermalization sweeps and 10^5 measured configurations. Some earlier MC results were used[5]. Results from exploring the blocking method have previously been reported [8].

2.7.1 Low T Results

It is of interest to investigate what low T means in terms of physical temperatures. In the dimensionless units of eq. (1), room temperature (290K) corresponds to T_r=0.837808. We have computed r_{ee}/N , where $r_{ee}=\sqrt{\langle r_{ee}^2\rangle}$, using the low-$T$ expansion corresponding to eq. (A5) for different chain sizes N at $T = T_r$. In fig. 1, comparisons are made between these low-T results and MC data. Also shown in fig. 1 is the T=0 solution (cf. eq. (7)). Not surprisingly the low-T approximation becomes more accurate as N increases since it corresponds to a lower $\hat{T}$. For N=1024 the error is less than 3%, which is quite impressive. Computing r_{ee} for N=1024 using eq. (A5) is $\sim$ 200 times faster than using MC. The computational demand for both methods grows like N^3.

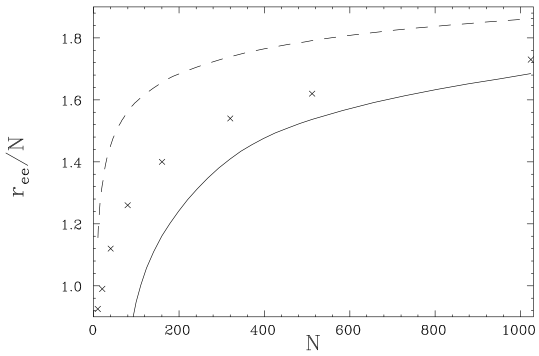

Figure 1: r_{ee}/N as a function of N for a Coulomb chain at $T{=}T_r$. Dashed line, full line and crosses represent $T{=}0$ (eq. (7)), first order low-T expansion (eq. (A5)) and MC results, respectively.

2.7.2 Scaling

Next we test the scaling properties expected from the high temperature expansions (eq. (10) and Appendix B) against numerical results. In figs. 2 and 3, r_{ee}/N and E_C/N are shown as functions of $\hat{T} = N/T$. The predictions from the high-T expansion for r_{ee} fit extremely well for $\hat{T} > 0.2$, whereas for E_C the validity region of this expansion is located at much larger $\hat{T}$. Also shown are the finite-N effects from eqs. (B5,B6), which are larger for E_C than for r_{ee} as can be understood from eqs. (B2,B5,B6). The deviation from scaling in fig. 3 for $\hat{T} > 1$ is almost entirely due to finite-N effects.

3 Debye Screened Chains

Next we turn to the case of the Coulomb chain being screened by the surrounding medium. We model this effect by using the Debye-Hückel potential (being fully aware of its limitations).

3.1 The Model

The energy of the Debye screened chain takes the following form [5]:

$$E(\mathbf{r}) = E_G + E_C = \frac{1}{2}\sum_{i=1}^{N-1} \mathbf{r}_i^2 + \sum_{\sigma} \frac{e^{-\kappa r_\sigma}}{r_\sigma} \tag{23}$$

where the additional parameter κ is the inverse screening length. In what follows we assume that κ is independent of T.

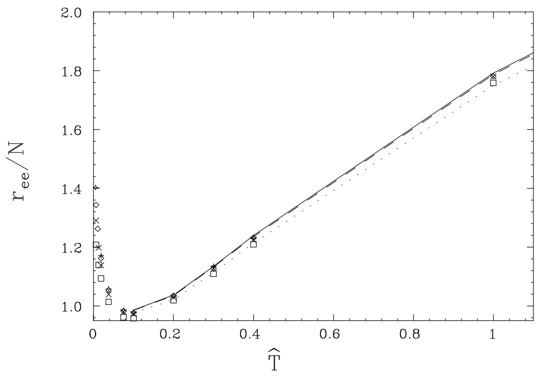

Figure 2: r_{ee}/N as a function of $\hat{T}$ for a Coulomb chain from MC results for N=20 (□), 40 ($\times$), 80 ($\diamond$) and 160 ($+$). The lines show second order high-T expansion results for N=20 (dotted), 80 (dashed) and ∞ (full) from eqs. (B5,B6).

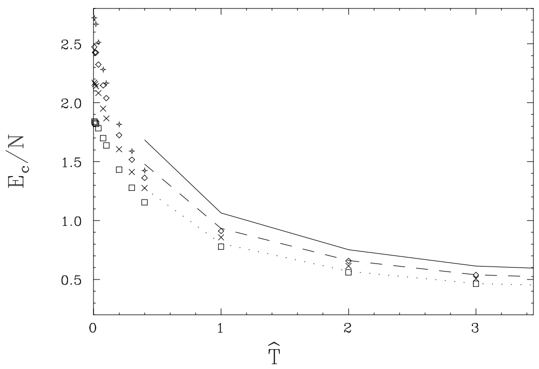

Figure 3: E_C/N as a function of $\hat{T}$ for a Coulomb chain from MC results for N=20 (□), 40 ($\times$), 80 ($\diamond$) and 160 ($+$). The lines show leading order high-T results for N=20 (dotted), 80 (dashed) and ∞ (full) from eqs. (B5,B6).

In the screened case, a proper virial identity relating the average bond and interaction energies does not exist (cf. eq. (4)). Still, one has the slightly less useful identity [5].

$$2\langle E_G\rangle - \langle E_C\rangle - \kappa\left\langle\sum_\sigma e^{-\kappa r_\sigma}\right\rangle = 3(N-1)T \tag{24}$$

3.2 Zero Temperature

Since the screened interaction is short-range, the ground-state configuration can, for large enough N, be considered translation-invariant, with a constant, N-independent nearest-neighbour distance a. The energy then becomes

$$E \approx N\left(\frac{a^2}{2} + \frac{1}{a}\sum_{l=1}^{\infty}\frac{e^{-\kappa a l}}{l}\right) \tag{25}$$

which upon minimization gives (defining $\eta \equiv \kappa a$)

$$a^3 = \frac{\eta}{e^{\eta}-1} - \log(1-e^{-\eta}) \tag{26}$$

valid for $N\eta \gg 1$. This gives a implicitly as a function of κ, and we have, for small κ:

$$\begin{aligned} a &\approx (-\log\eta)^{1/3} \\ \kappa &\approx \frac{\eta}{(-\log\eta)^{1/3}} \\ \Rightarrow a &\approx (-\log\kappa)^{1/3} \end{aligned} \tag{27}$$

while for large κ, we obtain

$$\begin{aligned} a &\approx \left((\eta+1)e^{-\eta}\right)^{1/3} \\ \kappa &\approx \frac{\eta}{\left((\eta+1)e^{-\eta}\right)^{1/3}} \\ \Rightarrow a &\approx 3\frac{\log\kappa}{\kappa} \end{aligned} \tag{28}$$

Similarly, we have for the energy per monomer

$$E_G/N = \frac{a^2}{2} \tag{29}$$

$$E_C/N = -\frac{1}{a}\log\left(1-e^{-\eta}\right) \tag{30}$$

3.3 Low Temperature Expansions

Also in the screened case, observables can be expanded in a low temperature series, analogous to the Coulomb case, although the details are slightly modified (cf. Appendix A). The expression for $\langle E\rangle$, eq. (8), depends only on the number of degrees of freedom and is still valid, while the expressions for $\langle E_C\rangle$ and $\langle E_G\rangle$ separately (eqs. A13, A14) are less transparent than the corresponding unscreened equations (9).

3.4 High Temperature Expansions

Assuming a T-independent κ, and a large N, we have in the high-T limit

$$\langle r_{ee}^2 \rangle \approx 3(N-1)T + 4\sqrt{\frac{2}{\pi}} N^{3/2} \kappa^{-2} T^{-3/2} \tag{31}$$

$$\langle E_C \rangle \approx \zeta(\frac{3}{2}) \sqrt{\frac{2}{\pi}} N \kappa^{-2} T^{-3/2} \tag{32}$$

while $\langle E_G \rangle$ in this limit is given by $\frac{3}{2}(N-1)T + \frac{3}{2}\langle E_C \rangle$. In this case, there are no obvious scaling properties.

A Flory estimate of the free energy for the Debye-Hückel potential gives a radius of the chain

$$r \sim \frac{N^{3/5}}{\kappa^{2/5}} \tag{33}$$

indicating that the chain will behave like a self-avoiding walk in the large-N limit. Both Flory scaling and the leading order terms in the high temperature expansion, eq. (31), are consistent with a more general scaling behaviour:

$$\frac{r^2}{NT} \sim f\left(\frac{N}{\kappa^4 T^5}\right) \tag{34}$$

where the function $f(x)$ behaves as $3 + 3.2\, x^{1/2}$ for small x, while an asymptotic behaviour $f(x) \sim x^{1/5}$ would correspond to Flory scaling.

Scaling window

A reasonable assumption is that the relevant scaling region is where the range of the potential is small compared to the chain size, and large compared to the monomer-monomer separation, i.e.

$$1 \ll \kappa^2 NT \ll N \tag{35}$$

In this window, the leading expression for $\langle E_C \rangle$, eq. (32), has to be modified (see Appendix B) into

$$\langle E_C \rangle \approx 2N\kappa^{-1}T^{-1} \tag{36}$$

with $\langle E_G \rangle = \frac{3}{2}(N-1)T + \langle E_C \rangle$, while the expression for $\langle r_{ee}^2 \rangle$, eq. (31), is unaffected.

This is consistent with a naive scaling behaviour stemming from the continuum formulation

$$\hat{E}^{(N)} = \int_0^1 d\tau \frac{1}{2} \dot{\mathbf{y}}(\tau)^2 + \int_0^1 d\tau \int_{\tau+1/N}^1 d\tau' \frac{e^{-\hat{\kappa}|\mathbf{y}(\tau') - \mathbf{y}(\tau)|}}{|\mathbf{y}(\tau') - \mathbf{y}(\tau)|} \tag{37}$$

with $\hat{\kappa} = N\kappa$, when ignoring the short distance cutoff $1/N$, i.e.

$$\langle E_C \rangle \approx N f(\hat{\kappa}, \hat{T}), \quad \langle r_{ee}^2 \rangle \approx N^2 g(\hat{\kappa}, \hat{T}) \tag{38}$$

where f and g are given by eqs. (31,36)

$$\begin{aligned} f(\hat{\kappa}, \hat{T}) &\approx 2\hat{\kappa}^{-1}\hat{T}^{-1} \\ g(\hat{\kappa}, \hat{T}) &\approx 3\hat{T} + 4\sqrt{\frac{2}{\pi}}\hat{\kappa}^{-2}\hat{T}^{-3/2} \end{aligned} \tag{39}$$

3.5 Blocking Degrees of Freedom

Despite the fact that the linear chain approximation is of more limited validity in the screened case, one still can devise a blocking approach. Indeed, for low enough temperatures the approach works quite well [8].

In this case the discrete derivation of the correction term is more convenient. Again, starting out from a discrete blocked energy

$$E_{\mathrm{B}}^{(K)} = \frac{1}{2Q}\sum_{i=1}^{K-1} r_{i,i+1}^2 + \frac{3}{2}(N-K)T \,+\, Q^2\sum_i\sum_{j>i}\frac{e^{-\kappa r_{ij}}}{r_{ij}} + \sum_{i=1}^{K} W(r_{i,i+1}) \tag{40}$$

following the same steps as in the unscreened case, one arrives at

$$W(r) = -\frac{Q^2}{r}\left[\log\left(1 - e^{-\kappa r/Q}\right) - \log\left(1 - e^{-\kappa r}\right)\right] \tag{41}$$

In this way, the longitudinal behaviour will be rather accurately reproduced by the blocked system. However, at low T, the transverse fluctuations will dominate, as indicated by eq. (A9) and the subsequent discussion. These are probably more difficult to reproduce than the longitudinal fluctuations.

3.6 Numerical Comparisons

In this section we investigate the validity regime of the high- and low-temperature expansions of r_{ee} for the screened chain. In addition, we test the approximate scaling indicated by eq. (34), and the corresponding scale-breaking arising outside the scaling window given by eq. (35).

In fig. 4 the high- and low-T expansions of the end-to-end distance, eqs. (31, A12), are compared to MC data. Clearly, an increase in κ enlarges the high-T interval and decreases the low-T interval. Quantities at room temperature T_r, for biologically relevant values of κ, are hard to estimate from both high- and low-T expansions.

The approximate scaling as suggested by high temperature expansions and supported by Flory arguments (eq. (34)) is shown in fig. 5 to hold almost too

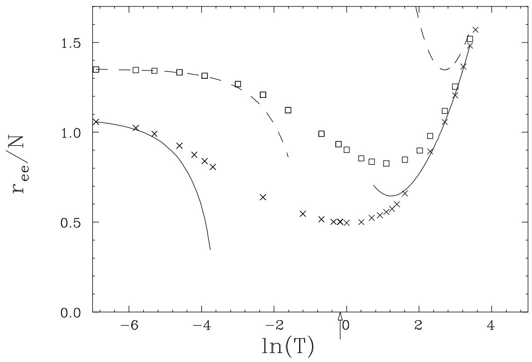

Figure 4: r_{ee}/N as a function of T for a screened, N=40, Coulomb chain with $\kappa = 0.1(\Box)$ and 0.63 $(\times)$. The lines show second order high-T expansion results (κ=0.1 (dashed), 0.63 (solid)) and the corresponding first order low-T expansions. T_r is marked with an arrow.

good for the somewhat arbitrary cut $N\kappa^2 T \in (8, 0.3N)$. In fig. 6 the deviation from this behaviour is shown by plotting $\ln(r_{ee}^2/NT)$ as a function of $\ln N\kappa^2 T$ for fixed values of $N/(\kappa^4 T^5)$. Small values of $N\kappa^2 T$ then are equivalent to a high temperature Coulombic limit, while large values ($\gg N$) correspond to a low temperature Gaussian limit. Hence in both limits the curve approaches the Gaussian value, which is $\ln 3$.

A noticeable feature of fig. 6 is the seemingly N-independent rise to the left, indicating that in this region $\langle r_{ee}^2 \rangle$ depends only on $N/\kappa^4 T^5$ and $N\kappa^2 T$, or, equivalently, on $\hat{T} = T/N$ and $\hat{\kappa} = N\kappa$. This is equivalent to stating that a naive (i.e. without the extra nearest-neighbour term) blocking approach should work well there. The scale-breaking seen in the right part of fig. 6, where the curves bend downwards, occurs when $N\kappa^2 T$ becomes comparable to N, violating the assumed scaling condition, eq. (35). For an infinite N, this scale-breaking would be absent, and the corresponding curve would never bend down.

4 Summary

Scaling and scale-breaking properties of thermodynamic and conformational properties for simple models of charged polymer chains have been established. These properties are deduced from high-and low-T expansions by means of a perturbative treatment of the interaction for both Coulomb and Debye-Hückel screened chains. In addition to the naive high-T limit with fixed κ for the screened chains we also consider a restricted limit where $T \to \infty$ and $\kappa \to 0$

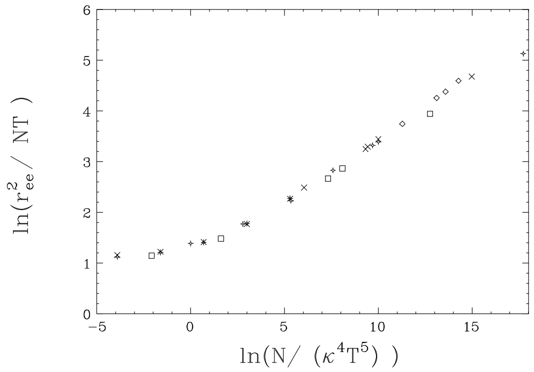

Figure 5: $\ln r_{ee}^2/NT$ as a function of $\ln N/\kappa^4 T^5$ with $N\kappa^2 T \in (8, 0.3N)$.

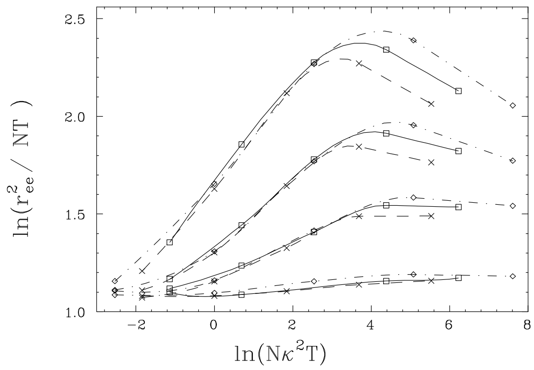

Figure 6: $\ln(r_{ee}^2/NT)$ as a function of $\ln(N\kappa^2 T)$. The four collections of curves correspond to four different values of $\ln N/(\kappa^4 T^5)$: from top to bottom 5.30, 2.99, 0.69 and -3.91 for $N = 40(\square)$, $80(\times)$ and $160(\diamond)$. The lines are only intended to guide the eye.

while keeping $N\kappa^2 T$ large and $\kappa^2 T$ small.

For the Coulomb chain, an increase in N makes the chain stiffer due to the long-range character of the electrostatic interaction. The same effect is obtained by lowering the temperature; indeed, thermodynamic quantities for long chains are well approximated by a low-temperature expansion. The relevant variable of the chain is the rescaled temperature $\hat{T} = T/N$, as further supported by high-T expansions which for large N become equivalent to high-$\hat{T}$ expansions.

For the screened chain the situation is somewhat different due to the appearance of a new length scale – the inverse screening length κ^{-1}. For κ^{-1}-values in a window between the bond length and the chain length, scaling, i.e. dominating contributions from large length scales, are observed both for conformational and thermodynamical observables.

The scaling properties in terms of $\hat{T} = T/N$ provides a firm theoretical basis for the real space blocking scheme[8]; a detailed derivation is given. As reported[8] this approach is very powerful for computing r_{ee} and E_C, both for Coulomb and screened chains, with low errors. Nothing prohibits the extension of the blocking scheme to include titration and multi-chain systems.

For relatively small temperatures, the low-T expansion[5] is further developed into an efficient computational tool for computing conformational properties. In the Coulomb case results at room temperatures with low errors emerge from this scheme. For the screened case the low-T approach is not viable, at least for reasonable values of N, T and κ.

Appendix A. Low T Expansions

Coulomb Chains

This section has a certain unavoidable overlap with a previous paper[5]. Low-T expansions for $\langle E_C \rangle$ and $\langle E_G \rangle$ are given in eq. (9). Computing low-T corrections to r_{ee} is somewhat more elaborate.

In terms of the zero temperature bond lengths defined by $b_i \equiv \sum_{\sigma \ni i} \frac{1}{b_\sigma^2}$ we define the tensors

$$
\begin{aligned}
B_{ij} &= \sum_{\sigma \ni i,j} \frac{1}{b_\sigma^3} && \text{(A1)} \\
C_{ijk} &= \sum_{\sigma \ni i,j,k} \frac{1}{b_\sigma^4} && \text{(A2)}
\end{aligned}
$$

In addition, we need the two matrices related to B,

$$
\begin{aligned}
U &= (1+2B)^{-1} && \text{(A3)} \\
V &= P(1-B)^{-1}P && \text{(A4)}
\end{aligned}
$$

where P denotes the projection matrix onto the subspace orthogonal to b, which is a zero-mode of $1-B$. The transverse fluctuations (V) will dominate the expansion due to the presence of eigenvalues of B close to one.

In terms of these tensors, we have the quadratic expectation-values at low-T:

$$
\begin{aligned}
\langle \mathbf{r}_i \cdot \mathbf{r}_j \rangle &= b_i b_j + T \Bigg(U_{ij} + 2V_{ij} + \frac{4 b_i b_j}{3 \sum_k b_k^2} \\
&\quad + 3 \sum_{klm} C_{klm} (b_i U_{jk} + b_j U_{ik})(U_{lm} - V_{lm}) \Bigg) + O(T^2) \qquad \text{(A5)}
\end{aligned}
$$

where the first two terms of the T coefficient are the naive contributions from the longitudinal and transverse fluctuations. The rest are corrections due to the rotational degeneracy of the $T=0$ configuration, which is also responsible for the transverse zero-modes (of $1-B$). In terms of this expression, $\langle r_{ee}^2 \rangle$ is obtained by summing independently over i and j, while $\langle E_G \rangle$ is obtained by summing over $i=j$ and dividing by two. The summation for $\langle E_G \rangle$ can be done exactly

$$
\begin{aligned}
\sum_{i=j} \langle r_i \cdot r_j \rangle &= \sum b_i^2 + T \left(\mathrm{Tr}\ (U+2V) + \frac{4}{3} + 2 \sum_{klm} C_{klm} b_l (U_{lm} - V_{lm}) \right) \\
&= \sum b_i^2 + T \left(\mathrm{Tr}\ \{(1+2B)U + 2(1-B)V\} + \frac{4}{3} \right)
\end{aligned}
$$

$$= \sum b_i^2 + T\left(3N - \frac{11}{3}\right) \tag{A6}$$

and again the result of eq. (9) is obtained.

Screened Chains

For a screened chain, with b_i still denoting the (now κ dependent) zero temperature bond lengths, the tensors take the following form

$$B = \sum_{\sigma \ni i,j} \frac{e^{-\kappa b_\sigma}}{b_\sigma^3}(1 + \kappa b_\sigma) \tag{A7}$$

$$U = \left(1 + \kappa^2 \sum_{\sigma \ni i,j} \frac{e^{-\kappa b_\sigma}}{b_\sigma} + 2B\right)^{-1} \tag{A8}$$

$$V = P(1-B)^{-1}P \tag{A9}$$

The dominance by the transverse fluctuations in the expansions will in the screened case be even more pronounced since the off-diagonal values of B are exponentially suppressed. Two versions of the C-tensor are needed, one related only to parallel fluctuations $C^{(ppp)}$ and the other, $C^{(ptt)}$, coupled to one parallel and two transverse fluctuations.

$$C_{ijk}^{(ptt)} = \sum_{\sigma \ni i,j,k} \frac{e^{-\kappa b_\sigma}}{b_\sigma^4}\left(1 + \kappa b_\sigma + \frac{\kappa^2 b_\sigma^2}{3}\right) \tag{A10}$$

$$C_{ijk}^{(ppp)} = \sum_{\sigma \ni i,j,k} \frac{e^{-\kappa b_\sigma}}{b_\sigma^4}\left(1 + \kappa b_\sigma + \frac{\kappa^2 b_\sigma^2}{2} + \frac{\kappa^3 b_\sigma^3}{6}\right) \tag{A11}$$

In terms of these tensors we have, to first order in the low-T expansion, the expectation values

$$\begin{aligned}\langle \mathbf{r}_i \cdot \mathbf{r}_j \rangle = \; & b_i b_j + T\Bigg(U_{ij} + 2V_{ij} + 2\frac{\sum_k b_k\,(b_j U_{ik} + b_i U_{jk})}{\sum b_k^2} \\ & + 3\sum_{klm}\left(C_{klm}^{(ppp)} U_{lm} - C_{klm}^{(ptt)} V_{lm}\right)(b_j U_{ik} + b_i U_{jk})\Bigg)\end{aligned} \tag{A12}$$

$$
\begin{aligned}
\langle E_C \rangle &= \sum_\sigma \frac{e^{-\kappa b}}{b} \\
&\quad -T \sum_i \left(2\frac{\sum_j b_i b_j U_{ij}}{\sum b_k^2} + 3\sum_{klm} \left(C^{(ppp)}_{klm} U_{lm} - C^{(ptt)}_{klm} V_{lm} \right) b_i U_{ik} \right) \\
&\quad -\frac{T}{2} \left(\mathrm{Tr}\ U + 2\mathrm{Tr}\ V \right) + \frac{3N-5}{2} T \qquad \text{(A13)} \\
\langle E_G \rangle &= \frac{1}{2} \sum_i b_i^2 \\
&\quad +T \sum_i \left(2\frac{\sum_j b_i b_j U_{ij}}{\sum b_k^2} + 3\sum_{klm} \left(C^{(ppp)}_{klm} U_{lm} - C^{(ptt)}_{klm} V_{lm} \right) b_i U_{ik} \right) \\
&\quad +\frac{T}{2} \left(\mathrm{Tr}\ U + 2\mathrm{Tr}\ V \right) \qquad \text{(A14)}
\end{aligned}
$$

Appendix B. High T Expansions

Sums at large N

In what follows, we will encounter sums over subchains like the following for large N

$$
S_\alpha \equiv \sum_\sigma L_\sigma^\alpha \equiv \sum_{k=1}^{N} (N-k) k^\alpha \qquad \text{(B1)}
$$

where L_σ is the length (i.e. the number of bonds) of the subchain σ. Obviously, there exist $N-k$ distinct subchains of length k.

In particular, we will encounter the following sums:

$$
\begin{aligned}
S_{1/2} &= \frac{4}{15} N^{5/2} + BN - \frac{1}{12} N^{1/2} - A + \dots \\
S_{-1/2} &= \frac{4}{3} N^{3/2} + CN - B - \frac{1}{12} N^{-1/2} + \dots \qquad \text{(B2)} \\
S_{-3/2} &= DN - 4N^{1/2} - C - \frac{1}{12} N^{-3/2} + \dots
\end{aligned}
$$

where the numerical values of the constants A, B, etc. are

$$
A \approx -.02548, \quad B \approx -.20789, \quad C \approx -1.46035, \quad D \equiv \zeta(3/2) \approx 2.612375 \qquad \text{(B3)}
$$

In addition, we need

$$
\zeta(3) \approx 1.202057 \qquad \text{(B4)}
$$

High T expansions for a Coulomb chain

For a system of N monomers, we have the following high-T expansions, which are obtained by considering the Coulomb interaction as a perturbation,

$$\begin{aligned}
\langle r_{ee}^2 \rangle &\approx 3(N-1)T + \sqrt{\frac{2}{\pi}} T^{-1/2} \sum_\sigma L_\sigma^{1/2} \\
\langle E_G \rangle &\approx \frac{3}{2}(N-1)T + \frac{1}{2}\sqrt{\frac{2}{\pi}} T^{-1/2} \sum_\sigma L_\sigma^{-1/2} \\
\langle E_C \rangle &\approx \sqrt{\frac{2}{\pi}} T^{-1/2} \sum_\sigma L_\sigma^{-1/2}
\end{aligned} \tag{B5}$$

At large N these simplify to

$$\begin{aligned}
\langle r_{ee}^2 \rangle &\approx 3(N-1)T + \frac{4}{15}\sqrt{\frac{2}{\pi}} T^{-1/2} N^{5/2} \\
\langle E_G \rangle &\approx \frac{3}{2}(N-1)T + \frac{2}{3}\sqrt{\frac{2}{\pi}} T^{-1/2} N^{3/2} \\
\langle E_C \rangle &\approx \frac{4}{3}\sqrt{\frac{2}{\pi}} T^{-1/2} N^{3/2}
\end{aligned} \tag{B6}$$

The corresponding high-T expansions for a blocked system ($N \to K = N/Q$) yield identical expressions to the order shown, as long as K is large. This can be understood by considering the blocked Hamiltonian of eq. (19), with E_G defined to include the constant $\frac{3}{2}(N-K)T$, and E_C to include the corrective nearest-neighbour interaction. The latter term, given by eq. (20), does not contribute in the high-T limit: it is needed only at low T.

Generic Perturbation Expansion for Screened Chain

For a Debye screened chain, one must distinguish between two distinct high-T limits – (1) the naive one, where $T \to \infty$ with a constant κ, and (2) a modified limit, corresponding to the scaling window, eq. (34), where $T \to \infty$ and $\kappa \to 0$ keeping $\kappa^2 T$ small and $N\kappa^2 T$ large. The latter of course requires a large N.

In both cases the analysis is based on a perturbative treatment of the interaction, which to a few orders yields the following results for a screened chain of N monomers.

$$\begin{aligned}
\langle r_{ee}^2 \rangle &\approx 3(N-1)T + \sqrt{\frac{2}{\pi}} \kappa^3 T \sum_\sigma L_\sigma^2 F_2(\kappa\sqrt{L_\sigma T}) \\
\langle E_G \rangle &\approx \frac{3}{2}(N-1)T + \frac{1}{2}\sqrt{\frac{2}{\pi}} \kappa^3 T \sum_\sigma L_\sigma F_2(\kappa\sqrt{L_\sigma T})
\end{aligned} \tag{B7}$$

$$\langle E_C \rangle \approx \sqrt{\frac{2}{\pi}}\kappa \sum_{\sigma} F_1(\kappa\sqrt{L_\sigma T})$$

where the $F_k()$ are erf-related functions, defined by

$$F_k(x) = (2k-1)!!\exp(x^2/2)\int_x^\infty dy\; y^{-2k}\exp(-y^2/2) \tag{B8}$$

At small x the leading order behaviour of F_1 and F_2 respectively are given by

$$F_1 \sim \frac{1}{x}, \quad F_2 \sim \frac{1}{x^3} \tag{B9}$$

while the corresponding high-x expansions are

$$F_1 \sim \frac{1}{x^3}, \quad F_2 \sim \frac{3}{x^5} \tag{B10}$$

Conventional High T expansion for a Screened Chain

In the $T \to \infty$ limit with a constant κ and a fixed large N, the argument $(\kappa\sqrt{L_\sigma T})$ of the F_k's in eqs. (B7) is always large and equations (B10) can be used. Then the sum in the expression for $\langle r_{ee}^2 \rangle$ is dominated by the large L terms (scaling) and can be approximated by an integral. In contrast, the sums in $\langle E_C \rangle$ and $\langle E_G \rangle$ are dominated by small L (no scaling), and must be explicitly summed. We thus obtain

$$\begin{aligned}
\langle r_{ee}^2 \rangle &\approx 3(N-1)T + 4\sqrt{\frac{2}{\pi}}N^{3/2}\kappa^{-2}T^{-3/2} \qquad \text{(B11)}\\
\langle E_G \rangle &\approx \frac{3}{2}(N-1)T + \frac{3}{2}\langle E_C \rangle \\
\langle E_C \rangle &\approx \zeta(\frac{3}{2})\sqrt{\frac{2}{\pi}}N\kappa^{-2}T^{-3/2}
\end{aligned}$$

The corresponding high-T expansions for a blocked system, based on eqs. (40, 41) with large K and large Q, yield for $\langle r_{ee}^2 \rangle$ the same as above. However, $\langle E_G \rangle$ and $\langle E_C \rangle$ become too large,

$$\begin{aligned}
\langle E_G \rangle &\approx \frac{3}{2}(N-1)T + \frac{3}{2}\langle E_C \rangle \qquad \text{(B12)}\\
\langle E_C \rangle &\approx \sqrt{\frac{2}{\pi}}\zeta\left(\frac{3}{2}\right)N\kappa^{-2}T^{-3/2}\left(Q^{-1/2} + \frac{\zeta(3)}{\zeta(\frac{3}{2})}Q^{3/2}\right)
\end{aligned}$$

This is due to an overshooting by the corrective term, eq. (41), which gives rise to the $Q^{3/2}$ term in the expression for $\langle E_C \rangle$. On the other hand, upon omitting the corrective term, $\langle E_C \rangle$ becomes too small by a factor $Q^{-1/2}$, due to the lack of scaling mentioned above. Obviously, for thermodynamic properties, the blocking method does not apply in this limit.

Modified High T expansion for Screened Coulomb

With the restriction of staying within the scaling window, $\kappa^2 T \ll 1 \ll N\kappa^2 T$, the sums in (B7) get contributions from both small and large arguments ($\kappa\sqrt{L_\sigma T}$) and one cannot solely rely on the large argument expansions. In turns out however that in a continuum approximation i.e. $\sum_\sigma f(L_\sigma) \rightarrow \int_1^N (N-L)f(L)dL$ the integrals can be performed exactly and one finds that all three sums scale, i.e. they are dominated by the large-L terms. While the expression for $\langle r_{ee}^2\rangle$ remains unchanged, we obtain for $\langle E_G\rangle$ and $\langle E_C\rangle$ in this limit

$$\begin{aligned} \langle E_G \rangle &\approx \frac{3}{2}(N-1)T + \langle E_C\rangle \\ \langle E_C \rangle &\approx 2N\kappa^{-1}T^{-1} \end{aligned} \qquad \text{(B13)}$$

For a system blocked into K effective monomers, these expressions are reproduced, provided also the blocked system is in the scaling window, i.e. if $\kappa^2 TQ \ll 1$; otherwise it yields to too small values for $\langle E_C\rangle$ and $\langle E_G\rangle$.

References

[1] G. A. Christos and S. L. Carnie, *J. Chem. Phys.* **91**, 439 (1989).

[2] H.H. Hooper and H.W. Blanch and J. M. Prausnitz, *Macromolecules* **23**, 4820 (1990).

[3] P.G. Higgs and H. Orland *J. Chem. Phys.* **95**, 4506 (1991).

[4] M. Ullner and B. Jönsson and P.-O. Widmark, *J. Chem. Phys.***100**, 3365 (1994).

[5] B. Jönsson, C. Peterson and B. Söderberg, *J. Phys. Chem.* **99**, 1251 (1995).

[6] M.J. Stevens and K. Kremer, *J. Chem. Phys.* **1669**, 4 (1995).

[7] B. Jönsson, C. Peterson and B. Söderberg, *Phys. Rev. Lett.* **71**, 376 (1994).

[8] C. Peterson, O. Sommelius and B. Söderberg, *Phys. Rev. Lett.* **76**, 1079 (1996).

[9] P.G. deGennes, *Scaling Concepts in Polymer Physics*, Cornell University Press, Ithaca 1979.

[10] M.G. Bawendi and K.F. Freed, *J. Chem.Phys.* **84**, 449 (1986).

[11] P.J. Flory, *J. Chem. Phys.* **17**, 303 (1949).

[12] M. Lal, *Mol. Phys.* **17**, 57 (1969);
N. Madras and A.D. Sokal, *J. Stat. Phys.* **50**, 109 (1988).

[13] A. Irbäck, *J. Chem. Phys.* **101**, 1661 (1994).

Paper V

LU TP 96-28
December 1996

Local Interactions and Protein Folding: A 3D Off-Lattice Approach

Anders Irbäck[1], Carsten Peterson[2], Frank Potthast[3] and Ola Sommelius[4]

Complex Systems Group, Department of Theoretical Physics
University of Lund, Sölvegatan 14A, S-223 62 Lund, Sweden

To appear in *Journal of Chemical Physics*

Abstract:

The thermodynamic behavior of a three-dimensional off-lattice model for protein folding is probed. The model has only two types of residues, hydrophobic and hydrophilic. In absence of local interactions, native structure formation does not occur for the temperatures considered. By including sequence independent local interactions, which qualitatively reproduce local properties of functional proteins, the dominance of a native state for many sequences is observed. As in lattice model approaches, folding takes place by gradual compactification, followed by a sequence dependent folding transition. Our results differ from lattice approaches in that bimodal energy distributions are not observed and that high folding temperatures are accompanied by relatively low temperatures for the peak of the specific heat. Also, in contrast to earlier studies using lattice models, our results convincingly demonstrate that one does not need more than two types of residues to generate sequences with good thermodynamic folding properties in three dimensions.

[1]irback@thep.lu.se
[2]carsten@thep.lu.se
[3]frank@thep.lu.se
[4]ola@thep.lu.se

1 Introduction

In the process of unveiling central issues in the thermodynamics and kinetics of protein folding, simplified models where the amino acid residues constitute the basic entities seem to exhibit many non-trivial and interesting properties [1]. In particular lattice model approaches with contact interactions only have become increasingly popular. The lattice and contact term approximations may seem drastic. Nevertheless, it turns out that such simple models are able to catch non-trivial aspects of the folding problem. This is interesting and encouraging. However, it does not imply that the approximations involved are understood. It is therefore crucial to pursue the study of alternative models, e.g. exploring off-lattice models with Lennard-Jones interactions.

The major advantage of lattice models is computational efficiency, at least for small chain sizes. With improved algorithms and faster computers this advantage is losing in importance. In this paper we propose and study an extension to three dimensions (3D) of a two-dimensional (2D) off-lattice model [2] that was successfully studied previously by Irbäck *et al.* [3, 4] This model contains only two types of amino acids, hydrophobic and hydrophilic, and the key part of the energy function is a species-dependent term that favors the formation of a hydrophobic core. However, as will be demonstrated below, this term alone is not sufficient in order to have thermodynamically dominant native states. This observation is reminiscent of existing lattice model results [5, 6], and could be taken as an indication that it is essential to have more than two different types of amino acids. In this paper we explore another possibility; do the folding properties depend on species-independent local interactions sticking to two amino acid types only? It should be noted that both lattice and 2D off-lattice models implicitly contain local interactions. In the lattice case the mere presence of a discretized space "stiffens" the dynamics locally, and in two dimensions the continuum movements are hampered by compressing one dimension.

The purpose of this work is to construct and numerically study a 3D generalization of the 2D model. [3, 4] As design criteria for such a model we have:

- The model should give rise to thermodynamically dominant states – i.e. be biologically plausible from a stability point of view.
- The local interactions should be chosen to at least qualitatively reproduce bond and torsional angle distributions and local correlations found in functional proteins.

We propose a simple form for the local interactions, which are found to play an important role. Without any local interaction in the model, the local structure of the chains is much more irregular than for proteins. It turns out that one can obtain a local structure qualitatively similar to that of proteins, by adjusting the strength of the local interactions. Having chosen the local interactions in this way, we reexamine the overall thermodynamic behavior. We find that not only have the local properties improved, but the native states have also become more stable.

Furthermore, we examine the structure formation and the properties of the folding transition by studying the temperature dependence of various thermodynamic and structural variables, and the distributions of these quantities at the folding temperature. These results can be understood in terms of a gradual collapse to compact structures where the (sequence dependent) folding transition occurs. The qualitative aspects of this picture confirm what has been found in lattice model calculations. [1, 8] However, it turns out that our results differ from lattice approaches in that bimodal energy distributions are not observed and that high folding temperatures are accompanied by relatively low temperatures for the peak of the specific heat.

The paper is organized as follows. In Sec. 2 the 3D model is defined and in Sec. 3 we extract local properties and correlations for functional proteins from the PDB data base [9]. Monte Carlo (MC) methods and measurements are described in Sec. 4. The results and the summary are found in Sec. 5 and 6 respectively.

2 The Model

We start by defining the simplified geometry of the model. Each residue is represented by a single site located at the C^α position. These sites are linked by rigid bonds of unit length, $\hat{b}_i$, to form linear chains living in three dimensions. The shape of an N-mer is either specified by the $N-1$ bond vectors $\hat{b}_i$ or by $N-2$ bond angles τ_i and $N-3$ torsional angles α_i (see Fig. 1).

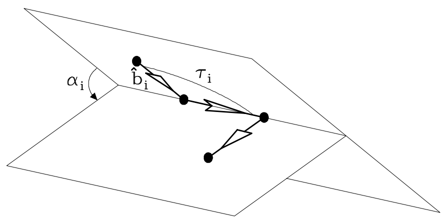

Figure 1: Definition of $\hat{b}_i$, τ_i and α_i.

The model contains two kinds of residues, A and B, which behave as hydrophobic (σ_i=+1) and hydrophilic ($\sigma_i = -1$) residues respectively. The energy function is given by

$$E(\hat{b};\sigma) = -\kappa_1 \sum_{i=1}^{N-2} \hat{b}_i \cdot \hat{b}_{i+1} - \kappa_2 \sum_{i=1}^{N-3} \hat{b}_i \cdot \hat{b}_{i+2} + \sum_{i=1}^{N-2} \sum_{j=i+2}^{N} E_{\text{LJ}}(r_{ij};\sigma_i,\sigma_j) \quad (1)$$

where $r_{ij} = r_{ij}(\tau_{i+1},\ldots,\tau_{j-1};\alpha_{i+1},\ldots,\alpha_{j-2})$ denotes the distance between residues i and j, and $\sigma_1,\ldots,\sigma_N$ is a binary string that specifies the primary sequence. The *species-dependent* global interactions are given by the Lennard-Jones potential,

$$E_{\text{LJ}}(r_{ij};\sigma_i,\sigma_j) = 4\epsilon(\sigma_i,\sigma_j)\left(\frac{1}{r_{ij}^{12}} - \frac{1}{r_{ij}^{6}}\right) . \quad (2)$$

The depth of the minimum of this potential, $\epsilon(\sigma_i,\sigma_j)$, is chosen to favor the formation of a core of A residues

$$\epsilon(\sigma_i,\sigma_j) = \begin{cases} 1 & \text{AA} \\ \frac{1}{2} & \text{BB, AB} \end{cases} \quad (3)$$

The two parameters of the energy function, κ_1 and κ_2, determine the strength of *species-independent* local interactions. The model will be explored for different values of these two parameters, and our final choice will be $\kappa_1 = -1$ and $\kappa_2 = 0.5$.

The behavior of the model at finite temperature T is given by the partition function

$$Z(T;\sigma) = \int \left[\prod_{i=1}^{N-1} d\hat{b}_i\right] \exp(-E(\hat{b};\sigma)/T) . \quad (4)$$

Let us stress that the interactions in Eq. 1 are not chosen so as to stabilize the native state of some particular sequence. Rather, our goal is to study general sequences for a given energy function. We have attempted to choose this energy function as simple as possible. Anticipating some of results to be presented in Sec. 5, let us here briefly discuss the relevance of the different interaction terms.

Species-dependent interactions. It is obvious that the global interactions play a key role in the model; these interactions are responsible for the compactification of the chain, and for the formation of a hydrophobic core. For functional proteins, we find that probability distributions of bond and torsional angles depend only weakly on the hydrophobicity pattern for the residues involved. In our model, the form of these distributions is very sensitive to the choice of global interactions, and it can be strongly sequence dependent. In order to avoid this, we have chosen the potentials for the three different types of residue pairs to be fairly similar; they are all attractive at large separations, and the location of the minimum is the same.

Species-independent interactions. It is less clear how important the local interactions are. When studying the behavior of several different sequences in the absence of the local interactions ($\kappa_1 = \kappa_2 = 0$), the stability of the native state tends to be very low. Furthermore, we find that local correlations along such chains are weak, which is in line with the findings of Socci *et al.* [10] For functional proteins the corresponding correlations are fairly strong, which is a manifestation of the presence of secondary structure. For these reasons we decided to incorporate the local interactions in the model. In this way one gets stiffer chains, which implies stronger local correlations. In addition, the stability of the native states tends to improve, as we will see below.

We have studied the model for many different choices of κ_1 and κ_2. The general behavior of the system is fairly insensitive to small changes of these parameters. Below we will focus on the results obtained for the three choices (κ_1, κ_2)=(0,0),(-1,0) and (-1,0.5).

3 Local Structures in Functional Proteins

In a 3D off-lattice model, it is possible to check the local properties against those for functional proteins in a direct way. We have probed the local structure in two different ways. First we consider the distributions of bond and torsional angles. Second we study local correlations along the chain. In this section we describe the results one finds for functional proteins. These results will be used in Sec. 5 to compare with the qualitative local behavior of our model.

Distributions of bond and torsional angles. These distributions for functional proteins are well-known [11, 12] and are included here for completeness. We consider the structure defined by the backbone of C^α atoms. The results were obtained using a set of 505 selected sequences [13, 14] from the Protein Data Bank. [9] This set was obtained by allowing for a maximum of 25% sequence similarity for aligned subsequences of more than 80 residues. [15] Within this set of 505 minimally redundant sequences, 491 contained complete backbone information; the others were excluded from our analysis.

In Fig. 2 the distributions of bond and torsional angles are shown together with a scatter plot for these two quantities. Note that the calculation of the torsional angle α_i requires four consecutive C^α atoms, while the bond angle τ_i requires only three. The additional fourth C^α atom needed for α_i is taken in the N-terminus direction.

From Fig. 2 it is evident that there are strong regularities in the local structure. The τ_i and α_i distributions both exhibit a clear two-peak structure, which can be associated with two well-populated regions in the (τ_i, α_i)-plane. One of these regions, $\tau_i \in$ [85°,100°] and $\alpha_i \in$ [35°,70°], corresponds to right-handed α-helix and the other, $\tau_i \in$ [105°,145°] and $\alpha_i \in$ [170°,250°], corresponds to β-sheet.

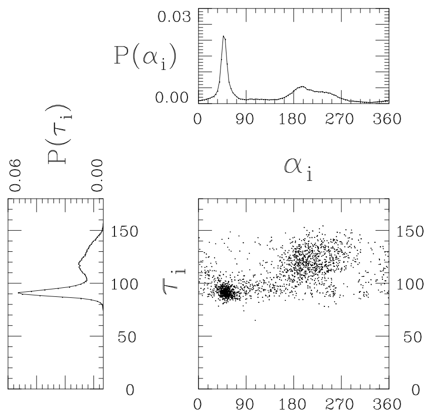

Figure 2: Bond (τ_i) and torsional (α_i) angle distributions for functional proteins.

Local correlations. We study local correlations using the function

$$C_b(d) = \frac{1}{N-d-1} \sum_{i=1}^{N-d-1} \hat{b}_i \cdot \hat{b}_{i+d} \tag{5}$$

where $\hat{b}_i$ are normalized (virtual) bond vectors. Local correlations along protein chains have been studied by Socci *et al.* [10], using a correlation function slightly different from that in Eq. 5. In Fig. 3a we show the correlation function $C_b(d)$ for functional proteins. As can be seen from this figure, there are significant correlations at least out to separations of about eight residues. The oscillations present can be related to the presence of α-helix structure, which has a period of 3.6.

4 Methods

4.1 Monte Carlo Method

Numerical simulations have been performed for a variety of different choices of (κ_1, κ_2) and different sequences and temperatures. At low temperatures conventional Monte Carlo methods tend to become extremely time-consuming, due to the presence of high free-energy barriers. As in previous work [3, 4] we have therefore chosen to employ the dynamical-parameter method, which means that some parameter of the model is taken as a dynamical variable which takes values ranging over a definite set. In this way it is possible to greatly improve the frequency of transitions between the different free-energy valleys;

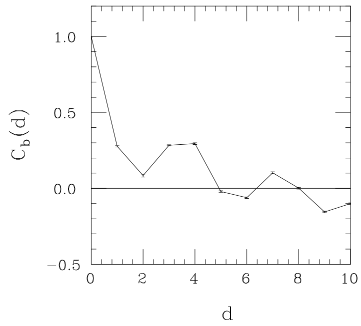

Figure 3: The correlation function $C_b(d)$ for functional proteins (see Eq. 5).

for the 2D model speedup factors of 10^3–10^4 were observed [3], compared with conventional methods.

In the present work the temperature is treated as a dynamical variable ("simulated tempering" [16]). More precisely, the joint probability distribution

$$P(\hat{b}, k) \propto \exp(-g_k - E(\hat{b}, \sigma)/T_k) \tag{6}$$

is simulated, where T_k, $k = 1, \ldots, K$, are the allowed values of the temperature. The g_k's are tunable parameters which must be chosen carefully for each sequence. Details on how to determine these parameters can be found elsewhere. [3, 4] The joint distribution $P(\hat{b}, k)$ is simulated by using separate Metropolis steps [17] in k and $\hat{b}$. For $\hat{b}$ we use two types of elementary moves: rotations of single bonds and moves of pivot type. [18]

In our simulations we used a set of $K = 25$ allowed temperatures, which are equidistant in $1/T$ and ranging from 0.15 to 3.0.

In order to study the energy level spectrum we use a quenching procedure; in the course of the simulations the system is quenched to zero temperature at regular intervals. For this purpose we employ a conjugate gradient method. We found this method more efficient than using a Monte Carlo algorithm with $T = 0$. Also, we tested two different conjugate gradient algorithms. In the conjugate gradient method successive minimizations are carried out along different lines. Information about the gradient is needed to define the lines, and may or may not be utilized for the minimizations. For the present problem we found that minimization without gradient calculation is faster. The quenching procedure only accounts for a small portion of the total computing time.

In Fig. 4 we show the evolution of the quenched and unquenched energies in a typical simulation of a $N = 20$ chain.

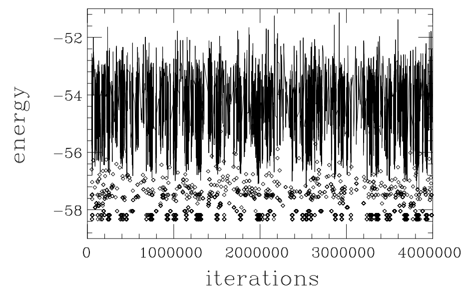

Figure 4: Evolution of the quenched (diamonds) and unquenched (line) energies in the simulation of sequence 1 (see Table 1). Measurements were taken every 10 iterations. Shown are the data corresponding to the lowest allowed temperature. The thermalization phase of 50000 sweeps is not shown.

4.2 Measurements

In Sec. 3 we discussed measurements of local properties of the chains. In order to study the stability of the full native structure, further information is needed. To this end we have studied the distribution of the mean-square distance between configurations, δ^2_{ab}. For two configurations a and b, δ^2_{ab} is defined as

$$\delta^2_{ab} = \min \frac{1}{N} \sum_{i=1}^{N} |\bar{x}_i^{(a)} - \bar{x}_i^{(b)}|^2 \tag{7}$$

where $|\bar{x}_i^{(a)} - \bar{x}_i^{(b)}|$ denotes the distance between the sites $\bar{x}_i^{(a)}$ and $\bar{x}_i^{(b)}$, and where the minimum is taken over translations, rotations and reflections. The corresponding distribution, $P(\delta^2)$, for fixed temperature and sequence, reads

$$P(\delta^2) = \frac{1}{Z(T;\sigma)^2} \int d\hat{b}^{(a)} d\hat{b}^{(b)} \delta(\delta^2 - \delta^2_{ab}) \mathrm{e}^{-E(\hat{b}^{(a)};\sigma)/T} \mathrm{e}^{-E(\hat{b}^{(b)};\sigma)/T} \tag{8}$$

where $\delta(\cdot)$ denotes the Dirac delta function. For convenience, we often use the mean

$$\langle \delta^2 \rangle = \int d\delta'^2 P(\delta'^2) \delta'^2 \tag{9}$$

rather than the full distribution $P(\delta^2)$.

We have also measured the specific heat C_V and gyration radius r_{gyr}, defined by

$$C_V = \frac{1}{T^2} \left(\langle E^2 \rangle - \langle E \rangle^2 \right) \tag{10}$$

$$r_{\text{gyr}}^2 = \frac{1}{N}\sum_{i=1}^{N}\left(\langle\bar{x}_i^2\rangle - \langle\bar{x}_i\rangle^2\right) \tag{11}$$

The specific heat has a maximum in the vicinity of the folding transition. To accurately determine the height and location of this maximum we use the multihistogram method. [19, 20]

In addition to these measurements, we employ the quenching procedure described above. Removing the thermal noise in this way is of great help in monitoring the evolution of the system, but requires a substantial amount of computer time. Therefore, we have performed these calculations at larger intervals than other measurements, and only at the lowest of the temperatures studied.

The quenching procedure provides us with a set of low-lying local energy minima. The mean-square distance to the global minimum will be denoted by δ_0^2 (cf Eq. 7). Using the corresponding distribution, $P(\delta_0^2)$, we define a probability p_0 of finding the system within a small neighborhood of the global minimum. We take

$$p_0 = \int_0^{\Delta} P(\delta_0^2)d\delta_0^2 \tag{12}$$

with the parameter $\Delta = 0.04$; this choice of Δ is motivated by the δ_0^2 distributions (cf Figs. 12 a and b). Let us stress that the distribution $P(\delta_0^2)$ is different from the distribution $P(\delta^2)$ introduced earlier; $P(\delta^2)$ measures general fluctuations rather than deviations from a given state.

The degree of folding may be defined in terms of the quantity p_0. Alternatively, it may be defined as

$$Q = \frac{n^o}{n} \tag{13}$$

where n^o is the number of occupied native contacts, and n is the total number of native contacts. Two monomers i and j are taken to be in contact if $r_{ij}^2 < 1.75$; this cutoff is motivated by the distribution $P(r_{ij}^2)$ (not displayed in this paper). We have $Q = 1$ for the native structure. Also, it is useful to divide the set of native contacts into local and global contacts. A contact between monomers i and j will be called local if $2 \leq |i-j| \leq 4$ and global if $|i-j| > 4$. We set $Q_l = n_l^o/n_l$, where n_l^o is the number of occupied local native contacts and n_l is the total number of local native contacts. Similarly, we define Q_g as the fraction of occupied global native contacts.

5 Results

The model is defined by two parameters, κ_1 and κ_2, which set the strengths of the local interactions. In order to investigate the importance of these interactions, we first performed preliminary runs for a number of different (κ_1, κ_2)

no.	sequence	T_s	$C_V^{\max}$	T_f
1	$BAAA\ AAAB\ AAAA\ BAAB\ AABB$	0.361	51.4	< 0.15
2	$BAAB\ AAAA\ BABA\ ABAA\ AAAB$	0.319	55.9	< 0.15
3	$AAAA\ BBAA\ AABA\ ABAA\ ABBA$	0.298	65.8	0.23
4	$AAAA\ BAAB\ ABAA\ BBAA\ ABAA$	0.273	61.5	0.22
5	$BAAB\ BAAA\ BBBA\ BABA\ ABAB$	0.327	49.8	< 0.15
6	$AAAB\ BABB\ ABAB\ BABA\ BABA$	0.257	62.6	0.15

Table 1: The six sequences studied. The errors in T_s and $C_V^{\max}$ are less than 0.005 and 0.3 respectively. The errors in T_f are approximately 0.02.

values. In particular, these explorations aimed at establishing the balance between the local and global interactions — the overall scale of (κ_1, κ_2). More extensive simulations were then carried out for three different choices

$$(\kappa_1, \kappa_2) = \begin{cases} (0,0) \\ (-1,0) \\ (-1,0.5) \end{cases} \tag{14}$$

using sequences of length $N = 20$. It turns out that shorter chains exhibit less interesting and discriminative behavior. The sequences, which were deliberately chosen to represent a variety of behavior, are listed in Table 1. In this section we first compare the behavior of the model at the three values of (κ_1, κ_2) with respect to the local interactions and low T properties in order to single out one set of (κ_1, κ_2) values. We then examine the folding properties and thermodynamic behavior for $(\kappa_1, \kappa_2) = (-1, 0.5)$ in some detail.

5.1 The Local Interactions

Prior to investigating folding properties for different choices of (κ_1, κ_2), we compare the bond and torsional angle distributions and the local correlations of the chains with those of functional proteins. In Figs. 5 and 6 the model counterparts of Figs. 2 and 3 are shown. The data in Fig. 5 were obtained at a fixed temperature, $T = 0.15$, while those in Fig. 6 were obtained using quenched low energy structures. In both cases we expect the data to reflect the behavior for a wide range of not too high temperatures.

The results strongly indicate the need for local interactions when it comes to mimicking functional proteins; the strong regularities in the local structure observed for proteins are to a large extent missing for a pure Lennard-Jones

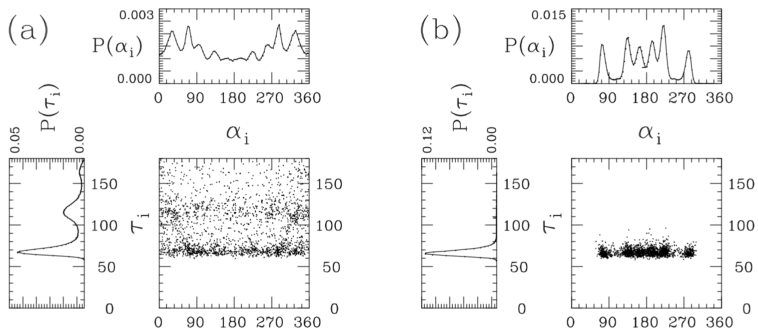

Figure 5: Bond (τ_i) and torsional (α_i) angle distributions at $T = 0.15$ for the six simulated sequences, **(a)** pure Lennard-Jones potential $(\kappa_1, \kappa_2) = (0, 0)$ and **(b)** $(\kappa_1, \kappa_2) = (-1, 0.5)$. The potential corresponding to $(\kappa_1, \kappa_2) = (-1, 0)$ yields a similar distribution as in (b).

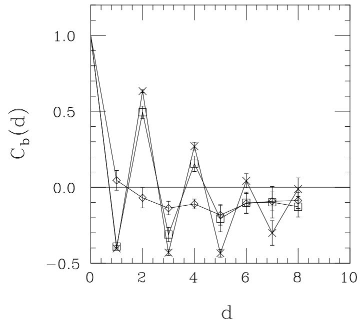

Figure 6: The correlation function $C_b(d)$ (Eq. 5) averraged over the six sequences in Table 1 using (κ_1, κ_2)=(0,0) ($\diamond$), (-1,0) ($\Box$) and (-1,0.5) ($\times$).

potential. This can be seen from the torsional angle distribution and the correlation function $C_b(d)$. The torsional angle α_i varies over the whole range of 360°, without any strongly suppressed regions, and the correlation $C_b(d)$ is very weak for all $d > 0$. The conclusion that local correlations are weak for a pure Lennard-Jones potential is in good agreement with the findings of Socci *et al.* [10]

From the Figs. 5 and 6 it is also clear that changing κ_1 from 0 to -1 leads to a significant improvement; the torsional angle distribution becomes concentrated to a few relatively small regions, and local correlations become stronger. The range of the correlation $C_b(d)$ is for $\kappa_1 = -1$ comparable to what it is

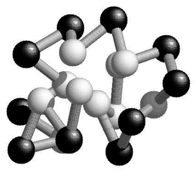

Figure 7: A representative native state (seq. 6) for $(\kappa_1, \kappa_2) = (-1, 0.5)$ illustrating the formation of a hydrophobic core. The hydrophobic (A) and hydrophilic (B) monomers are represented by white and black spheres respectively.

for proteins. Needless to say, the model is not intended to reproduce the precise form of the correlations. However, it is encouraging that the qualitative behavior of this very simple model is consistent with the one from functional proteins.

The remaining question is whether a non-zero κ_2 is called for. No conclusive evidence can be drawn from Figs. 5 and 6 alone in this respect, although one may argue that the range of the correlation $C_b(d)$ is still somewhat short for $(\kappa_1, \kappa_2) = (-1, 0)$.

Next we investigate how the choice of parameters affects the key folding property [4] — the δ^2 distribution should be peaked for low δ^2. In Fig. 8, $P(\delta^2)$ is shown for sequence 4 in Table 1. In contrast to the local properties discussed above, $P(\delta^2)$ is strongly sequence dependent. Nevertheless, Fig. 8 illustrates some general trends seen in the data. First, the pure Lennard-Jones interaction yields a very broad distribution of δ^2, implying that folding properties are poor. This is true for all the six sequences studied. Second, although the behavior is different for one of the six sequences, the $\kappa_2 \neq 0$ choice appears to have a distinct edge over the one ignoring the torsional angle interaction.

In summary, our results show that local interactions are essential in order to get a regular local structure and structural stability. When comparing the results for $(\kappa_1, \kappa_2) = (-1, 0)$ and (-1,0.5), we find that the structural stability tends to be highest for $(\kappa_1, \kappa_2) = (-1, 0.5)$. In what follows we will focus on this choice of parameters for the six sequences in Table 1.

In Fig. 7 a representative example of ground state structure for $(\kappa_1, \kappa_2) = (-1, 0.5)$ is shown — the local structure is regular and the global structure is such that the A monomers form a core. Such formation of a hydrophobic core is observed for all sequences studied.

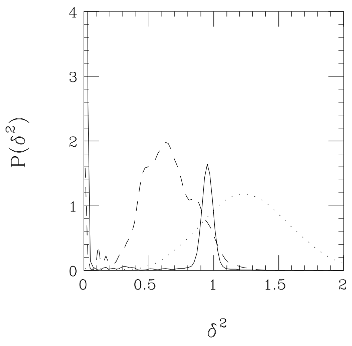

Figure 8: $P(\delta^2)$ at $T = 0.15$ for sequence 4 (cf Table 1); (κ_1,κ_2)=(0,0) (dots), (-1,0) (dashes), and (-1,0.5) (solid). The low-δ^2 peak for (κ_1,κ_2)=(-1,0.5) extends to 37.

5.2 2D Revisited

In the work by Irbäck *et al.* [3, 4], a similar model [2] was studied in 2D using somewhat different Lennard-Jones parameters and local interactions corresponding to $(\kappa_1, \kappa_2)=(\frac{1}{4}, 0)$ (cf Eq. 1). Here, we briefly discuss the importance of local interactions for this 2D model.

For this purpose, we leave out the local interaction term, i.e. we set $(\kappa_1, \kappa_2)=(0, 0)$. Using this pure Lennard-Jones potential, we redo the simulations for 15 sequences. At $T = 0.15$, we find a strong correlation between the $\langle\delta^2\rangle$'s for the two types of potentials; thus $\langle\delta^2\rangle$ varies widely with sequence even for the $(\kappa_1, \kappa_2)=(0, 0)$ potential. This is in contrast to our findings in 3D, where all the sequences studied have a large $\langle\delta^2\rangle$ for $(\kappa_1, \kappa_2)=(0, 0)$.

5.3 Folding Properties

When investigating the folding properties of the chains we focus on the thermodynamics. This is in part inspired by earlier results [4], where the thermodynamic properties exhibited strong sequence dependence. Initially we examine the various thermodynamic quantities defined in Sec. 4.2 over the entire probed T range. Then we proceed with the "magnifying glass" to the 0.15$< T <$0.50 region, where the different chains exhibit strongest difference in behavior and the folding properties can be studied in some detail.

5.3.1 Thermodynamic Behavior

In Fig. 9 the behavior of the different thermodynamic quantities are shown over the entire T range. The overall size of the molecule, as measured by

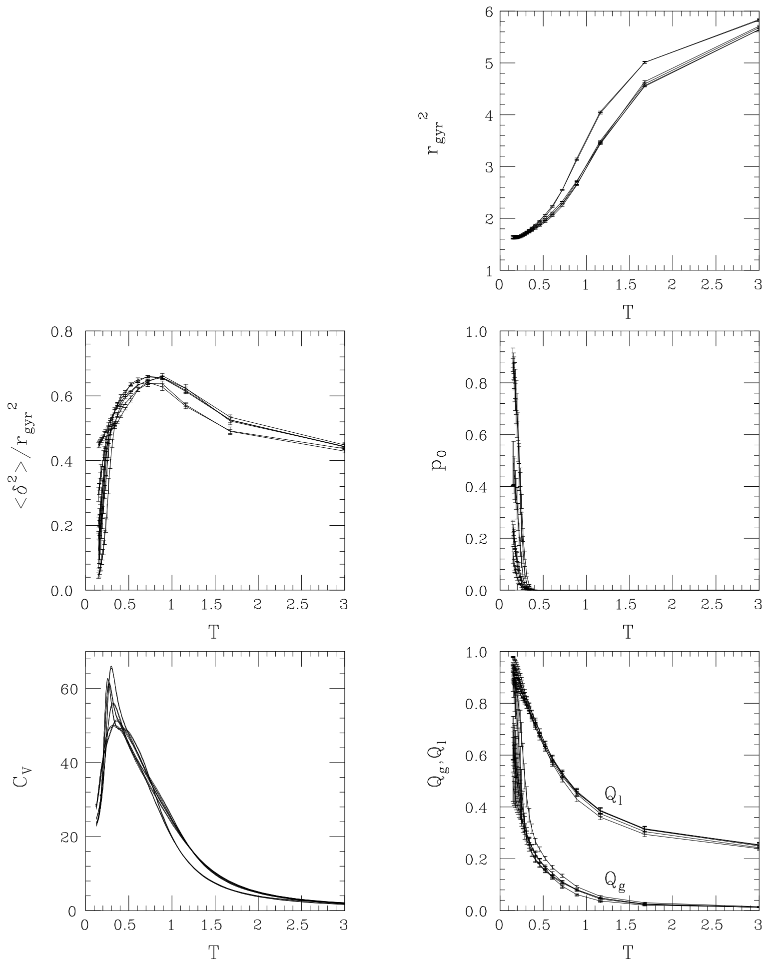

Figure 9: Thermodynamic properties for the six chains in Table 1 using (κ_1, κ_2)=(-1,0.5).

r^2_{gyr}, decreases substantially when T decreases from 3 to 0.15, as can be seen from Fig. 9. This decrease is gradual. The data points essentially fall onto two different curves. The upper curve corresponds to the sequences 5 and 6 with composition 10A+10B, and the lower curve to the sequences 1–4 with composition 14A+6B.

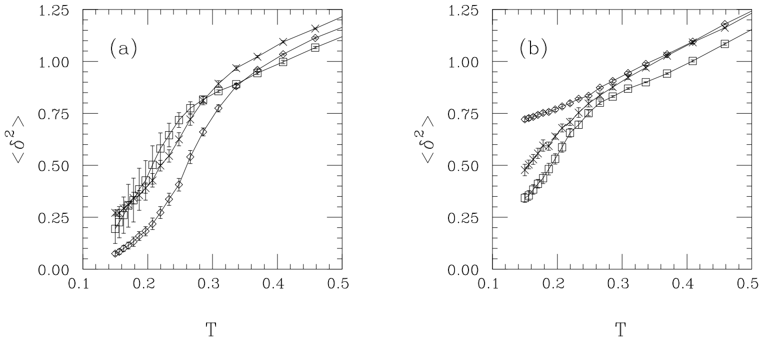

Figure 10: $\langle\delta^2\rangle$ as a function of T for the sequences of Table 1 using (κ_1,κ_2)= (-1,0.5) : **(a)** 4 ($\square$), 2 ($\times$) and 3 ($\diamond$). **(b)** 6 ($\square$), 1 ($\times$) and 5 ($\diamond$).

Next we turn to $\langle\delta^2\rangle$, which measures the size of the fluctuations. In Fig. 9 we show the relative magnitude $\langle\delta^2\rangle/r^2_{\rm gyr}$. This ratio exhibits a peak between $T=0.6$ and 0.9, and is fairly sequence independent down to $T=0.4$. At the lowest temperatures studied the situation is different. Here $\langle\delta^2\rangle$ and $\langle\delta^2\rangle/r^2_{\rm gyr}$ are strongly sequence dependent. In Fig. 10 the results are shown for $\langle\delta^2\rangle$ in the low-T region.

In order to understand the low-T behavior it is useful to consider p_0, which measures the relative population of the lowest energy state (Eq. 12). A comparison of the data for $\langle\delta^2\rangle$ and p_0 shows that small $\langle\delta^2\rangle$ values are associated with large p_0 values. Therefore, it is reasonable to define the folding temperature T_f as the temperature where $p_0=1/2$. Estimates of T_f are given in Table 1. For three of the six sequences T_f is smaller than 0.15, as can be seen from Fig. 11a. It should be stressed that the shape of the molecule is very compact already above T_f. This will be discussed in more detail below for one of the sequences.

From Figs. 9 and 11b it can be seen that the specific heat exhibits a peak in the low-T region, slightly above T_f. The height, $C_V^{\rm max}$, and location, T_s, of the peak are given in Table 1. We find that $C_V^{\rm max}$ is large for the sequences with high T_f, which is in accordance with the results from lattice model studies [8]. However, our results for T_s are somewhat different from these [8]. In our model T_s is relatively low for sequences with high T_f, while the lattice results [8] show the opposite behavior. Thus, the separation T_s-T_f exhibits a stronger sequence dependence in our model.

Also shown in Fig. 9 is the T dependence for the occupancy of local and global native contacts. In the vicinity of T_f, Q_l is large and varies slowly, whereas Q_g changes rapidly. In particular, this demonstrates that the formation of local native structure, like the compactification, is a gradual process

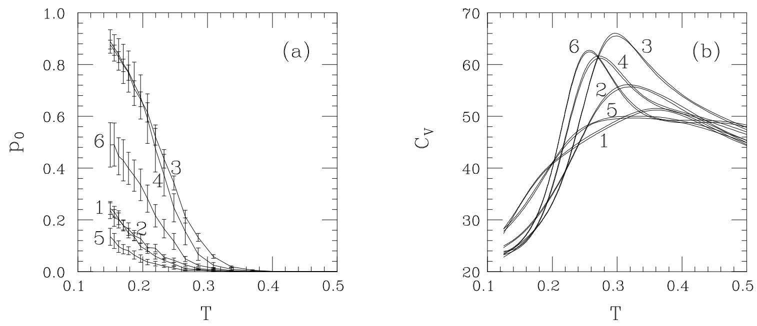

Figure 11: Enlargements of **(a)** p_0 and **(b)** C_V in Fig. 9, (κ_1, κ_2)=(-1,0.5). The bands in (b) correspond to $C_V \pm \sigma$, where σ is the standard deviation.

that to a large extent takes place above T_f.

5.3.2 The Folding Transition Region

In this subsection we study the behavior at the folding temperature T_f, where $p_0 = 1/2$, in some more detail. Two different sequences are considered, 4 and 6. Sequence 4 has a fairly high T_f value, whereas sequence 6 represents a more typical T_f.

In Figs. 12 a and b we show histograms of δ_0^2, the mean-square distance to the lowest energy state, near $T = T_f$. Both histograms exhibit a multi-peak structure, with a narrow peak at low δ_0^2 that corresponds to the native state. The thermodynamic weight of the native state is, by definition, approximately 50% in both cases. However, the distributions differ in shape, which is important from the viewpoint of kinetics. From Figs. 12 a and b one concludes that the δ_0^2 distribution is much more rugged for sequence 6 than for sequence 4. This suggests that, at $T = T_f$, folding is fastest for sequence 4, the sequence with highest T_f. We also explored using Q rather than δ_0^2 as reaction coordinate, with similar results.

The Q distribution at T_f has been studied previously, using a lattice model. [7] Here the distributions for a folding and a non-folding sequence were compared, and these were found to be almost identical. This may seem to contradict our findings, and suggest that there is a difference between the two models. However, it should be remembered that Šali *et al.* [7] did not study the full Q distribution, but rather the Q distribution corresponding to maximally compact structures only.

In Figs. 12 c and d we show the probability distributions of E and $r_{\rm gyr}^2$ at $T \approx T_f$ for sequence 4. Also shown are the contributions to these distributions from conformations with $\delta_0^2 < 0.04$ and $\delta_0^2 > 0.04$, respectively. This corresponds to a simplified two-state picture where each conformation is classified as either native-like or not. The shape of the δ_0^2 distribution shows that such a classification is feasible in an essentially unambiguous way.

As one might have expected from the sharpness of the peak in the specific heat, Fig. 12 c shows that these two "states" differ significantly in energy, although the total E distribution is unimodal. However, the average size of the molecule is very similar for the two states. This fact clearly demonstrates that the compactification occurs prior to the dominance of the native state setting in.

These results may be compared with those of Socci *et al.* [8], where a detailed study of the behavior at T_f was carried out for a lattice model. Here the total number of contacts, C, rather than r^2_{gyr} was used as a measure of compactness. In contrast to the results shown in Figs. 12 c and d, the probability distributions of both E and C were found to be bimodal for a sequence with high T_f. This may reflect a genuine difference between lattice and off-lattice models.

6 Summary

We have extended the off-lattice protein model of Irbäck *et al.* [4] to three dimensions. In doing so, one key issue has been the choice of species-independent local interactions that balance the species-dependent non-bonded Lennard-Jones interactions. The local bond and torsional angle interactions were chosen to satisfy two criteria:

- The resulting low temperature configurations should at least qualitatively reproduce the local angle distributions and correlations of functional proteins, in particular the range over which structural correlations exist. In order to reproduce the precise shape of the correlation function, and that of bond and torsional angle distributions, one would have to work at a different level of detail, which is beyond the scope of this paper.

- It should be possible to produce good folders; i.e. there should be sequences with thermodynamically stable structures at not too low temperatures.

It turns out that the presence of local interactions is necessary for satisfying these criteria. Among the two local interactions, the bond angle one is the most crucial one in this respect.

After having specified the interaction to meet these requirements we study the thermodynamic behavior for six different sequences. The following generic behavior emerges:

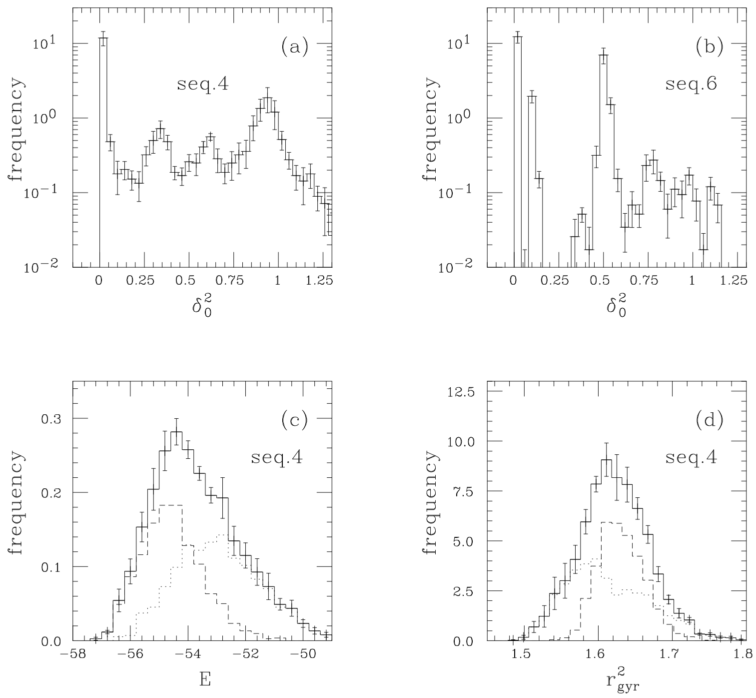

Figure 12: Histograms at $T \approx T_f$ for sequence 4 ($T = 0.22$) and 6 ($T = 0.15$), $(\kappa_1, \kappa_2) = (-1, 0.5)$. **(a)** δ_0^2 for seq. 4. **(b)** δ_0^2 for seq. 6. **(c)** E for seq. 4. **(d)** r^2_{gyr} for seq. 4. The dashed and dotted lines in (c) and (d) represent the contributions corresponding to $\delta_0^2 < 0.04$ and $\delta_0^2 > 0.04$, respectively.

- As the temperature is decreased, a gradual compactification takes place.
- In the compact state a sequence dependent folding transition occurs, where the good folding sequences are characterized by a higher folding temperature. In terms of the specific heat, these good folders also have more pronounced peaks.
- In the state from which the transition to the native state occurs, a large fraction of the native contacts are already formed. The contacts missing are mainly those corresponding to large topological distance along the chain.

This picture is consistent with what is observed for lattice models. [1, 8] A few minor, but significant, differences should be mentioned though.

- We do not observe bimodal distributions of energy or compactness as in the work by Socci *et al.* [8] In a simplified two-state picture, the two coexisting states at the folding temperature do correspond to different energy distributions, but the overlap between the two is large enough to blur this effect.

- For the sequences studied, high folding temperature is accompanied by a relatively low temperature for the peak of the specific heat. This is in contrast to what has been previously reported. [8]

Finally, we stress the fact that we have studied sequences with only two types of residues. In the work by Shakhnovich *et al.* [5, 6] a number of binary (two-letter code) sequences were studied in a 3D lattice model. The two-letter code was found to be insufficient in the sense that these sequences did not have unique native structures. In our model, many binary sequences do have unique native structures.

Our ability to map out the thermodynamics of the 3D off-lattice model, relies heavily upon the efficiency of the dynamical-parameter algorithm. [3, 4] As it stands, the results for each $N = 20$ chain require 70 CPU hours on an Alpha DecStation 200. We feel confident that additional algorithmic efficiency improvements can be made, which will enable us to probe longer and more 3D chains than reported in this work.

References

[1] For a review, see M. Karplus and A. Šali, "Theoretical Studies of Protein Folding and Unfolding", *Curr. Opin. Struct. Biol.* **5**, 58 (1995).

[2] F.H. Stillinger, T. Head-Gordon and C.L. Hirshfeld, "Toy Model for Protein Folding", *Phys. Rev.* **E 48**, 1469 (1993).

[3] A. Irbäck and F. Potthast, "Studies of an Off-Lattice Model for Protein Folding: Sequence Dependence and Improved Sampling at Finite Temperature", *J. Chem. Phys.* **103**, 10298 (1995).

[4] A. Irbäck, C. Peterson and F. Potthast, "Identification of Amino Acid Sequences with Good Folding Properties", *Phys. Rev.* **E 55**, 860 (1997).

[5] E.I. Shakhnovich, "Proteins with Selected Sequences Fold into Unique Native Conformation", *Phys. Rev. Lett.* **72**, 3907 (1994).

[6] K. Yue, K.M. Fiebig, P.D. Thomas, H.S. Chan, E.I. Shakhnovich and K.A. Dill, "A Test of Lattice Protein Folding Algorithms", *Proc. Natl. Acad. Sci. USA* **92**, 325 (1995).

[7] A. Šali, E. Shakhnovich and M. Karplus, "Kinetics of Protein Folding. A Lattice Model Study of the Requirements for Folding to the Native State", *J. Mol. Biol.* **235**, 1614 (1994).

[8] N.D. Socci and J.N. Onuchic, "Kinetic and Thermodynamic Analysis of Proteinlike Heteropolymers: Monte Carlo Histogram Technique", *J. Chem. Phys.* **103**, 4732 (1995).

[9] F.C. Bernstein, T.F. Koetzle, G.J.B. Williams, E.F. Meyer, M.D. Brice, J.R. Rodgers, O. Kennard, T. Shimanouchi and M. Tasumi, "The Protein Data Bank: A Computer Based Archival File for Macromolecular Structures", *J. Mol. Biol.* **112**, 535 (1977).

[10] N.D. Socci, W.S. Bialek and J.N. Onuchic, "Properties and Origins of Protein Secondary Structure", *Phys. Rev.* **E 49**, 3440 (1994).

[11] M. Levitt, "A Simplified Representation of Protein Conformations for Rapid Simulation of Protein Folding", *J. Mol. Biol.* **104**, 59 (1976).

[12] A. Godzik, A. Kolinski and J. Skolnick, "Lattice Representations of Globular Proteins: How Good are They?", *J. Comp. Chem.* **14**, 1194 (1993).

[13] U. Hobohm and C. Sander, "Enlarged Representative Set of Protein Structures", *Protein Sci.* **3**, 522 (1994).

[14] The May 1996 edition was used

[15] U. Hobohm, M. Scharf, R. Schneider and C. Sander, "Selection of a Representative Set of Structures from the Brookhaven Protein Data Bank", *Protein Sci.* **1**, 409 (1992).

[16] E. Marinari and G. Parisi. "Simulated Tempering: A New Monte Carlo Scheme", *Europhys. Lett.* **19**, 451 (1992).

[17] N.A. Metropolis, A.W. Rosenbluth, M.N. Rosenbluth, A. Teller and E. Teller, "Equation of State Calculations by Fast Computing Machines", *J. Chem. Phys.* **21**, 1087 (1953).

[18] M. Lal, "Monte Carlo Computer Simulations of Chain Molecules", *Molec. Phys.* **17**, 57 (1969).

[19] A.M. Ferrenberg and R.H. Swendsen, "New Monte Carlo Technique for Studying Phase Transitions", *Phys. Rev. Lett.* **61**, 2635 (1988); **63**, 1658 (1989) (Erratum), and references given in the erratum.

[20] A.M. Ferrenberg and R.H. Swendsen, "Optimized Monte Carlo Data Analysis", *Phys. Rev. Lett.* **63**, 1195 (1989).

Paper VI

LU-TP 96-30
December 1996

The Electrostatic Persistence Length Calculated from Monte Carlo, Variational and Perturbation Methods

Magnus Ullner[1] and Bo Jönsson[2]
Physical Chemistry 2, Chemical Center, University of Lund
Box 124, S-221 00 Lund, Sweden

Carsten Peterson[3], Ola Sommelius[4] and Bo Söderberg[5]
Complex Systems Group, Department of Theoretical Physics
University of Lund, Sölvegatan 14A, S-223 62 Lund, Sweden

To appear in *Journal of Chemical Physics*

Abstract:

Monte Carlo simulations and variational calculations using a Gaussian ansatz are applied to a model consisting of a flexible linear polyelectrolyte chain as well as to an intrinsically stiff chain with up to 1000 charged monomers. Addition of salt is treated implicitly through a screened Coulomb potential for the electrostatic interactions.

For the flexible model the electrostatic persistence length shows roughly three regimes in its dependence on the Debye-Hückel screening length, κ^{-1}. As long as the salt content is low and κ^{-1} is longer than the end-to-end distance, the electrostatic persistence length varies only slowly with κ^{-1}. Decreasing the screening length, a controversial region is entered. We find that the electrostatic persistence length scales as $\sqrt{\xi_p}/\kappa$, in agreement with experiment on flexible polyelectrolytes, where ξ_p is a strength parameter measuring the electrostatic interactions within the polyelectrolyte. For screening lengths much shorter than the bond length, the κ^{-1} dependence becomes quadratic in the variational

[1]fk2mul@dix.fkem2.lth.se
[2]fk2boj@grosz.fkem2.lth.se
[3]carsten@thep.lu.se
[4]ola@thep.lu.se
[5]bs@thep.lu.se

calculation. The simulations suffer from numerical problems in this regime, but seem to give a relationship half-way between linear and quadratic.

A low temperature expansion only reproduces the first regime and a high temperature expansion, which treats the electrostatic interactions as a perturbation to a Gaussian chain, gives a quadratic dependence on the Debye length.

For a sufficiently stiff chain, the persistence length varies quadratically with κ^{-1} in agreement with earlier theories.

1 INTRODUCTION

During the last decade or so a large number of simulations of charged polymers have appeared in the literature. Many of these have been devoted to the study of conformational properties in bulk solution [1, 2, 3, 4, 5, 6], while a few have focused on the dramatic effects polyelectrolytes can produce in charged colloidal dispersions [7, 8]. In the former case the polymer chain is quite often characterized by a few geometric parameters like the end-to-end separation or the radius of gyration. The behaviour of a polyelectrolyte has also been analyzed in terms of its persistence length. The subject of persistence length may sometimes appear confusing due to the number of definitions and different ways to calculate the quantity. The general concept of persistence length is however the same — it is a measure of stiffness, a characteristic length over which a polymer chain remembers its direction. Of course, even a neutral polymer will have a non-zero persistence length and it has become common practice to divide the total persistence length into an electrostatic, $l_{p,e}$, and a non-electrostatic or "bare" part, $l_{p,0}$,

$$l_{p,t} = l_{p,0} + l_{p,e}. \tag{1}$$

Odijk [9] and, independently, Skolnick and Fixman [10] (OSF) derived equivalent models to calculate the influence of electrostatic interactions on the persistence length and in particular the effect of screening from added salt. For some time there has been a controversy in the literature over conflicting results for the ionic strength dependence [11, 12, 13, 14] and it is the purpose of this communication to resolve the conflict.

Experimentally the OSF result, which suggests a quadratic dependence on the Debye length, κ^{-1}, for the electrostatic persistence length, has been confirmed for intrinsically very stiff polyelectrolytes, like DNA [15] and poly(xylylene tetrahydrothiophenium chloride) [16], but although it has been claimed that the theory is also valid for long, flexible chains [17, 18], the experimental findings generally points towards a linear relationship, i.e. $l_{p,e} \sim \kappa^{-1}$, for flexible polyelectrolytes [19, 20, 21, 22]. An objection to the OSF theory is the neglect of entropy. Taking this into account, variational calculations also give the linear relationship [23, 11, 12]. Simulations usually show deviations from the OSF theory, and the exponent p in $l_{p,e} \sim \kappa^{-p}$ may vary from 1.5 [24] down to 0.3-0.9 [13]. However, $p \approx 1$, in agreement with experiment, have also been reported [3, 6].

It is our conclusion that an almost linear relationship does exist for a flexible polyelectrolyte when the screening length is shorter than the dimensions of the chain, but longer than the monomer-monomer separation. For an intrinsically stiff chain, however, we find a quadratic dependence in agreement with the OSF theory.

2 THE PERSISTENCE LENGTH

Prior to discussing the models and our different approaches we review different definitions of the persistence length and briefly discuss the OSF theory. Given a linear chain with N monomers, the microscopic approach to the persistence length is simply to sum the average scalar products of bond vectors with respect to a certain bond, i.e. to calculate the average sum of directional cosines,

$$l_{p,i} = \frac{1}{a} \sum_{k=0}^{N-1-i} \langle \mathbf{r}_i \cdot \mathbf{r}_{i+k} \rangle = a \sum_{k=0}^{N-1-i} \langle \cos\theta_{i+k} \rangle. \tag{2}$$

where $\mathbf{r}_i = \mathbf{x}_{i+1} - \mathbf{x}_i$ is the bond vector between monomer i and $i+1$, whereas $\mathbf{x}_i$ represents the coordinate of monomer i and a is an average bond length. In the following a will represent the root-mean-square monomer-monomer separation,

$$a^2 = \frac{1}{N-1} \sum_{j=1}^{N-1} \langle \mathbf{r}_j^2 \rangle, \tag{3}$$

which, of course, is the same as the bond length for a chain with rigid bonds. Usually, i denotes the central bond and the cosines are calculated from the average of the scalar products in both directions and not just for subsequent bonds as written in Eq. (2). One may also calculated $l_{p,N/2}$ as an average over both directions. The average over all the local and uni-directional persistence lengths, $l_{p,i}$, is related to the mean-square end-to-end separation,

$$R_{ee}^2 \equiv \langle (\mathbf{x}_N - \mathbf{x}_1)^2 \rangle = \langle \sum_{i=1}^{N-1} \mathbf{r}_i \cdot \sum_{j=1}^{N-1} \mathbf{r}_j \rangle = \sum_{i=1}^{N-1} \langle \mathbf{r}_i^2 \rangle + 2 \sum_{i=1}^{N-2} \sum_{j=i+1}^{N-1} \langle \mathbf{r}_i \cdot \mathbf{r}_j \rangle, \tag{4}$$

i.e.

$$l_{p,R} \equiv \frac{1}{N-1} \sum_{i=1}^{N-1} l_{p,i} = \frac{R_{ee}^2}{2(N-1)a} + \frac{a}{2}. \tag{5}$$

In the case of an infinite chain, all bonds are equivalent and so are the persistence lengths of Eqs. (2) and (5). We may in fact treat the polymer as infinite and disregard the index i in Eq. (2), if the chain is long enough to make end-effects unimportant, i.e., for most bonds $\langle \cos\theta_{i+k} \rangle$ will become zero before k reaches the end and most of the chain will be described by the same orientational correlation function, C_k. This function is normally expected to to decay exponentially with a characteristic length scale, $l_{p,x}$,

$$C_k \equiv \langle \cos\theta_k \rangle = \mathrm{e}^{-ka/l_{p,x}}. \tag{6}$$

Planning ahead, we might be tempted to fit the correlation function to an exponential function, e.g. by linear regression of $\ln C_k$ *vs.* k, and simply calculate $l_{p,x}$ from the slope in this case. This is not such a good idea, however, because we are disregarding one of the fitting parameters. It is a little optimistic to think that the fitting would reproduce the exact value, $C_0 = 1$, as the prefactor of the exponential (or the intercept $\ln C_0 = 0$ in the linear regression). In order to take both parameters into account, it is better to integrate

$$l_{p,\infty} = a \int_0^\infty C_0 \mathrm{e}^{-ka/l_{p,x}} dk = C_0 l_{p,x}. \tag{7}$$

We see that when $C_0 = 1$ we get $l_{p,x}$ back and at the same time we have a natural way to incorporate a fitted $C_0 \neq 1$. The integral is essentially the sum in Eq. (2) and here we have the connection between the microscopic and exponential definitions. There is a difference, however. The sum in Eq. (2) is truncated at the end of the chain regardless if C_k has decayed to zero or not, while the integral in Eq. (7) extrapolates the result to that of an infinite chain. The significance of this will become evident when we look at the results.

The correlation function C_k is discrete since we are considering a polymer with discrete bonds. We will get a continuous function, however, if we make the bonds or segment lengths infinitesimally small, $a \to ds$, and the number of segments infinitely large, while keeping the contour length, $L = (N-1)a = \sum_{i=1}^{N-1} a = \int_0^L ds$, fixed. This is the worm-like chain model [25, 26]. In the chain with discrete bonds there is automatically an intrinsic stiffness, even in the absence of interactions. This results, in the well-known mean-square end-to-end distance for a freely jointed chain or random walk with a fixed step length a,

$$R_{ee}^2 = \sum_{i=1}^{N-1} a^2 C_0 + 2 \sum_{k=1}^{N-1} (N-1-k) a^2 C_k = (N-1)a^2, \tag{8}$$

since there are $N-1-k$ scalar products of the type $\langle \mathbf{r}_i \cdot \mathbf{r}_{i+k} \rangle$ [cf. Eq. (4)] and without interactions one has

$$C_k = \begin{cases} 1 & \text{for } k = 0 \\ 0 & \text{otherwise} \end{cases} . \tag{9}$$

For the worm-like chain we need to specify $C(s) \equiv \langle \cos\theta(s) \rangle$, where $s = \int_0^s ds$ is a distance along the contour of the chain, in order to calculate [cf. Eq. (8)]

$$R_{ee}^2 = 2 \int_0^L (L-s)\, C(s)\; ds. \tag{10}$$

Returning to the assumption of an exponential decay, i.e. $C(s) = \exp\left(-s/l_{p,w}\right)$, we get

$$R_{ee}^2 = 2 L l_{p,w} - 2 l_{p,w}^2 \left(1 - \mathrm{e}^{-L/l_{p,w}}\right). \tag{11}$$

If R_{ee} is known, $l_{p,w}$ can be obtained from 11. This method is often used to extract an apparent persistence length from experimental data [27, 3, 21], although what is usually measured is the radius of gyration, R_G, defined as

$$R_G^2 \equiv \frac{1}{N}\sum_{i=1}^{N}\langle(\mathbf{x}_i - \mathbf{x}_{cm})^2\rangle = \frac{1}{N^2}\sum_{i=1}^{N}\sum_{j=i+1}^{N}\langle x_{ij}^2\rangle, \tag{12}$$

where $\mathbf{x}_{cm}$ is the centre of mass coordinate and x_{ij} is the distance between atoms i and j. The worm-like chain expression used is

$$\begin{aligned} R_G^2 &= \frac{2}{L^2}\int_0^L ds'\,(L-s')\int_0^L ds\,(s'-s)\,\mathrm{e}^{-L/l_{p,w}} \\ &= \frac{Ll_{p,w}}{3} - l_{p,w}^2 + 2\frac{l_{p,w}^3}{L} - 2\frac{l_{p,w}^4}{L^2}\left(1-\mathrm{e}^{-L/l_{p,w}}\right) \end{aligned} \tag{13}$$

or its long chain limit ($L \gg l_{p,w}$)

$$R_G^2 \approx \frac{Ll_{p,w}}{3}. \tag{14}$$

For a worm-like chain with an exponentially decaying correlation function, Eqs. (11) and (13) are equivalent. In other cases the obtained persistence lengths would hardly be identical, but the trends are expected to be the same. For convenience we will be using Eq. (11).

The persistence lengths discussed above are all total persistence lengths, where the "bare" part, the persistence length in the absence of electrostatic interactions, depends on the chain (model) itself. For example, for the freely jointed chain $l_{p,0}$ is equal to the bond length [cf. Eqs. (5) and (8)] and, experimentally, a value extrapolated to infinite amounts of salt is often used. In order to calculate the electrostatic part, the OSF theory considers the electrostatic contribution to the bending energy, which is quadratic in the curvature or bending angle, for a very stiff worm-like chain ($l_{p,0} \gg \kappa^{-1}$), whose electrostatic interactions are described by the Debye-Hückel approximation, i.e. a screened Coulomb potential

$$u_{sc}(r) = k_B T l_B \frac{\mathrm{e}^{-\kappa r}}{r}, \tag{15}$$

where k_B is Boltzmann's constant, T is the absolute temperature and $l_B = e^2/(4\pi\epsilon_r\epsilon_0 k_B T)$ is the Bjerrum length, with e the elementary charge, ϵ_r the dielectric constant of the solution and ϵ_0 the permittivity of vacuum. The Debye screening length, κ^{-1}, is given by $\kappa^2 = 8\pi l_B N_A I 1000$, where N_A is Avogadro's number and I is the ionic strength in units of molar concentration (SI units are implied for the other quantities). The Debye-Hückel approximation is expected to be reasonable for a 1:-1 salt (and a weakly charged polyelectrolyte), in which case the ionic strength is just the molar salt concentration, i.e. $I = C_s$. The predicted electrostatic persistence length is

$$l_{OSF} = \frac{l_B Z^2}{12}\left[3y^{-2} - 8y^{-3} + \mathrm{e}^{-y}(y^{-1} + 5y^{-2} + 8y^{-3})\right], \tag{16}$$

with $y \equiv \kappa L$ and Z the amount of elementary charges on the chain. For large y this reduces to

$$l'_{OSF} = \frac{l_B}{4\kappa^2 A^2}, \tag{17}$$

where $A = L/Z$ is the length per unit charge. If we translate this to a model with a certain bond length a and a charge per monomer $\alpha = Z/N$ we get

$$l'_{OSF} = \frac{\alpha^2 l_B}{4\kappa^2 a^2}. \tag{18}$$

Besides the bond interactions, the models used in the simulations of the flexible polyelectrolyte chains only contain electrostatic interactions, which allows us to obtain a truly *electrostatic* persistence length. In the simulations of the stiff polyelectrolyte chains we also include a bond angle term. In a real polyelectrolyte other interactions, like excluded volume and attractive interactions, may be significant. Still, what we see here is in very good agreement with experiment.

3 MODELS

The polyelectrolyte is regarded as an infinitely diluted polyacid in a salt solution. The monomers form a linear chain where each monomer represents a charged site that carry one unit of negative charge. Three different models have been considered: Model 1 and 2 are freely jointed chains with harmonic and rigid bonds, respectively. In model 3 the rigid bonds have been augmented with an angular potential restricting the orientation of adjacent bonds. The harmonic bonds correspond to an approximately Gaussian distribution of bond lengths and can be viewed as an averaging over the conformational freedom of the covalent structure that implicitly joins the charged sites.

The solvent is treated as a dielectric continuum with a dielectric constant $\epsilon_r = 78.3$, corresponding to water at room temperature, and the salt ions are implicitly represented by the screening parameter κ. Thus, charged monomers interact via a screened Coulomb potential, E_C, which for the flexible bond model (model 1) is augmented with a Gaussian term, E_G, leading to a total interaction energy

$$E = E_G + E_C = \frac{k}{2}\sum_{i \neq N} r_{i,i+1}^2 + \frac{\alpha^2 e^2}{4\pi\epsilon_r\epsilon_0}\sum_i \sum_{j>i} \frac{\mathrm{e}^{-\kappa r_{i,j}}}{r_{i,j}}, \tag{19}$$

where N is the number of monomers, $r_{i,j}$ is the distance between monomer i and j, e is the electronic charge, ϵ_0 is the permittivity of vacuum and α the (fractional) amount of charge on a monomer i. The force constant, k, is given implicitly through the input parameter $r_0 = (e^2/4\pi\epsilon_r\epsilon_0 k)^{1/3}$, which is the equilibrium distance for a fully charged dimer.

The angular potential in model 3 is simply,

$$E_A = -k_B T \frac{l_B l_A^2}{r_0^3} \sum_{i=1}^{N-1} \cos\theta_i, \tag{20}$$

where θ_i is the angle between bond i and $i+1$. The angular potential is characterized by the length l_A and increasing l_A means increased stiffness in the chain.

4 METHODS

The key approach employed for studying the scaling properties of the persistence length is the Monte Carlo method. In this section, however, we also discuss what is expected from non-stochastic approaches; a variational method, high- and low-T expansions.

4.1 Monte Carlo simulation

The Monte Carlo (MC) simulations were performed with the traditional Metropolis algorithm [28] in a canonical ensemble. One polyelectrolyte chain at infinite dilution was simulated. The sampling of chain conformations was made highly efficient, compared to traditional Monte Carlo moves, by using a pivot algorithm, which allows chain lengths of more than 2000 monomers. The pivot algorithm was first described by Lal [29], and its efficiency for self-avoiding walks have been thoroughly discussed by Madras and Sokal [30]. Despite its excellent properties, it was only recently that the pivot algorithm started to gain wider recognition as a tool to enhance simulations of polymers and polyelectrolytes [31, 24, 32, 33].

In a traditional single-move algorithm only one or a few monomers are translated or rotated at a time. The number of interactions that has to be calculated is of the order N and a large number of attempts per monomer is needed to generate independent chain conformations. Similarly, in the pivot algorithm each monomer i (except the first one) is translated in turn but together with the rest of the chain (monomers $i+1$ to N). Furthermore, the last part of the polymer is then rotated as a rigid body around one of the coordinate axes with monomer i as origin. To be specific, if the bonds are flexible (model 1) they are both translated and rotated, while in the case of rigid bonds (models 2 and 3) only the rotation is performed. The number of interactions calculated in one step is of the order N^2 but independent conformations are obtained after a only a few attempted moves, on the order of one per monomer or N in total. The net effect is a greatly reduced simulation time for a given degree of precision and a computational cost that grows approximately as N^3.

One expects the pivot algorithm to have its maximal efficiency for unscreened and extended chains, but we have recently shown its efficiency even for screened chains with less elongated structure [34]. The pivot algorithm provides an effective sampling of global properties like R_{ee}, but it turns out to be superior also for local properties like the monomer-monomer separation. A more detailed investigation than the present, is needed to really map out the applicable range for the pivot algorithm.

4.2 Variational approach

In the variational approach the true Boltzmann distribution $P \propto \exp(-E/k_BT)$ is approximated by a trial distribution $P_V \propto \exp(-E_V/k_BT)$, having a set of free parameters. It yields a variational free energy

$$\hat{F} = \langle E \rangle_V - k_BTS_V \geq F, \tag{21}$$

bounded from below by the true free energy F. $\langle E \rangle_V$ is the average of the true energy in the trial Boltzmann distribution P_V and S_V is the corresponding variational entropy. By minimizing $\hat{F}$ with respect to the parameters of E_V, thermodynamic quantities can be estimated. In the case of model 1 (flexible chain), we consider an arbitrary pure Gaussian variational distribution [32], corresponding to

$$E_V/k_BT = \frac{1}{2}\sum_{ij} G_{ij}^{-1}\mathbf{r}_i \cdot \mathbf{r}_j, \tag{22}$$

where $\mathbf{r}_i$ denotes the ith bond vector. With the correlation matrix G optimized (numerically) so as to minimize $\hat{F}$, the variational estimate for the correlation matrix becomes

$$\langle \mathbf{r}_i \cdot \mathbf{r}_j \rangle_V = 3G_{ij}. \tag{23}$$

From this a variational estimate for the persistence length, e.g. as defined in Eq. (5), can be obtained.

4.3 High temperature expansion

For model 1 at high temperatures, the energy [Eq. (19)] will be dominated by the bond term, and the interaction E_C can be treated as a perturbation. A perturbative expansion for the thermal average of an arbitrary observable f

yields

$$\langle f\rangle = \langle f\rangle^0 - \frac{1}{k_BT}\langle fE_C\rangle_C^0 + \frac{1}{2(k_BT)^2}\langle fE_CE_C\rangle_C^0 + \ldots, \qquad (24)$$

where $\langle\,\rangle_C^0$ refers to connected expectation values in the unperturbed Boltzmann distribution.

In a continuum approximation, valid when the nearest-neighbour distance is small as compared to the range of the interaction, the first few terms in the perturbative expansion of the squared end-to-end distance R_{ee}^2 are given by [35] (assuming full charge, $\alpha = 1$)

$$\langle R_{ee}^2\rangle = \frac{Nr_0^3}{l_B}\left[3 + \gamma f_1(\mu) + \gamma^2 f_2(\mu) + \ldots\right]. \qquad (25)$$

where

$$f_1(\mu) = 4\sqrt{\frac{2}{\pi}} - 16\mu^{-1/2} + \mathcal{O}(\mu^{-1})\ ,\quad f_2(\mu) = -\left(\frac{32}{\pi} - \frac{56}{9}\right) + \mathcal{O}(\mu^{-1/2}) \quad (26)$$

with the dimensionless parameters μ and γ given by

$$\mu = \frac{N\kappa^2 r_0^3}{l_B}\ ,\quad \gamma = \frac{N^{1/2} l_B^{5/2}}{\kappa^2 r_0^{9/2}}. \qquad (27)$$

Note that μ is proportional to the squared unperturbed end-to-end distance in units of the screening length; in the parameter range we are studying, μ is large.

Keeping only the leading large-μ contribution to each term f_i yields a power series in γ, indicating that the expansion is valid for small γ. Unfortunately, for the parameter range we are studying γ is *not* small, and while the first order expansion is proportional to κ^{-2}, the next order term, proportional to κ^{-4}, is larger and has a negative value.

Similarly, for the average squared bond length we obtain in the continuum approximation the perturbative result

$$a^2 \equiv \langle r_{mm}^2\rangle = \frac{r_0^3}{l_B}\left[3 + 4\frac{l_B^2}{\kappa r_0^3} + \ldots\right]. \qquad (28)$$

The persistence length $l_{p,R}$ is then obtained by dividing R_{ee}^2 by Nr_{mm}. In the results section, we have included the first order perturbative result for comparison, although a good agreement cannot be expected since the parameter γ is not small.

4.4 Low temperature expansion

A similar approach can be followed for low temperatures, where the Boltzmann distribution is dominated by the minimal energy configuration. For small fluctuations around the ground state, the energy can to lowest order be considered Gaussian, with the corrections treated as a perturbation. The resulting correlation matrix $\langle \mathbf{r}_i \cdot \mathbf{r}_j \rangle$ [36] can be used to calculate the persistence length.

5 RESULTS AND DISCUSSION

5.1 Flexible polyelectrolyte

From the form of the Hamiltonian, being just a sum of screened Coulomb interactions [Eq. (15)], and the fact that the statistical mechanical weight of a conformation is given by $\exp(-E/k_BT)$, it is easy to see that the rigid bond model scales with the bond length a as the unit of length and that any scaled length, e.g. l_p/a, must be a function of the dimensionless numbers (scaled length scales) κa and the strength parameter

$$\xi_p = \frac{\alpha^2 l_B}{a}, \tag{29}$$

which measures the strength of the electrostatic interactions within the polyelectrolyte for a given N. As a visual proof, Fig. 1 shows that $l_{p,e}/a$ is constant for a given value of these parameters. Note that ξ_p is different from the so called Manning parameter [37], $\xi = l_B/A = \alpha l_B/a$, which measures the interactions between the polyelectrolyte and mobile ions. In a previous paper we found for a titrating polyelectrolyte that the approximation of putting full charges a distance A apart is inferior to having fractional charges on the actual titrating sites [38]. Thus, we may conclude that ξ_p is the more pertinent parameter in this context.

The results in Fig. 2 show two distinct regimes in the salt dependence of the electrostatic persistence length. For low salt concentrations, i.e. when the Debye screening length is longer than the dimensions of the chain ($\kappa^{-1} \gg R_{ee}$), $l_{p,e}$ is almost constant. Note that the symbols on the y-axis represent the values in the unscreened case ($\kappa = 0$). When $\kappa^{-1} \ll R_{ee}$ the relationship between $l_{p,e}$ and κ^{-1} is close to linear. There is actually a third regime when κ^{-1} is less than the bond length, but we will save that till the discussion of the variational results.

Experimentally, Reed *et al.* have found a linear dependence on both κ^{-1} and α for $l_{p,e}$ [21]. To us, this implies

$$l_{p,e} \sim \frac{\sqrt{\xi_p}}{\kappa} = \frac{\alpha}{\kappa}\sqrt{\frac{l_B}{a}} = \frac{\alpha}{\sqrt{8000\pi N_A I a}} \tag{30}$$

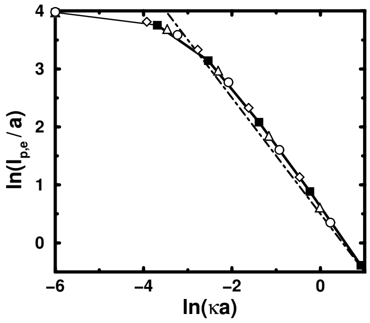

Figure 1: The logarithm of the scaled electrostatic persistence length, where $l_{p,e} = l_{p,R} - a$ [cf. Eq. (5)], as a function of $\ln(\kappa a)$ for rigid bond chains with $N = 320$ and fixed ξ_p. Filled squares represent $a = 24$ Å and $\alpha = 1$ and the open symbols represent $\alpha/a = 0.3536/3$ Å (triangles), $0.5/6$ Å (diamonds) and $0.707/12$ Å (circles), with the values on the y-axis showing the results for the salt-free case. The dot-dashed line marks a slope of -1.

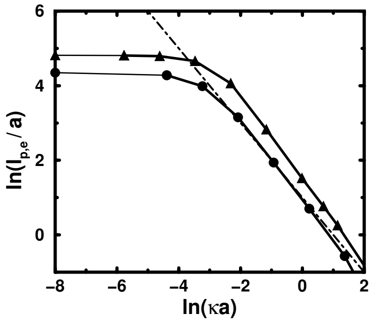

Figure 2: The logarithm of the scaled electrostatic persistence length, where $l_{p,e} = l_{p,R} - a$ [cf. Eq. (5)], as a function of $\ln(\kappa a)$. The results are for rigid bond chains with $N = 320$ and $a = 3$ Å (triangles) and 12 Å (circles) and fully charged monomers. The values on the y-axis are for the salt-free case, and are connected to the rest of the points by thinner lines. The dot-dashed line denotes a slope of -1.

at high salt concentrations, which is confirmed in Figs. 3 and 4. Note that $l_{p,e}$ is predicted to be temperature independent. Ha and Thirumalai (HT) have derived a similar expression, $l_p \sim \sqrt{(l_{p,0} l_B / A^2)}/\kappa$ for $l_{OSF} \gg l_{p,0}$ [12]. As long as $l_{p,0} = a$ the two expressions are the same, although l_p in their case appears to be the total persistence length. However, if we add a repulsive potential between next-nearest neighbours, which increases $l_{p,0}$ (but not too much, see below), Eq. (30) still holds, while the HT expression with the actual

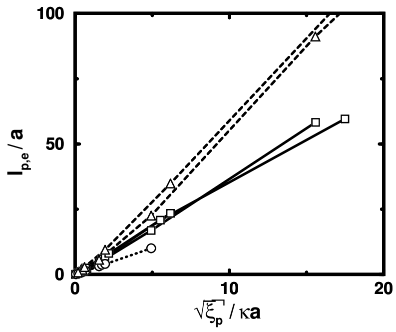

Figure 3: The scaled electrostatic persistence length, where $l_{p,e} = l_{p,R} - a$, as a function of $\sqrt{\xi_p}/\kappa a$. The results are for rigid bond chains with $N = 80$ (circles) and 320 (squares) with bond lengths 3 Å, 6 Å, 12 Å and 24 Å as well as $N = 1000$ with $a = 3$ Å and 12 Å (triangles). In order to clearly show the linear regime, only points where $\kappa^{-1} \leq R_{ee}/10$ are displayed.

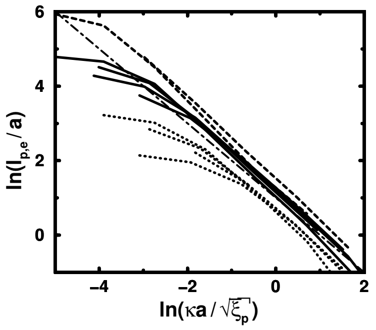

Figure 4: The logarithm of the scaled electrostatic persistence length, where $l_{p,e} = l_{p,R} - a$, as a function of $\sqrt{\xi_p}/\kappa a$. The lines represent the same combinations of a and α as in 3. The dot-dashed line marks a slope of -1.

intrinsic persistence length does not. The slope for the highly screened regime ($\kappa^{-1} \ll R_{ee}$) in Fig. 4 is roughly -1.1.

Equation (30) has no N dependence. Naively one may expect excluded volume behaviour in the high salt regime as a result of short ranged electrostatic interactions between monomers, which can also be far apart in the sequence as the chain loops back on itself. For a self-avoiding chain we have $R_{ee}^2 \sim N^{1.2}a^2$ [39], which from Eq. (5) would suggest $l_{p,e} \sim N^{0.2}$ for long chains. The slopes of the linear parts of Fig. 3, roughly 2.6, 4.3 and 7.3 for $N = 80$, 320 and 1000, respectively, give an N-exponent of 0.4.

So far we have used the "macroscopic" persistence length, Eq. (5), but the same conclusions are reached with other definitions as can be seen in Table 1

Table 1: End-to-end separation and electrostatic persistence lengths from different definitions, $l_{p,N/2} - a$ from Eq. (2), $l_{p,R} - a$ from Eq. (5), $l_{p,x} - a$ from Eq. (6), $l_{p,\infty} - a$ from Eq. (7), $l_{p,w} - a$ from Eq. (11) and l_{OSF} from Eq. (16), obtained for a 320-mer. The unit of length is 1 Å.

a	C_s/M	κ^{-1}	R_{ee}	$l_{p,N/2} - a$	$l_{p,R} - a$	$l_{p,x} - a$	$l_{p,\infty} - a$	$l_{p,w} - a$	l_{OSF}
	0	—	844	383	371	6969	5909	1182	10185
	0.00001	961	843	376	370	6494	5412	1169	9191
	0.0001	304	834	372	362	5246	4365	1071	5655
	0.001	96	781	334	317	2152	1713	699	1353
3	0.01	30	581	197	175	409	288	228	169
	0.1	9.6	316	58	51	117	56	52	18
	1	3.0	171	16	14	66	10	12	2
	10	0.96	101	5	4	52	-1	2	0.2
	100	0.30	68	0.9	0.9	62	-3	-0.6	0.02
	0	—	2680	1018	932	9158	5636	1433	10185
	0.00001	961	2586	943	867	7258	4231	1267	4605
	0.0001	304	2236	713	647	3300	1678	821	910
	0.001	96	1483	324	281	978	378	301	108
12	0.01	30	828	99	84	461	87	80	11
	0.1	9.6	481	27	24	256	14	18	1
	1	3.0	313	7	7	213	-11	0.8	0.1
	10	0.96	234	4	1	262	-12	-5	0.01
	100	0.30	217	1	0.2	420	-12	-6	0.001

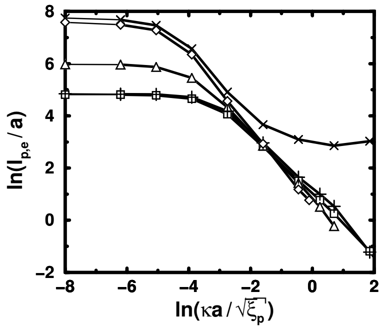

Figure 5: The logarithm of the electrostatic persistence length as a function of the logarithm of $\kappa a/\sqrt{\xi_p}$ for different definitions of $l_{p,e}$: $l_{p,N/2} - a$ from Eq. (2) (plus signs), $l_{p,R} - a$ from Eq. (5) (squares), $l_{p,x} - a$ from Eq. (6) (crosses), $l_{p,\infty} - a$ from Eq. (7) (diamonds), $l_{p,w} - a$ from Eq. (11) (triangles). The values are based on simulation results, either directly or through R_{ee}, of 320-mers with $a = 3$ Å.

and Fig. 5. The two persistence lengths obtained directly form the simulation, $l_{p,N/2}$ and $l_{p,R}$ [Eqs. (2) and (5)], are almost identical. $l_{p,R}$ is a global quantity and thus have better statistics than $l_{p,N/2}$, which has more local character. This becomes noticeable at high salt concentrations where the latter starts to suffer from insufficient averaging. The worm-like chain persistence length, Eq. (11), also give the same results for $\kappa^{-1} \ll R_{ee}$ and $\kappa^{-1} > a$. For screening lengths less than the bond length the true structure of the chain becomes important and the worm-like chain model breaks down and even gives negative persistence

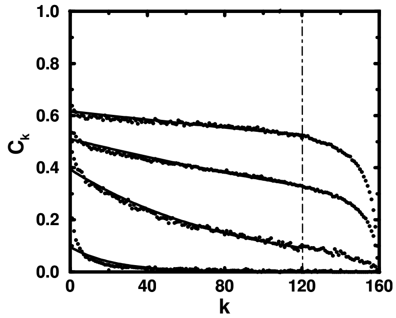

Figure 6: The orientational correlation function for a 320-mer with $a = 12$ Å and salt concentrations of 0, 0.1, 1, 100 mM (top to bottom) represented by small circles. The solid lines are exponentials fitted in the range k=0–120. The dot-dashed line just shows the upper limit of the fitting and the upper limit of the y-axis is a reminder that $C_0 = 1$.

lengths. To save the worm-like chain, a term corresponding to the last term of Eq. (5) would have been needed in Eq. (11).

$l_{p,x}$ [Eq. (6)] and $l_{p,\infty}$ have been obtained by fitting an exponential to the orientational correlation function. In order to avoid end-effects we have calculated C_k from the central bond and fitted the function only in the range k=0–120 (N=320). Figure 6 shows the correlation function together with the fitted exponential. It is clear that some information is lost at small values of k and that this is of greater importance at higher salt concentrations. In particular the initial part at $C_0 = 1$, which for the integrated persistence length $l_{p,\infty}$ corresponds to the intrinsic persistence length, $l_{p,0} = a$, is lost. Table 1 shows that if we did not subtract $l_{p,0}$ from $l_{p,\infty}$, this persistence length would be in good agreement with the microscopic definitions, not only at intermediate salt concentrations, but also at higher salt concentrations. Even more information is lost when calculating $l_{p,x}$. Note for example that the fitted exponentials have a prefactor (C_0) that is less than one and decreasing faster than C_1. In Fig. 5 we see that $l_{p,x}$ has a behaviour of its own. There is not a simple, consistent κ^{-1} dependence and an apparent exponent p in $l_{p,x} \sim \kappa^{-p}$ can have a range of values less than one, which is exactly the result of Micka and Kremer [13]. Their conclusions are thus a consequence of an unfortunate choice of persistence length definition.

The OSF persistence length also has an almost constant regime, with a salt-free limit $l_{OSF} = l_B Z^2/72$ (see Fig. 7). In this region the value of the electrostatic persistence length is sensitive to whether it includes end-effects, like $l_{p,i}$ and $l_{p,R}$, or is defined through a correlation function that is extrapolated

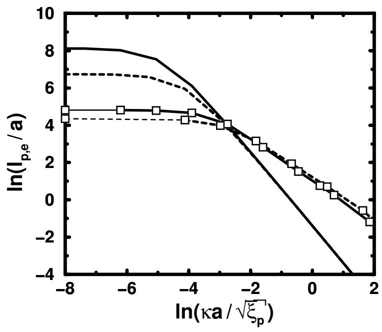

Figure 7: OSF theory [Eq. (16)] (no symbols) compared to the simulated electrostatic persistence length, $l_{p,e} = l_{p,R} - a$ from Eq. (5), (squares). The results are for 320-mers with $a = 3$ Å (solid lines) and $a = 12$ Å (dashed lines). The values on the y-axis are the results for the salt-free case.

to infinite chain lengths, like $l_{p,\infty}$ (and in principle $l_{p,x}$ if C_0 is close to one, cf. Eq. (7)). l_{OSF} belongs to the latter group and is actually in fair agreement with $l_{p,\infty}$ (and $l_{p,x}$) in this regime (see Table 1). The worm-like chain expression, Eq. (11), gives a behaviour intermediate between the two extremes and since the worm-like chain is often used to obtain persistence lengths from experimental data this is the behaviour expected to be reported experimentally. Such a report by Förster *et al.* appears to be at odds with both OSF theory and the notion of a power law for the κ dependence [40], but a comparison with the results here suggests that their experimental system just displays the constant regime and the subsequent cross-over region. This means that their comparison with OSF theory is rather unfair since they are using the high-salt version, Eq. (18).

In the second regime, l_{OSF} of course displays the well-known quadratic dependence on the Debye length, in disagreement with simulations. It is interesting to note that l'_{OSF}/a has the correct relationship between ξ_p and κa. It is essentially the square of the dimensionless form of the right-hand side of Eq. (30). This is a little bit tricky, however. Going from Eq. (17) to Eq. (18) the choice of the bond length a is arbitrary, because it is always balanced by α. This is no longer true if we are to scale l'_{OSF} by a. In that case we need the proper rigid bond model to get the correct bond length dependence, which is closely related to the above discussion about the difference between having an effective charge or an effective bond length, *i.e.* using ξ_p or the Manning parameter, ξ.

Figure 8 shows that the electrostatic persistence length obtained from the variational calculations is slightly higher than the simulation results for the same model. Otherwise, the agreement is excellent. The calculations have been made for a flexible bond chain with $r_0 = 6$ Å and the root-mean-square

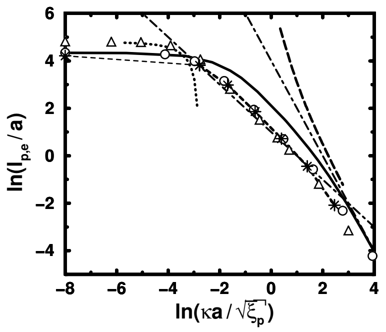

Figure 8: Comparison between simulations and variational and perturbational calculations. The simulation results are for 320-mers with rigid bonds of 3 Å (triangles) and 12 Å (circles) and flexible bonds with $r_0 = 6$ Å (dashed line, stars). The solid line represent the variational result for the latter, while the dotted line and the long dashed lines are low temperature and high temperature expansions, respectively, for a 512-mer with $r_0 = 6$ Å. The *symbols* on the y-axis are for the salt-free case and the dot-dashed lines mark a slope of -1 and -2, respectively.

bond length is around 12 Å, a little longer at low salt concentrations and a little shorter at high screening. As the simulation results show the behaviour is almost identical to that of a rigid bond chain with $a = 12$ Å. It is a general conclusion that models with flexible, harmonic bonds give the same results as rigid bond chains if the the actual, simulated root-mean-square monomer-monomer separation is used to represent the bond length. A pair similar to $r_0 = 6$ Å$/a = 12$ Å is $r_0 = 9$ Å$/a = 24$ Å.

When the Debye length is on the order of the bond length ($\kappa a \approx 1$) the variational result crosses over to a third regime where $l_{p,e}$ is proportional to κ^{-2}, i.e. we get a behaviour similar to the OSF prediction, which applies to stiff chains. Although the chain is highly flexible, it is stiff on the length scale of a bond and when κ^{-1} is of this order, the intrinsic persistence length, $l_{p,0} = a$, dominates the total persistence length. The OSF theory treats the electrostatic interactions as a perturbation to an intrinsic bending energy, which is quadratic in the bending angle. Analysing the high temperature expansion, Eq. (24), which is also a perturbational calculation, we would get a κ^{-2} dependence to the lowest order for the entire range of salt concentrations if $l_{p,e}$ were plotted as a function of $\sqrt{\xi_p}/\kappa$, but scaling with the bond length as in Fig. 8 the expansion result curves upwards at lower salt concentrations.

The simulation results appear also to cross over into a third regime at (ridiculously) high salt concentrations, although the exponent of κ^{-1} seems to be closer to 1.5 and slowly increasing. Seidel's large exponent, also 1.5, for κ^{-1} may be due to the fact that the Debye length was smaller than the distance

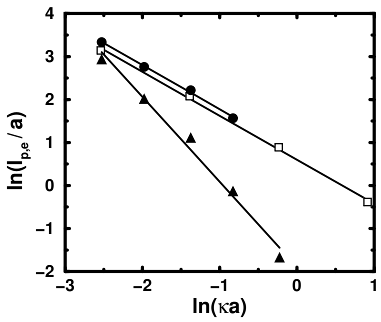

Figure 9: The electrostatic persistence length for a 320-mer with rigid bonds of $a = 24$ Å and an angular potential with $l_A = \sqrt{2000}$ Å (filled circles) and $l_A = \sqrt{20000}$ Å (filled triangles). The solid lines are least square fits, which have the slopes -1.0 and -2.0, respectively. Also shown is the corresponding chain without the angular potential (open squares).

between neighbouring charges [24].

Finally, the low temperature expansion, which corresponds to a rigid rod, gives the expected almost constant persistence length at low salt concentrations, but diverges when $\kappa R_{ee} \approx 1$ and the chain cannot bend as it is supposed to.

5.2 Stiff polyelectrolyte

Thus, we have shown that the OSF theory is not applicable for a flexible polyelectrolyte where the electrostatic persistence length is of the same order as the total persistence length. This should not come as a surprise, since the OSF theory was derived for a chain with a significant intrinsic stiffness and where the electrostatic persistence length only gives a minor contribution to the total persistence length.

One way to introduce a non-electrostatic stiffness beyond the bond length is via an angular potential [see Eq. (20)]. We have performed such simulations for a fully charged chain with 320 monomers and a fixed bond length $a = 24$ Å and found that the persistence length still scales like κ^{-1}. With increasing l_A, however, the dependence changes over to κ^{-2} in agreement with the OSF result. Figure 9 shows how a chain with $l_A = \sqrt{2000}$ Å and with an intrinsic persistence length, $l_{p,0} = 83$ Å decays like κ^{-1}, just like the flexible chain without the angular potential, i.e. $l_A = 0$ Å. Upon increasing the stiffness to $l_A = \sqrt{20000}$ Å and a $l_{p,0} = 759$ Å the κ dependence shifts to -2. The κ dependence at high salt concentration still seems to be quadratic although considerable numerical difficulties prevent an accurate analysis.

6 CONCLUSIONS

Simulating a flexible polyelectrolyte model that only has screened Coulomb interactions, besides the bond interactions, we find a linear relationship between the electrostatic persistence length and the Debye length in the controversial region where the Debye length is shorter than the chain dimensions ($\kappa^{-1} \ll R_{ee}$) and the interactions have become more local. Furthermore, we also find that the electrostatic persistence length is proportional to the square root of the strength parameter $\xi_p = \alpha^2 l_B/a$, which measures the internal interactions, i.e we have $l_{p,e} \sim \sqrt{\xi_p}/\kappa$. This is in agreement with experiment, but contradicts OSF theory, which predicts $l_{p,e} \approx \alpha^2 l_B/(2\kappa a)^2$.

The conclusions remain the same if different definitions of persistence length are used, although $l_{p,x}$ [Eq. (6)] may give erratic results when obtained by a simple fitting to the orientational correlation function.

Variational calculations agree with simulations. A small difference is seen at very high salt concentrations, where the variational results predict a κ^{-2} dependence as in the OSF theory. Here simulations give an exponent p between 1 and 2 for $l_{p,e} \sim \kappa^{-p}$. In this region, $\kappa^{-1} \ll a$, and the electrostatic interactions can be treated as a small perturbation to the harmonic interactions in the variational ansatz, similar to the perturbation of the quadratic bending energy in the OSF theory. A high temperature expansion carried to first order gives a quadratic dependence throughout the concentration range.

Finally, for a stiff chain where the electrostatic persistence length only gives a minor contribution to the the total stiffness, we find that theory due to Odijk and Skolnick and Fixman is valid. Under these conditions the electrostatic persistence length scales like κ^{-2}.

References

[1] J. P. Valleau, *Chem. Phys.* **129** , 163 (1989).

[2] H. H. Hooper and H. W. Blanch and J. M. Prausnitz, *Macromolecules* **23**, 4820 (1990).

[3] C. E. Reed and W. F. Reed, *J. Chem. Phys.* **94** , 8479 (1991).

[4] G. A. Christos and S. L. Carnie and T. P. Creamer, *Macromolecules* **25**, 1121 (1992).

[5] M. J. Stevens and K. Kremer, *J. Chem. Phys.* **103** 1669 (1995).

[6] C. Seidel and H. Schlacken and I. Müller, *Ber. Bunsenges. Phys. Chem.* **100**, 175–179 (1996).

[7] T. Åkesson and C. Woodward and B. Jönsson, *J. Chem. Phys.* **91**, 2461 (1989).

[8] T. Wallin and P. Linse, *J. Phys. Chem.* **100**, 17873 (1996).

[9] T. Odijk, *J. Polym. Sci., Polym. Phys. Ed.* **15**, 477 (1977).

[10] J. Skolnick and M. Fixman, *Macromolecules* **10**, 944 (1977).

[11] J.-L. Barrat and J.-F. Joanny, *Europhys. Lett.* **24**, 333 (1993).

[12] B. Y. Ha and D. Thirumalai, *Macromolecules* **28**, 577 (1995).

[13] U. Micka and K. Kremer, *Phys. Rev. E* **54** , 2653 (1996).

[14] U. Micka and K. Kremer, personal communication

[15] G. Maret and G. Weill, *Biopolymers* **22**, 2727 (1983).

[16] H. Mattoussi and S. O'Donohue and F. E. Karasz, *Macromolecules* **25**, 743 (1992).

[17] T. Odijk and A. C. Houwaart, *J. Polym. Sci., Polym. Phys. Ed.* **16**, 627 (1978).

[18] A. R. Khokhlov and K. A. Khachaturian, *Polymer* **23**, 1742 (1982).

[19] M. Tricot, *Macromolecules* **17**, 1698 (1984).

[20] S. Ghosh and X. Li and C. E. Reed and W. F. Reed, *Biopolymers* **30**, 1101 (1990).

[21] W. F. Reed and S. Ghosh and G. Medjahdi and J. Francois, *Macromolecules* **24**, 6189 (1991).

[22] V. Degiorgio and F. Mantegazza and R. Piazza, *Europhys. Lett.* **15**, 75 (1991).

[23] M. Schmidt, *Macromolecules* **24**, 5361 (1991).

[24] C. Seidel, *Macromol. Theory Simul.* **3**, 333 (1994).

[25] O. Kratky and G. Porod, *Recl. Trav. Chim. Pays-Bas* **68**, 1106 (1949).

[26] H. Yamakawa, "Modern Theory of Polymer Solutions", (Harper and Row, New York, 1971).

[27] M. Schmidt, *Macromolecules* **17**, 553 (1984).

[28] N. A. Metropolis and A. W. Rosenbluth and M. N. Rosenbluth and A. Teller and E. Teller, *J. Chem. Phys.* **21**, 1087 (1953).

[29] M. Lal, *Mol. Phys.* **17** , 57 (1969).

[30] N. Madras and A. D. Sokal, *J. Stat. Phys.* **50** , 109 (1988).

[31] M. Bishop and J. H. R. Clarke and A. Rey and J. J. Freire, *J. Chem. Phys.* **95**, 4589 (1991).

[32] B. Jönsson and C. Peterson and B. Söderberg, *J. Phys. Chem.* **99**, 1251 (1995).

[33] M. Ullner and B. Jönsson and P.-O. Widmark, *J. Chem. Phys.* **100**, 3365 (1994).

[34] M. Ullner and B. Jönsson and B. Söderberg and C. Peterson, *J. Chem. Phys.* **104**, 3048 (1996).

[35] B. Söderberg, unpublished.

[36] C. Peterson and O. Sommelius and B. Söderberg, *J. Chem. Phys.* **105**, 5233 (1996).

[37] G. S. Manning, *J. Chem. Phys.* **51**, 924 (1969).

[38] M. Ullner and B. Jönsson, *Macromolecules* **29**, 6645 (1996).

[39] P. J. Flory, "Principles of Polymer Chemistry", (Cornell University Press, Ithaca, 1992).

[40] S. Förster and M. Schmidt and M. Antonietti, *J. Phys. Chem.* **96**, 4008 (1992).

Paper VII

LU-TP 97-04
April 1997

On the Kinetic Behavior and Folding Properties of an Off-Lattice Heteropolymer Model

Ola Sommelius[1]

Complex Systems Group, Department of Theoretical Physics
University of Lund, Sölvegatan 14A, S-223 62 Lund, Sweden

Submitted to *Europhysics Letters*

Abstract:
The kinetic behavior of a three-dimensional off-lattice heteropolymer model is studied in terms of the time dependence of the average mean-square displacement between configurations. It is found that at short time-scales similar behavior is obtained even for sequences with very different thermodynamic properties. Furthermore, the degree of cooperativity in the folding process is examined by studying the residual number of degrees of freedom, obtained from an eigenvalue analysis of the correlation matrix, contributing to the structural fluctuations. In the compact state, a gradual decrease in this effective number of degrees of freedom takes place as the temperature is lowered. This can be interpreted as an increasing asymmetry of the energy landscape.

[1] ola@thep.lu.se

1 Introduction

In order to understand the characteristics of the energy landscape and to quantify the requirements needed for a protein to have a thermodynamical stable yet kinetically accessible native state, the introduction of simple models [1] is necessary. In these models the small length and time scales are effectively averaged out and the thermodynamics of the resulting coarse grained chain is described by an effective potential. The basic assumption for this is that a low-resolution description still captures features essential for describing folding properties.

Models which have been much studied are the lattice models where the protein is represented as chain of beads on a cubic lattice (see references in [1]). This approach has indeed proven to be very useful and one is able to describe several non-trivial aspects in the folding process. However it is important to study alternative off-lattice models both in order to understand the limitations of the lattice models and in their own right. In this work a 3D off-lattice model suggested in [2] is used. The model contains two types of amino acids, hydrophobic and hydrophilic, and the formation of a hydrophobic core is induced by a sequence dependent Lennard-Jones potential. In [2] the studies were focused on the thermodynamical behavior of this model.

For a sequence to be a good folder it must satisfy both thermodynamic and kinetic requirements. That is the ground state must be stable against thermodynamical fluctuations, which happens at low temperatures, and yet be kinetically accessible, which happens at higher temperatures. Therefore only sequences for which the thermodynamic stability persists at high enough temperatures can be classified as good folders. To understand the behavior of the structural fluctuations in this context the overall shape diffusion at short times is studied as well as the collective behavior of the conformational correlations in the chain.

This letter is organized as follows. Section two defines the model and the observables. Section three and four contain the results and a brief summary respectively.

2 The model

The model contains two kinds of residues, A and B, which behave as hydrophobic ($\sigma_i =$'A') and hydrophilic ($\sigma_i =$'B') residues, respectively. These monomers are joined by rigid bonds $\hat{b}_i$ to form a linear heteropolymer chain living in three dimensions. The shape of the chain is thus specified by the $N-1$ bond vectors

$\hat{b}_i$. The energy function is given by

$$E(\hat{b};\sigma) = -\kappa_1 \sum_{i=1}^{N-2} \hat{b}_i \cdot \hat{b}_{i+1} - \kappa_2 \sum_{i=1}^{N-3} \hat{b}_i \cdot \hat{b}_{i+2} + \sum_{i=1}^{N-2} \sum_{j=i+2}^{N} E_{\mathrm{LJ}}(r_{ij};\sigma_i,\sigma_j) \quad (1)$$

where $r_{ij} = r_{ij}(\hat{b}_i, \ldots, \hat{b}_{j-1})$ denotes the distance between sites i and j of the chain, and $\sigma_1, \ldots, \sigma_N$ is a binary string that specifies the primary sequence. The *species-dependent* global interactions are given by the Lennard-Jones potential,

$$E_{\mathrm{LJ}}(r_{ij};\sigma_i,\sigma_j) = 4\epsilon(\sigma_i,\sigma_j)\left(\frac{1}{r_{ij}^{12}} - \frac{1}{r_{ij}^{6}}\right) . \quad (2)$$

The depth of the minimum of this potential, $\epsilon(\sigma_i,\sigma_j)$, is chosen to favor the formation of a core of A residues, *i.e.* $\epsilon(A,A) = 1$ and $\epsilon(A,B) = \epsilon(B,B) = 1/2$. The two parameters of the energy function, κ_1 and κ_2, determine the strength of *species-independent* local interactions. The thermodynamic behavior of this model has been studied in Ref. [2]. It was found that the values $(\kappa_1,\kappa_2) = (-1, 0.5)$ give rise to local correlations qualitatively similar to those found in functional proteins. This choice favors anti-parallel nearest neighbour bonds and parallel next nearest neighbour bonds and will be used throughout this work. Furthermore it was found that, as the temperature is lowered, a gradual compaction occur. In the compact state this is then followed by a sequence dependent folding transition. For this model only a small fraction of random sequences have good folding properties. In 2D [3], where a more extensive investigation was done, only around 10 percent satisfied the folding criteria. This model to some extent resembles the IMP model [4, 5] which is a Gaussian chain augmented with a Lennard-Jones potential with an additional quenched disorder term $\sqrt{\epsilon}\,\eta_{ij}/r_{ij}^6$ representing a species-dependent interaction. The η_{ij}'s are stochastic variables having zero mean and unit variance, while ϵ is a measure of the strength of the quenched disorder.

In order to study the kinetics on a rugged energy landscape some kind of distance measure between conformations has to be defined. A natural choice [4] is the mean-square displacement between two configurations a and b, δ_{ab}^2:

$$\delta_{ab}^2 = \min \frac{1}{N} \sum_{i=1}^{N} |\mathbf{x}_i^a - \mathbf{x}_i^b|^2 \quad (3)$$

where $\mathbf{x}_i^{a(b)}$ denotes the position of monomer i in system $a(b)$. The minimization is to be performed over translations, rotations and reflections.

With δ_0^2 denoting the distance to the ground state, and $P(\delta_0^2)$ the corresponding probability distribution, we can define the probability for the system

no.	sequence	T_f
1	$BAAA\ AAAB\ AAAA\ BAAB\ AABB$	< 0.15
2	$BAAB\ AAAA\ BABA\ ABAA\ AAAB$	< 0.15
3	$AAAA\ BBAA\ AABA\ ABAA\ ABBA$	0.23
4	$AAAA\ BAAB\ ABAA\ BBAA\ ABAA$	0.22
5	$BAAB\ BAAA\ BBBA\ BABA\ ABAB$	< 0.15
6	$AAAB\ BABB\ ABAB\ BABA\ BABA$	0.15

Table 1: The six sequences studied. The errors in T_f are approximately 0.02.

to be found in the vicinity of the ground state as:

$$p_0 = \int_0^{0.04} P(\delta_0^2) d\delta_0^2 \tag{4}$$

The folding temperature T_f is then defined as the temperature where $p_0 = 1/2$.

3 Results

We use six sequences, of length $N = 20$ (Table 1), chosen in [2] to represent a variety of behavior, and examine their kinetic properties for short (intermediate) times. That is, the times should be large enough so as not depend on details of the MC-method (here the normal Metropolis algorithm) but smaller than the time scales necessary to equilibrate the systems. For each system $\mathcal{O}(100)$ Monte Carlo runs, each consisting of $3.3 \cdot 10^5$ steps were performed. The time averages of the mean-square displacement (eq. 3) $\langle \delta^2 \rangle_t$ are obtained by averaging over consecutive subsets of conformations with temporal extension t (this corresponds to an average time separation of $\approx t/3$). The simulations were performed at three different temperatures $T = 0.15, 0.23$ and 0.4. The two lowest correspond to folding temperatures of sequences 3 and 6 respectively (see Table 1), whereas $T = 0.4$ is low enough to correspond to compact states but high enough so that the ground state is almost completely de-populated. This can be seen from Fig. 1 (data from [2]), in which the population of the ground state p_0 and the radius of gyration (squared) is plotted versus temperature.

In Fig. 2 the time dependence of $\langle \delta^2 \rangle_t$ is displayed for short times. The data are well parametrized by a behavior of the type

$$\langle \delta^2 \rangle_t \propto t^\nu \tag{5}$$

with a temperature dependent exponent ν. For a harmonic chain one has $\nu = 1/2$ while the $T \to \infty$ limit gives $\nu = 1$ [5]. At short times the high temperature

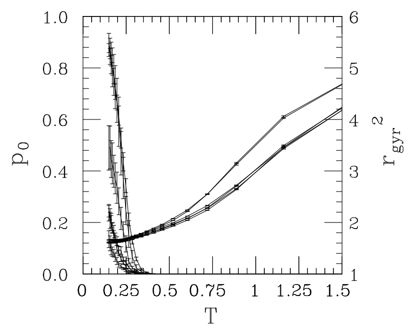

Figure 1: p_0 – the probability for the system to be found close to the native state, and r_{gyr}^2 – the radius of gyration squared, as a function of temperature.

limit is valid also for this model. For the sequences here examined ν grows with temperature (Table 2) in a roughly sequence independent manner. At a fixed (absolute) temperature there is a small difference in that the best folder is the chain with the slowest kinetics. This can partly be attributed to the fact that this system spend a lot of time in the vicinity of the native state although this effect mainly should affect the pre factor in eq. 5. On the other hand when

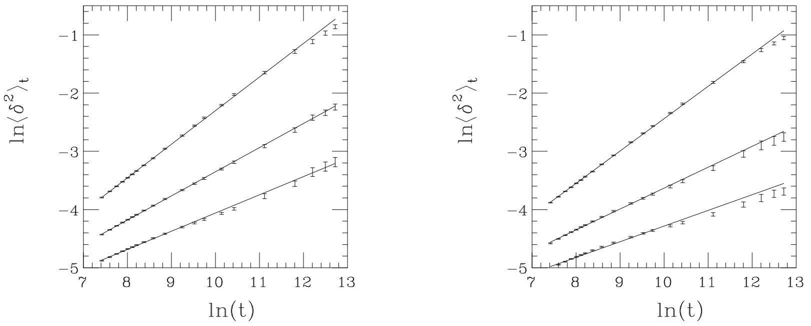

Figure 2: $\langle\delta^2\rangle_t$ as a function of t for sequence no. 1 and 3. The data correspond to, from top to bottom, the temperatures $T = 0.4, 0.23$ and 0.15. The solid lines are linear fits.

comparing the systems at the same "physical" temperature the difference is larger and in the other direction. The best folder now has the fastest kinetics. That is, when comparing the sequences at temperatures chosen such that the chains spend an equal amount of time in the native state, high thermodynamic stability implies fast kinetics. This means that the crucial requirement to be satisfied for a sequence to represent a good folder is thermodynamic stability

no.	T=0.15	0.23	0.4
1	0.31	0.41	0.58
2	0.31	0.40	0.57
3	0.27	0.36	0.56
4	0.29	0.37	0.56
5	0.32	0.42	0.59
6	0.30	0.40	0.58

Table 2: The exponent ν in eq. 5 for the different sequences at different temperatures. The errors are approximately 0.03

of the ground state. The more stable the ground state is the faster becomes the kinetics, at the folding temperature, towards this ground state. This is in line with what was found in [3]. With a somewhat different distance measure a similar study was performed for the IMP-model in [5]. The investigation was here focused on the behavior of the exponent ν at fixed temperature when the strength ϵ of the quenched disorder was changed. The results ranged from $\nu \approx 2/3$ for the ordered system ($\epsilon = 0$) to $\nu \approx 1/2$ for a chain with strong quenched disorder ($\epsilon = 10$). The difference between different realizations of the couplings η_{ij} at fixed value ϵ was found to be quite small although no distinction was made between these realizations in terms of their thermodynamic properties.

Next we study how the structural fluctuations decay as the temperature is lowered. All thermal averages where obtained with the "simulated tempering" method [6]. The torsional angles are defined by $\cos\phi_k = (\hat{b}_k \times \hat{b}_{k+1}) \cdot (\hat{b}_{k+1} \times \hat{b}_{k+2})$. In Fig. 3 the fluctuation in these angles, defined by $\langle \phi_k^2 \rangle - \langle |\phi_k| \rangle^2$ is showed as function of temperature. The lines represent a decreasing sequence of temperatures ranging from $T = 1.67$ (top) to $T = 0.15$ (bottom).

As can be seen, the sequence with good folding properties (seq. 3) have a more drastic "freeze out" of the (torsional) degrees of freedom, and at the lowest temperature, where $p_0 \approx 0.9$ only a few (3) of the torsion angles have significant fluctuations. For sequence 1 on the other hand $p_0(T = 0.15) \approx 0.25$, *i.e.* the thermodynamic stability requirement for the ground state is not yet satisfied, all the angles show rather large thermal fluctuations. These measurements do however not provide us with any information concerning the amount of correlations present in this process. In order to examine this issue we estimate an effective number of degrees of freedom for the chain, by calculating the eigenvalues to the correlation matrix

$$\rho_{ij} = \langle \hat{b}_i \cdot \hat{b}_j \rangle \tag{6}$$

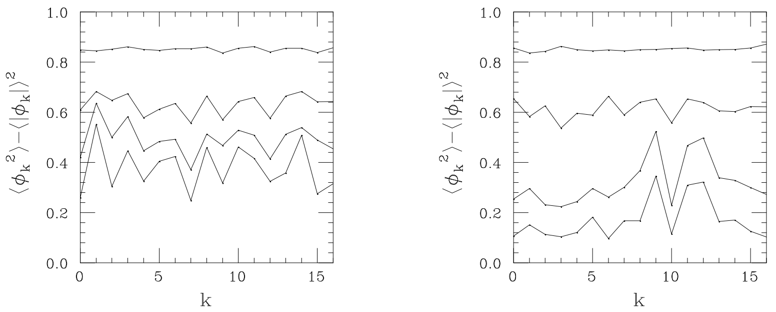

Figure 3: Fluctuation of torsional angels for sequences no. 1 and 3. The data corresponds to, from top to bottom, the temperatures $T = 1.67, 0.41, 0.23$ and 0.15.

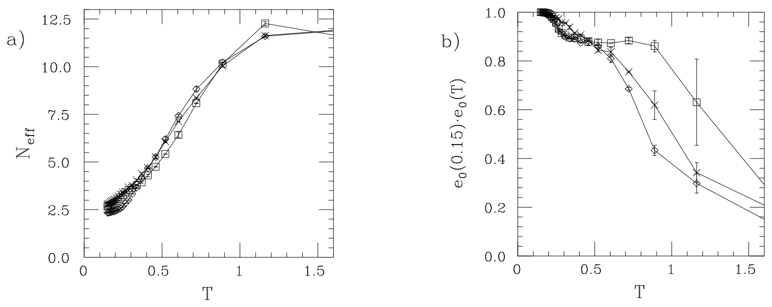

Figure 4: **a)** The "effective size" of the chain as a function of temperature. **b)** The scalar product of the leading eigenvector at T with the one at $T = 0.15$. The data correspond to seq. 1 ($\times$), seq. 7 ($\diamond$) and seq. 16 ($\Box$) respectively.

We define an "effective size" of the chain as

$$N_{\text{eff}} = \frac{\text{Tr } \rho}{\lambda_0} \tag{7}$$

where λ_0 is the largest eigenvalue of ρ. For this particular choice of correlation matrix the trace equals $N - 1$. As can be seen from Fig. 4 a there is a gradual decrease in the number of effective degrees of freedom as the temperature is lowered. This is in contrast to the behavior expected from a quadratic potential, for which N_{eff} would have been temperature independent. Thus the energy landscape becomes more and more asymmetric as the temperature goes down. Comparing with the behavior of r_{gyr}^2 and p_0 in Fig. 1 we see that this "freezing out" effect occurs mainly in the compact state but before the ground state is populated. In order to see how high in temperature the asymmetry defined at the lowest temperature persists we show in Fig. 4 b the scalar product between the dominant (normalized) eigenvector at $T = 0.15$, $e_0(0.15)$ with the corresponding one at temperature T, $e_0(T)$. This represents a measure on how similar the direction specifying the largest structural fluctuations is compared with the principal direction of the "valley" hosting the native state, or rather the dominating "valley" at $T = 0.15$. For seq. 3 and 4 at least these coincide. As can be expected at high temperatures there is no memory of this direction and although the qualitative behavior is similar for the different chains the sequence dependence is rather large compared to that of N_{eff}. This reflects the fact that $e_0(0.15) \cdot e_0(T)$ is directly related to the properties of the low-end of the energy spectrum while N_{eff} is more general in character.

4 Conclusions

We have studied the kinetic behavior of a 3D off-lattice protein model in terms of shape diffusion at short time scales in connection with folding. We find that sequences with very different thermodynamic behavior, e.g. with respect to the stability of the ground state, have fairly similar kinetic behavior at short time scales. This suggests that the crucial requirements for a chain to have good folding properties are mainly thermodynamic in nature. Furthermore, we examine the behavior of the structural fluctuations of the system – how large are the correlations in the process of freezing out the configurational fluctuations? By estimating an effective number of degrees of freedom present in the system we find that the collective effects in this process are indeed very high and that the asymmetry of the energy landscape is increased as the temperature is lowered.

References

[1] For a review, see M. Karplus and A. Šali, "Theoretical Studies of Protein Folding and Unfolding", *Curr. Opin. Struct. Biol.* **5**, 58 (1995).

[2] A. Irbäck, C. Peterson, F. Potthast and O. Sommelius "Local Interactions and Protein Folding: A 3D Off-Lattice Approach", to appear in *J. Chem. Phys.*

[3] A. Irbäck, C. Peterson and F. Potthast "Identification if Amino Acid Sequences with Good Folding Properties in an Off-Lattice Model", *Phys. Rev.* **E 55**, 860 (1997).

[4] G. Iori, E. Marinari and G. Parisi "Random Self-interacting Chains: a Mechanism for Protein Folding", *J. Phys. A.* **24**, 5349 (1991).

[5] P. Pliszka and E. Marinari "On Heteropolymer Shape Dynamics", *Europhys. Lett.* **22**, 3 (1993).

[6] E. Marinari and G. Parisi "Simulated Tempering: A New Monte Carlo Scheme", *Europhys. Lett.* **19**, 451 (1992).